SOUTHERN PLAINS
TRANSPORTATION CENTER

BEHAVIOR OF INTEGRAL ABUTMENT BRIDGES IN VARYING CLIMATE

Arash Hassanikhah, Ph.D.
Gerald A. Miller, Ph.D., P.E.
Kanthasamy K. Muraleetharan, Ph.D., P.E., G.E.

SPTC14.1-52-F

Southern Plains Transportation Center
201 Stephenson Parkway, Suite 4200
The University of Oklahoma
Norman, Oklahoma 73019

DISCLAIMER

The contents of this report reflect the views of the authors, who are responsible for the facts and accuracy of the information presented herein. This document is disseminated under the sponsorship of the Department of Transportation University Transportation Centers Program, in the interest of information exchange. The U.S. Government assumes no liability for the contents or use thereof.

TECHNICAL REPORT DOCUMENTATION PAGE

1. REPORT NO.	2. GOVERNMENT ACCESSION NO.	3. RECIPIENT'S CATALOG NO.
SPTC 14.1-52		

4. TITLE AND SUBTITLE	5. REPORT DATE
Behavior of Integral Abutment Bridges in Varying Climate	November 30, 2019
	6. PERFORMING ORGANIZATION CODE

7. AUTHOR(S)	8. PERFORMING ORGANIZATION REPORT
Arash Hassanikhah, Gerald A. Miller, and Kanthasamy K. Muraleetharan	Click here to enter text.

9. PERFORMING ORGANIZATION NAME AND ADDRESS	10. WORK UNIT NO.
School of Civil Engineering and Environmental Science, The University of Oklahoma, 202 West Boyd Street, Room 334 Norman, OK 73019	11. CONTRACT OR GRANT NO. DTRT13-G-UTC36

12. SPONSORING AGENCY NAME AND ADDRESS	13. TYPE OF REPORT AND PERIOD COVERED
Southern Plains Transportation Center 201 Stephenson Pkwy, Suite 4200 The University of Oklahoma Norman, OK 73019	Final August 2014 – November 2019
	14. SPONSORING AGENCY CODE

15. SUPPLEMENTARY NOTES

University Transportation Center

16. ABSTRACT

Integral Abutment Bridges (IABs) are jointless bridges without expansion joints in the bridge deck or between the superstructure and the abutments. An IAB provides many advantages during construction and maintenance of a bridge, but the soil-structure interactions occurring at the abutment in an IAB are complex. The impact of long term variations in soil moisture on the lateral load behavior of integral abutment piles is investigated. First, unsaturated seepage modeling is used to predict the variations in soil moisture content and associated matric suction profiles surrounding abutment piles through the end of this century in the U.S. Department of Transportation's (U.S. DOT) Region 6 states (Oklahoma, Texas, New Mexico, Arkansas, and Louisiana). Next, techniques were used to incorporate matric suction into the lateral load analysis of abutment piles. Finally, a sensitivity analysis of parameters such as soil profile, pile type and length, and pile orientation affecting the lateral load behavior of integral abutment piles was conducted. The parametric study showed that the pile orientation and foundation soil stiffness due to suction changes have a significant effect on the bending moment and lateral displacement behavior of abutment piles. The results also show that changing climate over the long term may result in net drying of soil profiles and increased matric suction around the top of the piles. Increases in matric suction in soil around the piles increases the strength and stiffness around the piles, which results in increased resistance to pile bending and greater curvature near the top of the pile where it enters the abutment. This in turn, increases the maximum bending moments near the top of the pile. Techniques such as orienting the piles in weak axis bending and reducing the stiffness of the soils surrounding the top of the piles should be considered to improve the performance of abutment-pile-soil systems in IABs.

17. KEY WORDS	18. DISTRIBUTION STATEMENT
Integral Abutment Bridge, Soil-pile interaction, Unsaturated soil, Soil moisture, Matric suction	No restrictions. This publication is available at www.sptc.org and from the NTIS

19. SECURITY CLASSIF. (OF THIS REPORT)	20. SECURITY CLASSIF. (OF THIS PAGE)	21. NO. OF PAGES	22. PRICE
Unclassified	Unclassified	119 + cover	

SI* (MODERN METRIC) CONVERSION FACTORS

APPROXIMATE CONVERSIONS TO SI UNITS

SYMBOL	WHEN YOU KNOW	MULTIPLY BY	TO FIND	SYMBOL
		LENGTH		
in	Inches	25.4	millimeters	mm
ft	Feet	0.305	meters	m
yd	yards	0.914	meters	m
mi	miles	1.61	kilometers	km
		AREA		
in^2	square inches	645.2	square millimeters	mm^2
ft^2	square feet	0.093	square meters	m^2
yd^2	square yard	0.836	square meters	m^2
ac	acres	0.405	hectares	ha
mi^2	square miles	2.59	square kilometers	km^2
		VOLUME		
fl oz	fluid ounces	29.57	milliliters	mL
gal	gallons	3.785	liters	L
ft^3	cubic feet	0.028	cubic meters	m^3
yd^3	cubic yards	0.765	cubic meters NOTE: volumes greater than 1000 L shall be	m^3
		MASS		
oz	ounces	28.35	grams	g
lb	pounds	0.454	kilograms	kg
T	short tons (2000 lb)	0.907	megagrams (or "metric ton")	Mg (or "t")
		TEMPERATURE (exact degrees)		
^oF	Fahrenheit	5 (F-32)/9 or (F-32)/1.8	Celsius	^oC
		ILLUMINATION		
fc	foot-candles	10.76	lux	lx
fl	foot-Lamberts	3.426	$candela/m^2$	cd/m^2
		FORCE and PRESSURE or STRESS		
lbf	poundforce	4.45	newtons	N
lbf/in^2	poundforce per square inch	6.89	kilopascals	kPa

APPROXIMATE CONVERSIONS FROM SI UNITS

SYMBOL	WHEN YOU KNOW	MULTIPLY BY	TO FIND	SYMBOL
		LENGTH		
mm	millimeters	0.039	inches	in
m	meters	3.28	feet	ft
m	meters	1.09	yards	yd
km	kilometers	0.621	miles	mi
		AREA		
mm^2	square millimeters	0.0016	square inches	in^2
m^2	square meters	10.764	square feet	ft^2
m^2	square meters	1.195	square yards	yd^2
ha	hectares	2.47	acres	ac
km^2	square kilometers	0.386	square miles	mi^2
		VOLUME		
mL	milliliters	0.034	fluid ounces	fl oz
L	liters	0.264	gallons	gal
m^3	cubic meters	35.314	cubic feet	ft^3
m^3	cubic meters	1.307	cubic yards	yd^3
		MASS		
g	grams	0.035	ounces	oz
kg	kilograms	2.202	pounds	lb
Mg (or "t")	megagrams (or "metric ton")	1.103	short tons (2000 lb)	T
		TEMPERATURE (exact degrees)		
^oC	Celsius	1.8C+32	Fahrenheit	^oF
		ILLUMINATION		
Lx	lux	0.0929	foot-candles	fc
cd/m^2	$candela/m^2$	0.2919	foot-Lamberts	fl
		FORCE and PRESSURE or STRESS		
N	newtons	0.225	poundforce	lbf
kPa	kilopascals	0.145	poundforce per square h	lbf/in^2

*SI is the symbol for the International System of Units. Appropriate rounding should be made to comply with Section 4 of ASTM E380.
(Revised March 2003)

BEHAVIOR OF INTEGRAL ABUTMENT BRIDGES IN VARYING CLIMATE

SPTC 14.1-52
Final Report

November 2019

Arash Hassanikhah, Ph.D.
Gerald A. Miller, Ph.D., P.E.
Kanthasamy K. Muraleetharan, Ph.D., P.E., G.E.

The University of Oklahoma
School of Civil Engineering and Environmental Science
202 W. Boyd St., Room 334, Norman, OK 73019

Southern Plains Transportation Center
201 Stephenson Pkwy, Suite 4200
The University of Oklahoma
Norman, OK 73019

Table of Contents

List of Figures

List of Tables

1. INTRODUCTION

1.1. Problem statement

Integral Abutment Bridges (IAB) are jointless bridges without expansion joints in the bridge deck or between the superstructure (deck and girders) and the abutments. The girders are cast into the back wall of the abutment eliminating the need for a bridge seat and bearings. An IAB provides many advantages during construction and maintenance of a bridge. Joints and bearings in a conventional bridge are expensive and costly to install and leaking joints lead to deterioration of girders and bearings and therefore higher maintenance costs. IABs also provide superior performance during extreme loading events such as earthquakes and blast loading. Due to these reasons, IABs are generally being built by agencies at an increasing rate in the U.S.A. The complex interactions occurring in an IAB between the superstructure, abutments, foundations, and soils, however, are still not fully understood. Furthermore, there are no national design standards for IABs and each state has adopted its own design and construction practice. This has led to a contradictory and confusing array of design and construction practices. IAB designers in the U.S. Department of Transportation (U.S. DOT) Region 6 states (Oklahoma, Texas, New Mexico, Arkansas and Louisiana) face additional challenges due to extreme variations in temperature and soil moisture in these states.

The research described in this report builds upon previous work that involved data collection from an instrumented Oklahoma IAB and subsequent modeling efforts (Muraleetharan et al. 2012; Kirupakaran 2013). Previous efforts focused on the influence of temperature extremes on IABs. Research presented herein focused on the

impact of variable moisture conditions on the lateral load behavior of the IAB abutment-pile system. The goal was to better understand the lateral load behavior of abutments-piles under varying weather conditions over months to years and develop design guidelines for IABs in Region 6 and other areas subjected to extreme variations in weather.

Research work began with the collection of available climate data and expected temperature, precipitation and other weather conditions across Region 6 were established for desired time periods. Then using the temporal weather variations as input, a computer program was used to model unsaturated seepage to predict variations in moisture content and matric suction in soil profiles over time. Finally, a soil-structure interaction model was used to study the lateral load behavior due to thermal loading of the pile-abutment system under varying moisture conditions.

As a part of the soil-structure interaction modeling, a parametric analysis was conducted to study the influence of different parameters on the lateral load response of the pile-abutment system. The parameters considered included: types, orientation, and length of abutment piles; different embankment and foundation soil conditions; various abutment backfill materials such as compacted and non-compacted granular fill; and length of the bridge. To model the soil-structure interaction the software LPILE (Ensoft 2007) was used; LPILE is an industry standard program for analysis of lateral loading of piles. For modeling unsaturated seepage into soil surrounding abutments and piles, the finite element based software SVFlux (SoilVision 2012) was used. SVFlux has advanced features for modeling transient moisture movement through soil due soil-atmospheric

interactions at the ground surface. The results of the modeling and parametric analysis were used to develop design guidelines for IABs in Region 6.

1.2. Purpose

While many important lessons were learned from prior field research and modeling, the purpose of this study was to extend the results of the previous work to encompass a variety of bridge, subsurface, and climatic conditions. Because instrumenting a large number of bridges and collecting the necessary data over large time frames was impractical, researchers with support of the SPTC conducted extensive parametric analyses to investigate important soil-structure interaction variables. A crucial outcome of the previous work was the calibration and validation of computer models to successfully mimic the observed behavior of an IAB under thermal loading. Building on this success, the goal of work described herein was to investigate the behavior of the IAB abutment-pile system in regard to the effects of bridge configuration (abutment and bridge length, etc.), foundation and pile type (pile bending stiffness, soil stiffness, etc.), backfill type (granular, controlled low strength material, etc.), embankment and foundation materials (type, stiffness, etc.), and impacts of seasonal temperature and moisture variations in the soil. The results of this extensive parametric analysis provided valuable insight into analysis and design of integral abutment bridges.

1.3. Research Objectives

The primary goal of the research was to develop design and construction guidelines for Integral Abutment Bridges in view of extreme variations in climate/weather and its impacts on the lateral load performance of the abutment-pile system. Research focused

on states associated with the SPTC in Region 6. Specific objectives and tasks of the research needed to accomplish this goal included:

Objective 1: Establish bridge and soil conditions representative of Region 6 states for use in the modeling studies.

Objective 1 Tasks: Review published literature and contact DOTs in Region 6 states to collect information regarding typical IAB bridge configurations and soil conditions.

Objective 2: Establish historical and future weather data that captures temporal variations across climate zones in Region 6, for use in unsaturated seepage modeling.

Objective 2 Tasks: Gather available weather data from Mesonet in Oklahoma and similar sources in Region 6 states, use available climate prediction tools to forecast future weather variations, establish representative weather data patterns for Region 6, and put the weather data in a format compatible with input into the unsaturated seepage computer program.

Objective 3: Establish temporal variations in soil moisture content and matric suction based on weather data established for states within Region 6. Variations in matric suction are needed as input into the soil-abutment-pile interaction analysis to capture the influence of variable soil saturation on the system behavior.

Objective 3 Tasks: Using weather data established under Objective 2 as input, conduct unsaturated seepage analyses using SVFlux, incorporating variations in weather and soil conditions representative of different climate zones across Region 6.

Objective 4: Reveal lateral load behavior of the abutment-pile system under varying abutment-pile configurations and varying weather and soil conditions representative of different climate zones across Region 6.

Objective 4 Tasks: Use LPILE to model abutment-pile-soil interactions under lateral loading due to thermal variations in the bridge structure, conduct a parametric analysis to investigate the influence of variable bridge configurations, soil conditions and moisture conditions representative of climate zones across Region 6. As part of this analysis, p-y curves had to be developed for lateral pile analysis with consideration given to the influence of matric suction on strength and stiffness of the soil.

Objective 5: Develop design and construction guidelines for IABs considering extreme weather variations and their influence on performance of the abutment-pile system.

Objective 5 Tasks: Based on information collected through the first four objectives, develop recommendations for practitioners to implement during design of abutment-pile systems.

2. BACKGROUND

2.1. Integral Abutment Bridges

Integral Abutment Bridges (IABs) are being increasingly used in Oklahoma and other parts of the country and have distinct advantages compared to conventional bridges. IABs are constructed without any expansion or construction joints and are also referred to as jointless bridges, rigid-frame bridges, and U-frame bridges. They are designed to transfer applied loads from superstructure through substructure to the stable foundation. Accommodation of superstructure lateral displacements due to thermally induced loads is different in IABs and conventional bridges. The expansion joints in conventional bridges accommodate the lateral displacement using various types of bearings and corrosion problems among these components is prevalent during their service life. The gradual degradation of materials used for bridge bearings and joints results from chemical reactions with surface water that enters the expansion joints. The replacement and maintenance of the expansion joints requires a costly and a time-consuming schedule, so the elimination of joints in an IAB is a considerable advantage over conventional bridges. However, since in an IAB thermal loads in the superstructure are transferred to the abutment and piles under lateral loading, it is important that the flexibility of the abutment-pile-backfill-foundation soil system is sufficient to prevent damage to the pile, abutment and bridge structure.

2.2. Background Information and Examples of IABs in Region 6

A survey of current practices for the design of IABs was performed by Kunin and Alampalli (2000). According to the survey, Oklahoma and Arkansas in Region 6, among the other states, were interested in responding to the inquiries. The Oklahoma engineers believed that the method of thermal loading applied to the bridges was conservative, resulting in less lateral movement than expected. Fifty IABs built in Oklahoma and only two IABs constructed in Arkansas until 2000, used precast concrete girders and steel girders with maximum lengths of 122 m and 91.5 m, respectively. The AASHTO (1996) standard specifications for highway bridges was followed by the States of Oklahoma and Arkansas. The recommended range of temperature for metal structures was 0 to 120°F for moderate climates and -30°F to 120°F for cold climates. Concrete structures were designed for 70°F variation in moderate climates and 80°F variation in cold climates.

According to a survey (Paraschos and Amde 2009), New Mexico built its first IAB in 1955 in an attempt to eliminate spalling of the abutment cap and diaphragms observed in some conventional bridges. The IABs were reported to have performed well largely due to elimination of the joint in the deck at the abutment. As Arkansas started to build this type of bridges in 2001 and the total number of IABs did not exceed 30 at the time of the survey, comprehensive assessment about the performance of IABs was not completed at that time. At the time of the survey, Texas had decided to stop building IABs due to economic issues. The cost of using steel piling for IABs instead of typically used drilled shafts or prestressed concrete piling was cited as a primary

economic reason for not building IABs. Oklahoma provided good feedback based on their experience dating back to 1980, when the first IAB was built in Oklahoma. The only problem reported was the settlement of the approach slabs across the state.

Information obtained from the State of Louisiana (Voyiadjis et al. 2016) shows that two fully integral abutment bridges have been built in recent years named Bodcau Bayou Bridge and Caminada Bay Bridge. The former one was built on a relatively lean and fat clay and the latter one was constructed on mainly fine sand and silty sand deposit. The total lengths of concrete deck of Bodcau Bayou Bridge and Caminada Bay Bridge were 300 feet and the average length of HP steel piles located in the embankments was 85 and 65 feet, respectively. As an example, Figure 2.1 shows a section of Bodcau Bayou Bridge. Two bridges were instrumented by the Louisiana Department of Transportation and Development (LaDODT) to monitor the pile deformation, soil pressure, and the rotation of the abutment wall for two years. Piles used in both bridges experienced the bending moments lower than the yielding bending moments. The numerical analysis for the given bridges showed that the smaller bridge displacement and backfill pressure were generated due to changing of soil stiffness surrounding the piles from soft to stiff values.

According to the New Mexico Department of Transportation (NMDOT) response, this state planned to build a fully integral abutment bridge named NM 122 over I-40, which has the total length equal to 180 feet and the average length of the HP steel piles supporting the abutments is 60 feet as shown in Figure 2.2. NMDOT uses the Current Edition of the AASHTO LRFD Bridge Design Specifications and the current interims as the

primary standards for the design of bridges in the State of New Mexico. However, a general guidance and interpretation of AASHTO LRFD Bridge Design Specifications was provided as a manual to the New Mexico design practice (2013). The manual describes the design procedure for materials used in bridges including reinforced concrete, prestressed concrete, steel, bearing devices and girder anchorages, deck joints, and substructure.

The State of Texas experiment regarding the fully integral abutment bridges is related to a bridge called FM-1905 over Anthony Road. The total length of this bridge was 222 feet and the average length of HP steel piles supporting the abutments was 36 feet as indicated in Figure 2.3. According to Texas engineers in the Department of Transportation, weathering steel (non-painted) was used to accommodate a low vertical clearance situation, and the designer knew that roadway drainage containing deicing salts leaking through expansion joints would be harmful to the steel. Thus, by making the bridge integral, the expansion joints were moved away from the steel girders and thus remove the corrosion potential. The successful performance of this bridge was related to soil conditions, which allowed the use of steel piles in a sandy soil. Recent information from Texas (Zornberg, 2016) shows that the department of transportation tends to continue the construction of IABs and establish a comprehensive research program across the state including: a review of US and international practices, as well as of existing data, to assess the applicability to conditions prevailing in Texas; a thorough evaluation of structures already constructed in Texas, as well as of an integral bridge

that was constructed in 2016 in Texas by FHWA Federal Lands; and a set of design details for using this technology in Texas conditions.

In the State of Oklahoma, the North-bound I-44 Bridge over Medicine Bluff Creek in Comanche County near Lawton was instrumented for 40 months starting in June 2009 and was selected as a case study to get preliminary results (Muraleetharan et al. 2012; Kirupakaran 2013). As shown in Figure 2.4, the I-44 Bridge has a total length of 210 feet and HP steel piles at the north and south abutments vary between 43 and 26 feet long, respectively. The numerical study conducted on the instrumented bridge by Kirupakaran (2013) showed that the abutment piles experienced bending moments greater than the yield bending moment, which was consistent with the recorded readings from the field data.

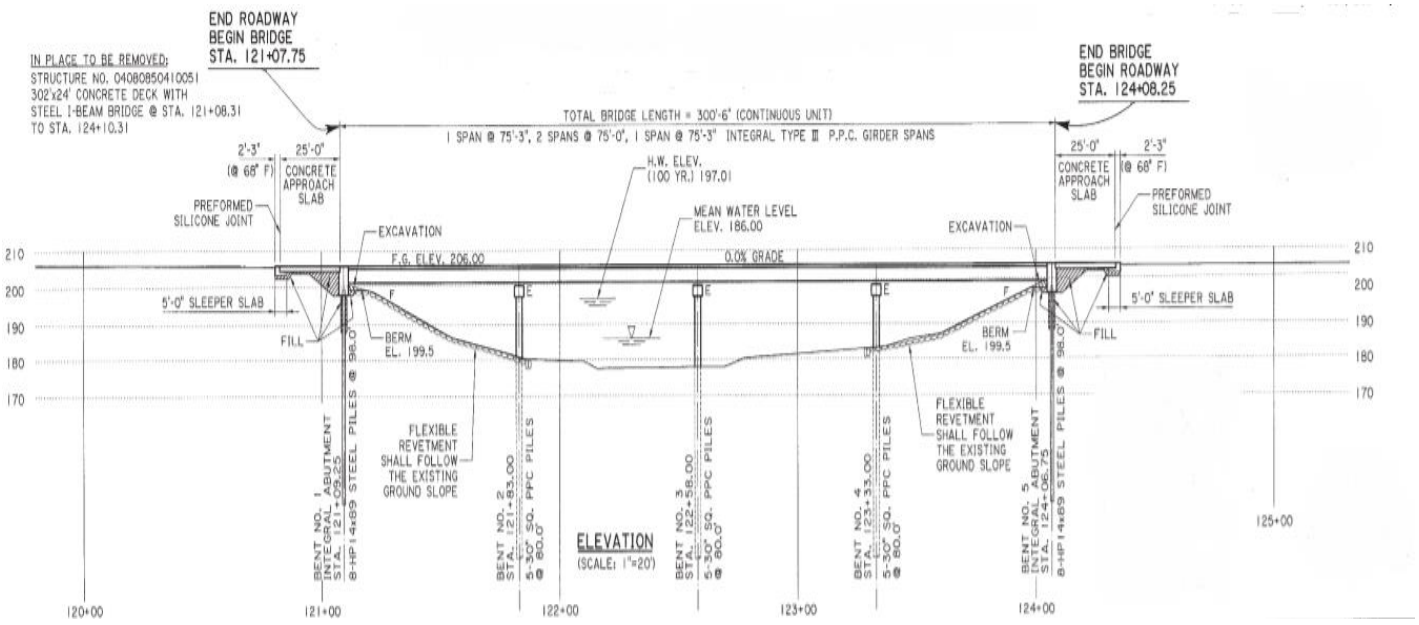

Figure 2.1. Profile of the LA 160 Bridge from Louisiana

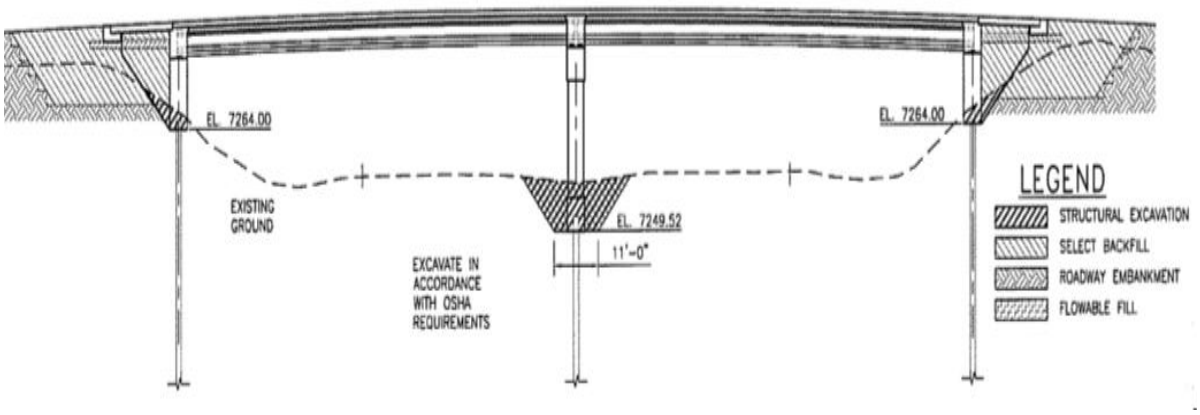

Figure 2.2. Profile of the NM 122 Bridge from New Mexico

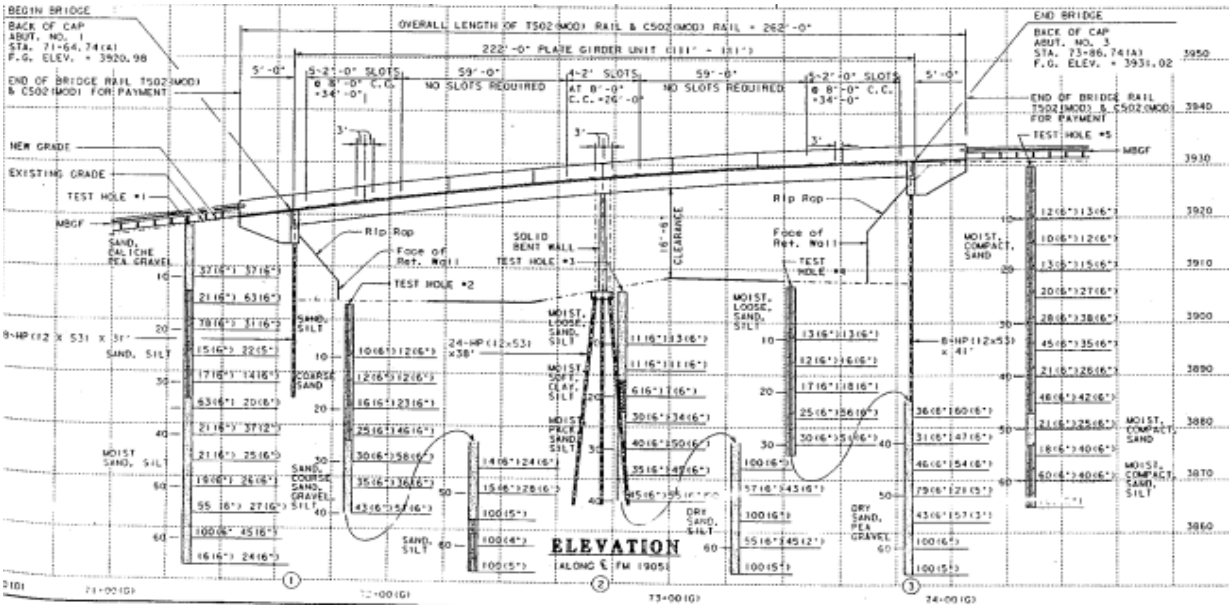

Figure 2.3. Profile of the FM 1905 Bridge from Texas

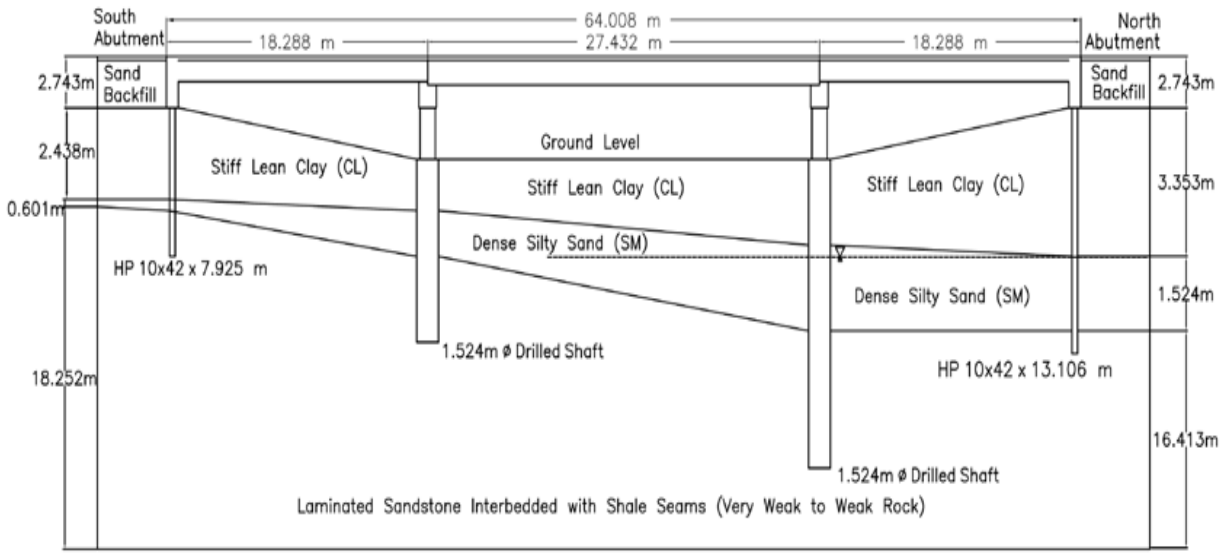

Figure 2.4. Profile of the I-44 Bridge from Oklahoma

2.3. Soil-Pile Interaction Numerical Models

Numerical methods are popular research methods widely used in the analysis of integral bridge problems. Several studies have been done using this method of analysis generating useful results. Some studies carried out on the integral bridge using the numerical method are discussed below.

Two different pile analysis methodologies including linear and non-linear methods were carried out using LPILE to investigate the influence of the lateral loading on the piles by Klaiber et al. (2004). They also proposed different abutment and pile systems such as micropiles, GRS structures, Geopier foundations, and sheet pile abutments instead of traditional deep foundation systems such as driven pile. In the linear method developed by Broms (1964a&b), a general uniform reaction of soil based on the undrained shear strength of soil and the width of pile was assumed in the lateral

pile analysis, whereas, in the non-linear method, a series of non-linear and horizontal springs was used to model the soil response. The maximum pile moments obtained from the linear and non-linear methods were compared; it was determined that the linear method was more conservative for most lateral load cases associated with bridge abutments. For stiff cohesive soils, the linear method was more conservative by 7 to 15 percent depending on the magnitude of the lateral pile loadings. However, the linear method produced less conservative maximum pile moments in soft cohesive soils by about 3 to 20 percent depending on the lateral pile loading. Finally, the maximum pile moments in cohesionless soils obtained from the linear method were more conservative by zero to three percent when compared to the non-linear analysis method.

Frosch and Lovell (2011) conducted a comprehensive study using LPILE and a finite element program named SAP2000, to investigate the effect of various characteristics on the long-term behavior of Integral Abutment Bridges (IABs). They developed and calibrated analytical models for design of IABs using field data obtained from instrumentation available for three IABs. They created a prototype of IAB in a quarter scale with 45^0 skew to study the effect of high degree of skew on the behavior of an IAB. They observed that the contraction movement of the abutment resulted in the maximum lateral pile displacement compared to the expansion movement. A steady-state cyclic movement was observed after approximately seven years of monitoring. The transverse movement of the abutment was more pronounced when the skew angle of bridge was greater than 30 degrees.

Dicleli (2005) employed a finite element software, SAP2000, to make a correlation between the internal forces in the abutment such as shear forces and bending moments and the thermal-induced displacements of the bridge. The abutment height, pile orientation and size, and sandy soil density were incorporated in their analysis. Dicleli and Albhaisi (2004a, 2004b, and 2005) also investigated the effects of clay stiffness around piles, pile size and orientation, pile connection to abutment, abutment height, and bridge size on the performance of integral bridges during thermal loading using SAP2000. The general results showed that the effect of backfill density can be negligible on the distribution and intensity of backfill pressure and more pronounced on the amount of internal forces in the abutment. The effect of size and orientation of the piles were not significant on the bending moments and shear forces generated in the abutments when the backfill and foundation soil were in the elastic zone. They also found the maximum length limits for different bridges supported by only HP piles driven in clay; the maximum length of concrete integral bridges was limited to 210 m in cold climates and 260 m in moderate climates and for the steel integral bridges, the limits were 120 m in cold climates and 180 m in moderate climates.

Abendroth and Greimann (2005) used experimental results to verify a 3-D model simulated using a finite element package, named ANSYS. They investigated the effects of loose versus dense sand behind the abutment and the stiffness of the soil around the piles when different vertical temperature distributions are applied over the depth of the superstructure. They found that the rotations and longitudinal displacement of

abutments predicted by ANSYS were more than those measured using the sensors in the field.

A nonlinear finite element model using GT STRUDL was employed by Civjan et al. (2007) to investigate the effects of backfill properties, foundation soil properties, and pile restraint on bridge distortion and pile moments during thermal loading. They found that the bridge expansion and contraction were influenced by different resisting elements such as backfill and foundation soil stiffness.

The compaction condition of sandy soil in predrilled holes, depth of predrilled holes, water table elevation, soil type around a pile and pile orientation were the parameters considered by Arockiasamy et al. (2004) in their analyses of IABs. They interpreted the results based on the displacements, moments and shear forces in H-piles supporting integral bridges subjected to thermal loading, using a finite element software, FB-Pier, and LPILE. They concluded that the piles installed into the predrilled holes filled with sand experienced low shear forces and bending moments due to the high flexibility. The effect of water table was recognized as insignificant based on the simple assumptions used in LPILE. The piles oriented in weak axis bending allowed larger lateral displacements before reaching yield bending moments compared to those installed in strong axis bending.

Using 2D finite element modeling, Arsoy et al. (1999) investigated the effects of the approach fill on pile stresses, abutment type, magnitude of thermal movement on the lateral resistance contribution of the abutment relative to the piles, and magnitude of the thermal induced lateral movement and the extent of settlement in the fill behind

the abutment. The finite element analyses showed that the vertical settlement in the fill behind the abutment occurred over a distance at the ground surface of three to four times the abutment height as measured from the back of the abutment. The low shear forces of pile head, which were computed around 12% to 26% of the total applied load, were also attributed to the small relative displacements between the pile and the surrounding ground.

Kamel et al. (1996) conducted a number of parametric studies addressing the influence of soil type (e.g. loose sand, dense sand, soft clay, and stiff clay), pile type (e.g. steel and prestressed concrete), and fixity of the pile head (e.g. hinged and fixed joints) using LPILE. They determined that the steel piles are more resistant to lateral loading compared to the prestressed concrete piles.

Faraji et al. (2001) modeled a three-dimensional Integral Abutment Bridge coupled with nonlinear springs representing the soil behind the abutment and piles using GT STRUDL. Four combinations of loose/loose, loose/dense, dense/loose, and dense/dense sand for soil behind the abutment/foundation soil was used in a parametric study. They found that the degree of compaction of foundation soil affected the bending moment of piles; however, it did not show any effect on the abutment moment and displacement.

Khodair and Hassiotis (2005) used a finite element program, Abaqus/Standard, to model a single HP pile surrounded by a sand-filled corrugated galvanized steel sleeve. The single pile was subjected to a lateral displacement created by an effective bridge temperature. The nonlinear form of Mohr-Coulomb failure criterion and elastic-

perfectly plastic model were assumed for soil and steel pile, respectively. They concluded that the increase of sand filled sleeve diameter surrounding an HP pile in finite element analysis increased the capacity of pile against the thermal loading.

Knickerbocker et al. (2005) used ANSYS to model an asymmetric integral abutment bridge in Tennessee. They conducted parametric studies including abutment depth, pile depth and skew angles for the sensitivity analysis of integral abutment bridge under thermal expansion and contraction loading of the superstructure. They found that in asymmetric bridges with respect to the abutments, the longer abutment was subjected to more movement due to the thermal loading compared to the shorter abutment.

Khodair and Abdel-Mohti (2014) conducted parametric studies to investigate the soil-pile interaction behavior using LPILE and finite element methods Abaqus/Cae and SAP2000. They have found that it is possible to make a correlation between the methods through change in parameters such as the soil's modulus of elasticity, radius of the soil surrounding the pile in Abaqus/Cae, and the number of springs in SAP2000.

The extensive parametric analyses of soil-pile interaction in the application of IABs by the former researchers showed that each mechanical component involved in the construction of an IAB was considered and could be designed effectively. However, the change of soil properties due to variable climate/weather was not considered in these studies. Since this is a primary focus of research discussed in this report, the following Section 2.4 discusses research on soil moisture prediction using different programs.

After validating the computer codes LPILE, GROUP (a group piles counterpart to LPILE) and a finite element code TeraDysac (Muraleetharan et al. 2003) using the I-44 field data, Kirupakaran (2013) conducted a parametric study to investigate various IAB configurations and abutment pile types. His results confirmed that I-44 abutment piles have indeed yielded at shallow depths. His results further revealed biaxial bending of abutment piles in IABs with skew. He recommended HP piles with smaller sections be placed in weak axis bending and in pre-drilled holes with low stiffness fill material, especially at shallow depths, to accommodate thermal movements in IABs and to reduce pile bending moments. He also recommended that abutment piles be placed in weak axis bending along the transverse direction for IABs with larger skew angles.

2.4. Soil Moisture Prediction Numerical Models

Several commercial software packages are available to model the moisture flow in soils, including SoilCover (Unsaturated Soils Group 1996), HYDRUS-2D (Simunek et al. 1999), Vadose/W (GeoSlope International Ltd. 2005), SVFlux (SoilVision Systems Ltd. 2007) and FlexPDE (PDE Solutions Inc.).

Scott et al. (2000) modeled one dimensional moisture movement in a soil profile over 8 years, using the model HYDRUS, which incorporates Richard's Equation. They concluded that there is substantial root zone recharge during wetter periods than normal winters. Modeled moisture fronts migrated as deep as 1.3 m during these years.

Collins and Znidarcic (2004) modeled a one-dimensional soil column using a saturated/unsaturated seepage finite element code, SEEP/W, to investigate infiltration

into an infinite slope. They found that the high rate of infiltration in slopes composed of coarse-grained soils leads to positive pore water pressures resulting in the slope failure at shallower depths. In contrast, the loss of suction in layers composed of fine-grained soils triggers the slope failure in deeper layers.

Chao et al. (2010) used Vadose/W to study the effect of precipitation, irrigation and deep underground water sources on the movement rate of a wetting front in a column of soil. The lowest, average, and the highest annual precipitation were used as three different climate conditions in the seepage analysis. Despite having soil layers with relatively low permeability, the results of the water seepage analyses indicated that depth of wetting continued to increase over a period of 40 years.

Rajeev et al. (2012) employed a finite element program, Vadose/W to predict the soil moisture and temperature variation due to real climate conditions. A one-dimensional model with an atmospheric boundary condition at the top and an impermeable boundary condition at the bottom was assumed for the seepage analysis. The required soil properties and initial conditions for the model were determined from samples collected from the field and tested in the laboratory. The soil moisture and temperature computed by the model were compared with the field data to validate the reliability of the model capabilities. Finally, the model was used to predict the long-term soil moisture variation using 20 years of weather data. They found that the soil moisture fluctuation in the layers close to the ground surface was more pronounced by the rainfall pattern compared to the relatively deep layers. However, the increase of moisture changes in the relatively deep layers associated with the fluctuation were

observed in the field measurement after an intensive rainfall preceded by a long period of drying.

Vanapalli et al. (2010) used Vadose/W to model a fully coupled transient seepage analysis of a soil profile that consisted mostly of expansive clay, and the predicted values of soil suction were then compared to published results. They observed that soil suction variations correlated well with environmental conditions on the surface boundary, such that these fluctuations decreased with depth.

Kang et al. (2014) conducted 1-D and 2-D seepage analyses using Vadose/W and compared the obtained results with 3-D seepage output implemented by the MODFLOW-SURFACT program. They conducted several field investigations and laboratory testing to characterize the subsurface soil profile such as determining the plasticity index, water content, percentage passing #200 sieve, the saturated hydraulic conductivity, and the depth of the ground water table. The minimum and maximum temperature, precipitation, maximum relative humidity, and wind speed were collected from weather stations and used as atmospheric boundary parameters. They concluded that the numerical seepage modeling can be conducted in one direction in cases that have minimal water flows from other perpendicular directions.

Gitrana et al. (2006), employed two commercial finite element packages, SVFlux and Vadose/W, to analyze seepage in a soil column due to precipitation, runoff, and evaporation. They described the development of partial differential equation (PDE) solutions in the packages to calculate the runoff and evaporation rate. Analyses

conducted using Vadose/W showed an overestimation and underestimation of runoff and actual evaporation rate, respectively, compared to using SVFlux.

Park and Fleming (2006) conducted a steady-state seepage analysis using SEEP/W to investigate the migration of moisture through an engineered cover system. The loss of suction through the cover soil due to infiltration was more pronounced when materials beneath the cover soil were composed of various barriers with different hydraulic conductivity functions (e.g. geotextile with rock flour).

Vadose/W and UNSAT-H were used by Benson et al. (2005) to predict a water balance for a one-dimensional soil column over three years by solving the modified Richard's equation. As a first note regarding the difference between two codes, they mentioned that Vadose/W uses the finite element method, whereas UNSAT-H utilizes the finite difference method to solve the water balance equation. The precipitation, evaporation, and vegetation parameters were measured at a research site as input parameters. The surface runoff overestimation was observed using the finite difference method, whereas the surface runoff predicted using finite element method was close to reality. The discrepancy between two codes to predict the surface runoff were attributed to the precipitation intensities, which were applied as a sinusoidal pattern and a constant default rate for Vadose/W and UNSAT-H, respectively.

The studies on the unsaturated seepage analysis conducted by the previous researchers showed that the good estimation of soil properties such as the hydraulic

conductivity and the water storage functions and modeling of proper boundary conditions are among the most important considerations for making good predictions.

3. WEATHER DATA COLLECTION IN REGION 6

3.1. Introduction

Historical and future weather data are required to predict soil moisture changes over depth and time. The Oklahoma Mesonet (www.mesonet.org) is a valuable resource for detailed historical weather data. The Oklahoma Mesonet consists of 120 automated stations throughout Oklahoma. There is at least one Mesonet station in each of Oklahoma's 77 counties. At each station weather parameters including: air temperature, relative humidity, total solar radiation, and wind speed are measured by a set of instruments at regular time intervals. The weather data are available from 1994 until now. Among the above-mentioned data from the weather station only precipitation and air temperature on a monthly basis are available from climate projections of future weather. The projected future weather data can be downloaded from the U.S. Geological Survey (USGS) using the National Climate Change Viewer (NCCV).

NCCV is a model visualization web application developed by Alder and Hostetler (2013). It includes the historical and future climate projections from 30 of the downscaled models for two of the Representative Concentration Pathway (RCP) emission scenarios for the years 1950-2099; RCP4.5 (Stabilized Emissions) and RCP8.5 (Unchecked Emissions) scenarios. The former emission scenario was employed in this report. RCP4.5 is one of the possible emissions scenarios in which atmospheric greenhouse gas (GHG) concentrations are stabilized so as not to exceed a radiative equivalent of 4.5 Wm^{-2} after 2100, about 650 ppm CO_2 equivalent. RCP8.5 is the most aggressive emissions scenario in which GHGs continue to rise unchecked through the

end of the century leading to an equivalent radiative forcing of 8.5 Wm^{-2}, about 1370 ppm CO_2 equivalent.

According to Alder and Hostetler (2013), "*worldwide climate modeling centers participating in the 5th Climate Model Intercomparison Program (CMIP5) provide climate information for the ongoing Fifth Assessment Report (AR5) of the Intergovernmental Panel on Climate Change (IPCC). The output from the CMIP5 models is typically provided on grids of ~1 to 3 degrees in latitude and longitude (roughly 80 to 230 km at 45° latitude). To derive higher resolution data for regional climate change assessments, NASA applied a statistical technique to downscale maximum and minimum air temperature and precipitation from 33 of the CMIP5 climate models to produce the NEX-DCP30 dataset on a very fine, 800-m grid over the contiguous United States (CONUS). The full NEX-DCP30 dataset covers the historical period (1950-2005) and 21st century (2006-2099) under four Representative Concentration Pathways (RCP) emission scenarios developed for AR5".*

3.2. Historical Weather Database

The historical weather data from four counties named Comanche, Beaver, Nowata, and McCurtain available in the Mesonet were selected and assumed to represent the variety of weather patterns in Oklahoma. Data from these four counties were utilized to conduct unsaturated seepage analyses representing the variety of weather conditions in Oklahoma. The locations of these counties are shown in Figure 3.1. The weather parameters including precipitation, average air temperature, relative humidity, total solar radiation, and wind speed measured in these four counties are shown in Figures

3.2(a) &(b), 3.3 (c)&(d), and 3.4(e). These figures and the seepage analyses discussed in Chapter 4, show that Beaver and McCurtain counties represent the driest and wettest counties, respectively. In the soil-pile interaction analyses discussed in Chapter 5, it is seen that the differences in pore water pressure distribution resulting from these differences in wetting play a key role in determination of soil stiffness and pile response.

The historical weather data was used to calibrate models for predicting future seepage based on future temperature and rainfall data. These calibrations, discussed in Chapter 4, developed for Oklahoma counties were applied to selected counties in neighboring Region 6 states based on similarities between projected future weather discussed in the next section.

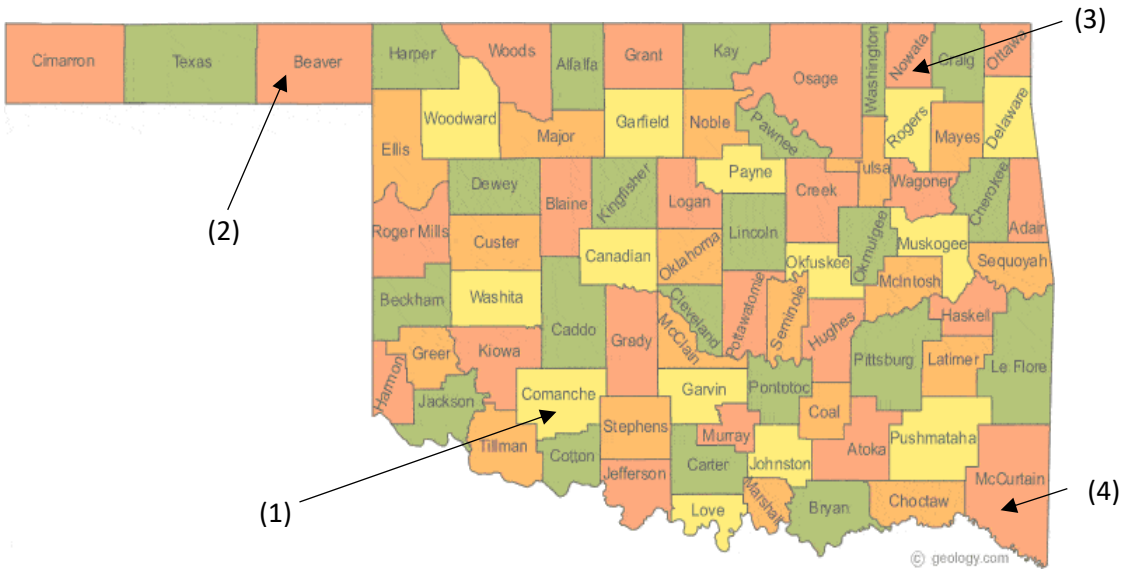

Figure 3.1. Oklahoma counties selected for seepage analysis (http://geology.com/state-map/oklahoma.shtml)

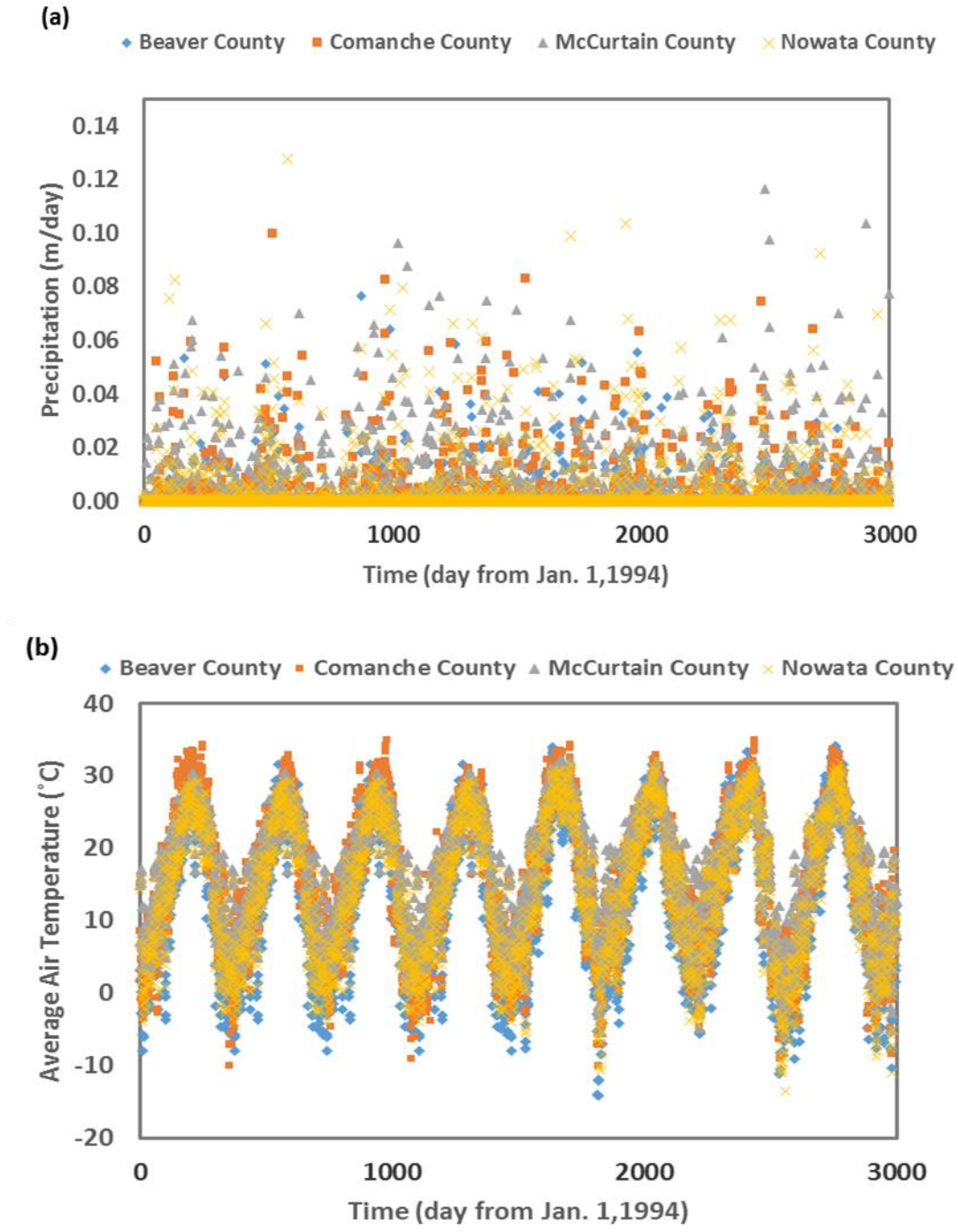

Figure 3.2. Weather data from Jan.1, 1994 to Jan.1, 2001. (a) Rainfall rate, (b) Average Air Temperature

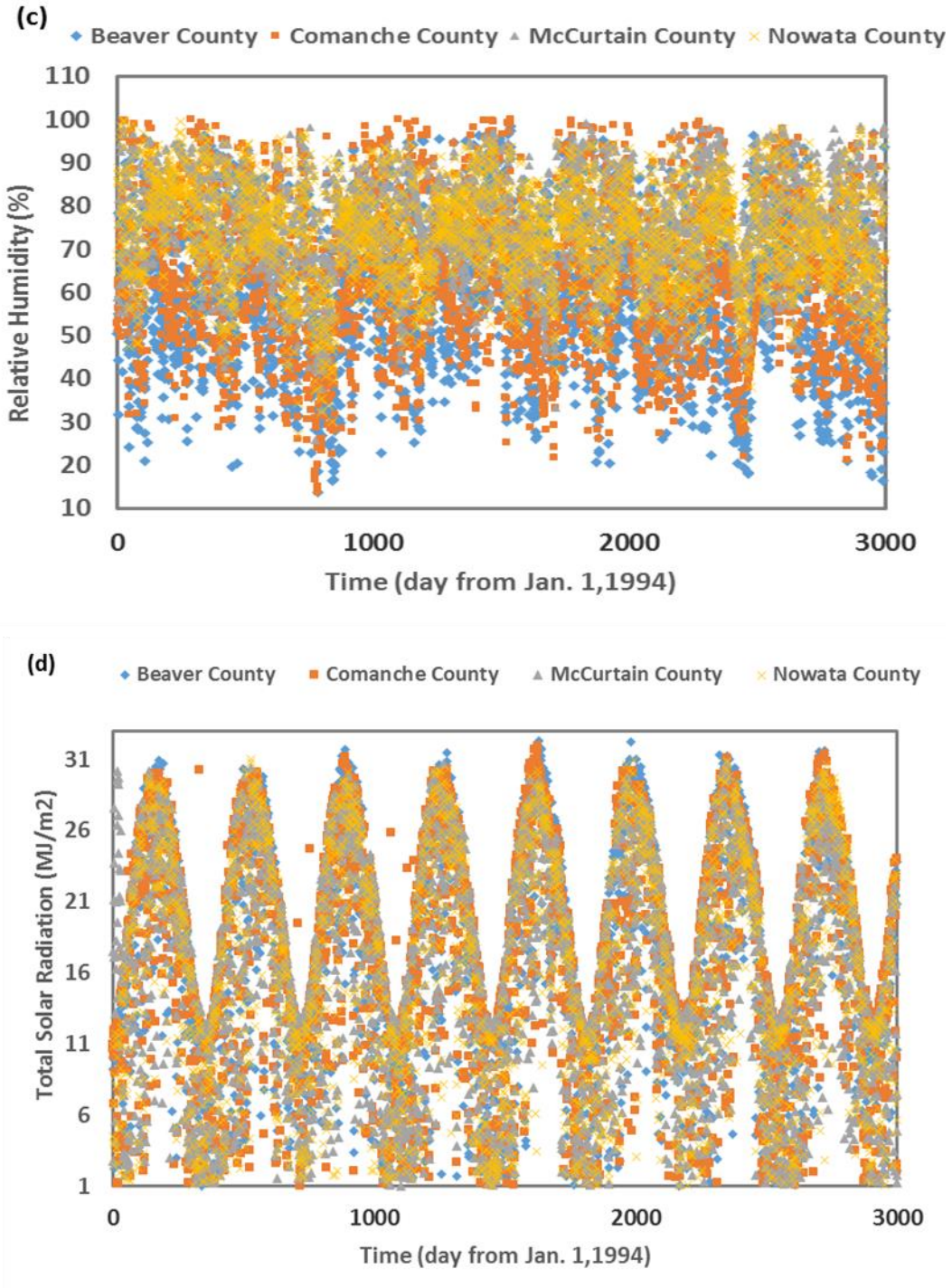

Figure 3.3. Weather data from Jan.1, 1994 to Jan.1, 2001. (c) Relative Humidity, (d) Total Solar Radiation

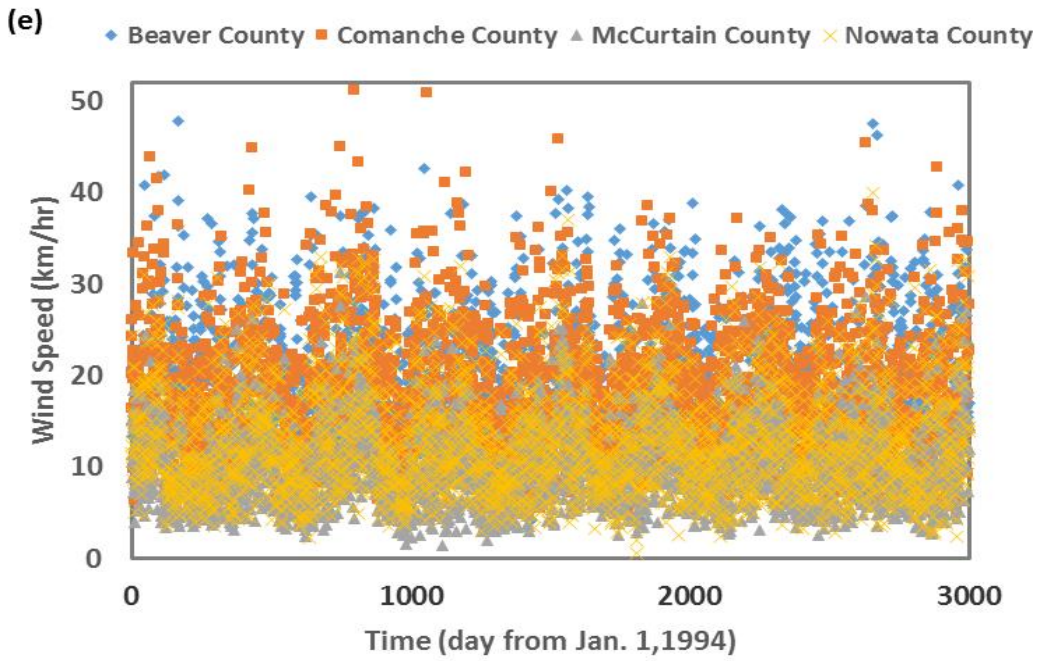

Figure 3.4. Weather data from Jan.1, 1994 to Jan.1, 2001. (e) Wind Speed

3.3. Future Weather Database

As mentioned, the future weather data available from the USGS NCCV was limited to air temperature and precipitation. Several counties in Region 6 states neighboring Oklahoma, as shown in Figure 3.5, were selected to represent the broad range of weather patterns across Region 6. Selected counties in other states in Region 6 were compared to weather patterns in the selected counties in Oklahoma to see if there were similarities that could be exploited in the seepage analysis. Because of the significant computing time involved with unsaturated seepage analysis, it was not practical to run

the seepage analyses for all of the Region 6 counties highlighted in Figure 3.5. Thus, to cut down the number of analyses, if weather patterns in selected counties in states neighboring Oklahoma were reasonably similar in terms of precipitation and average air temperature to one of the weather patterns in Oklahoma, then the same Oklahoma weather pattern was assumed for both. Given the large uncertainty in the projected future weather, this approach is practically warranted.

The selected counties for Arkansas and Louisiana showed a reasonably similar weather pattern compared to McCurtain County from Oklahoma as shown in Figures 3.6 through 3.9 and Figures A.1 through A.3 in Appendix A. All selected counties in New Mexico except one county (San Juan) showed similar weather to Beaver County, Oklahoma as shown in Figures 3.10 to 3.14. Two counties picked as representatives of the state of Texas were similar to McCurtain and Beaver counties from the State of Oklahoma as shown in Figures A.4 and A.5 in Appendix A.

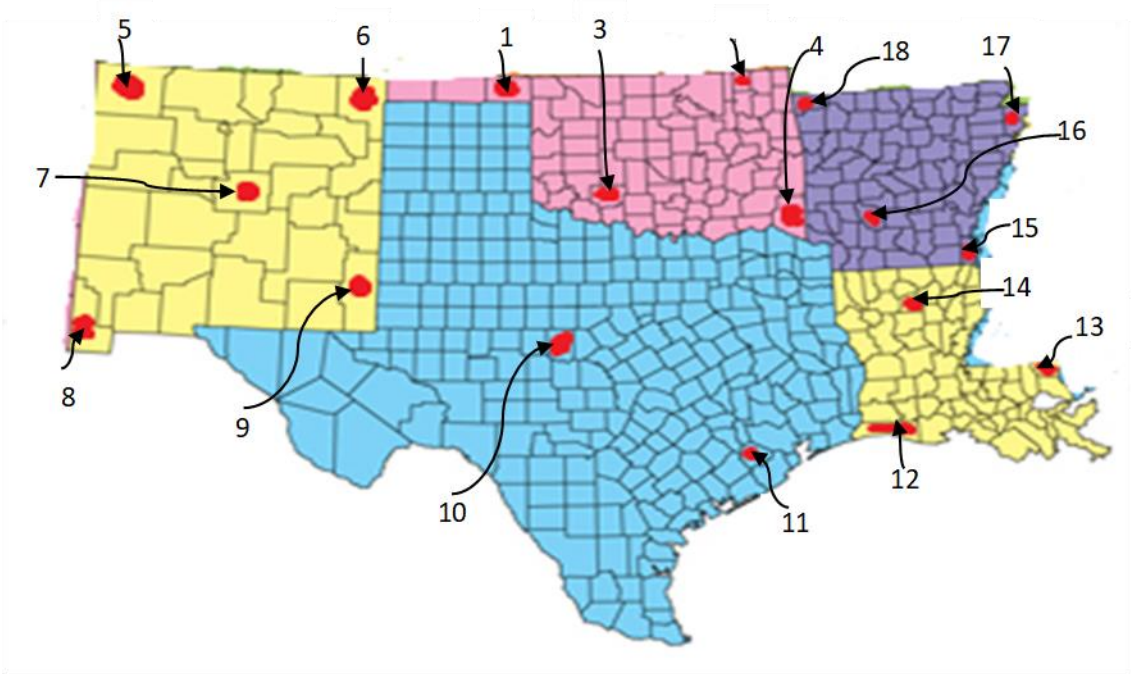

Oklahoma	New Mexico	Texas	Louisiana	Arkansas
1-Beaver	5-San Juan	10-Coleman	12-Cameron	15-Chicot
2-Nowata	6-Union	11-Fort Bend	13-Washington	16-Clark
3-Comanche	7-Torrance		14-Jackson	17-Mississippi
4-McCurtain	8-Hidalgo			18-Benton
	9-Lea			

Figure 3.5. Region 6 counties selected for climate comparison (http://ichizoku.us/county-map-of-us.html)

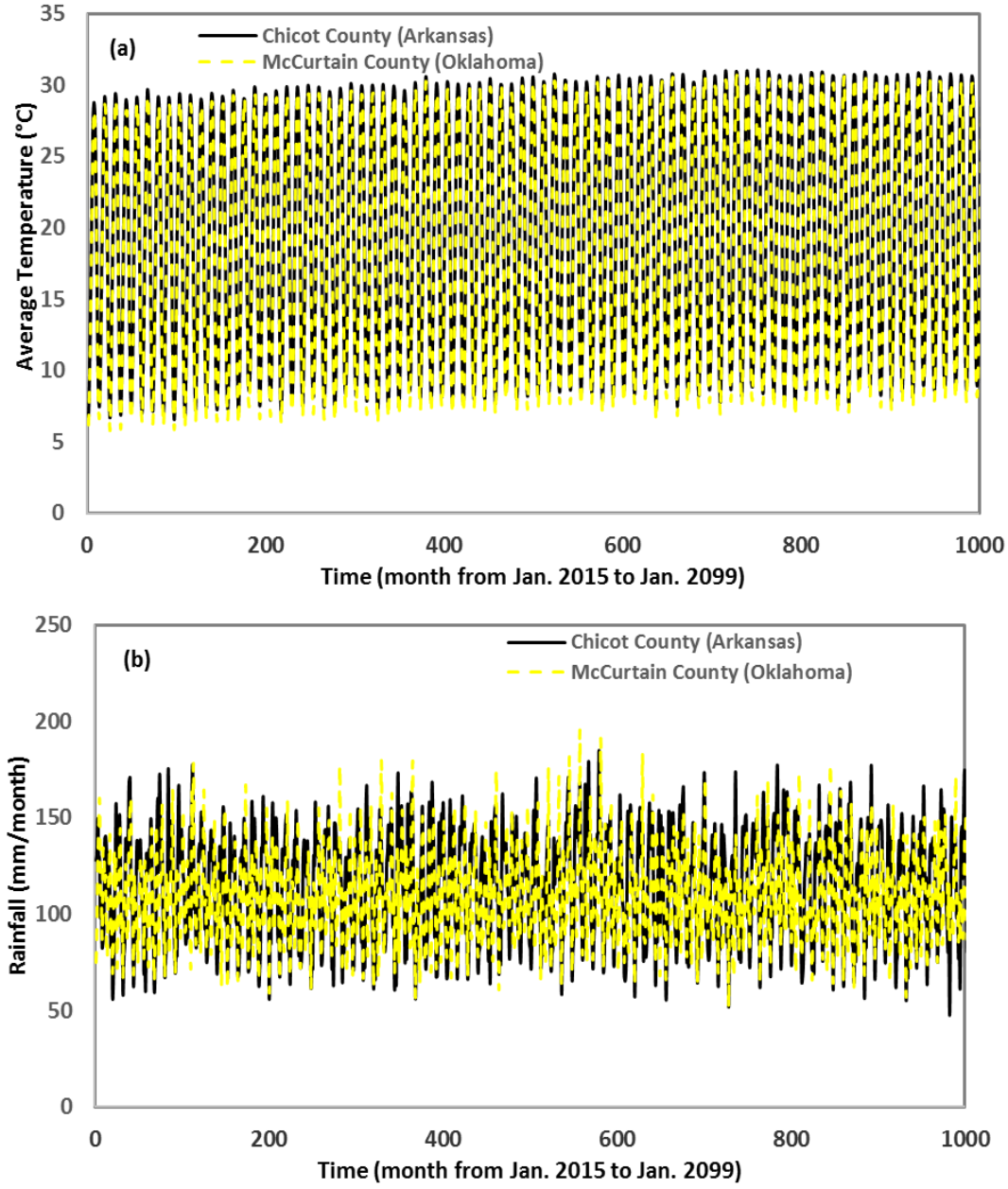

Figure 3.6. Average air temperature (a) and precipitation (b) comparison between Arkansas and Oklahoma (Chicot and McCurtain counties)

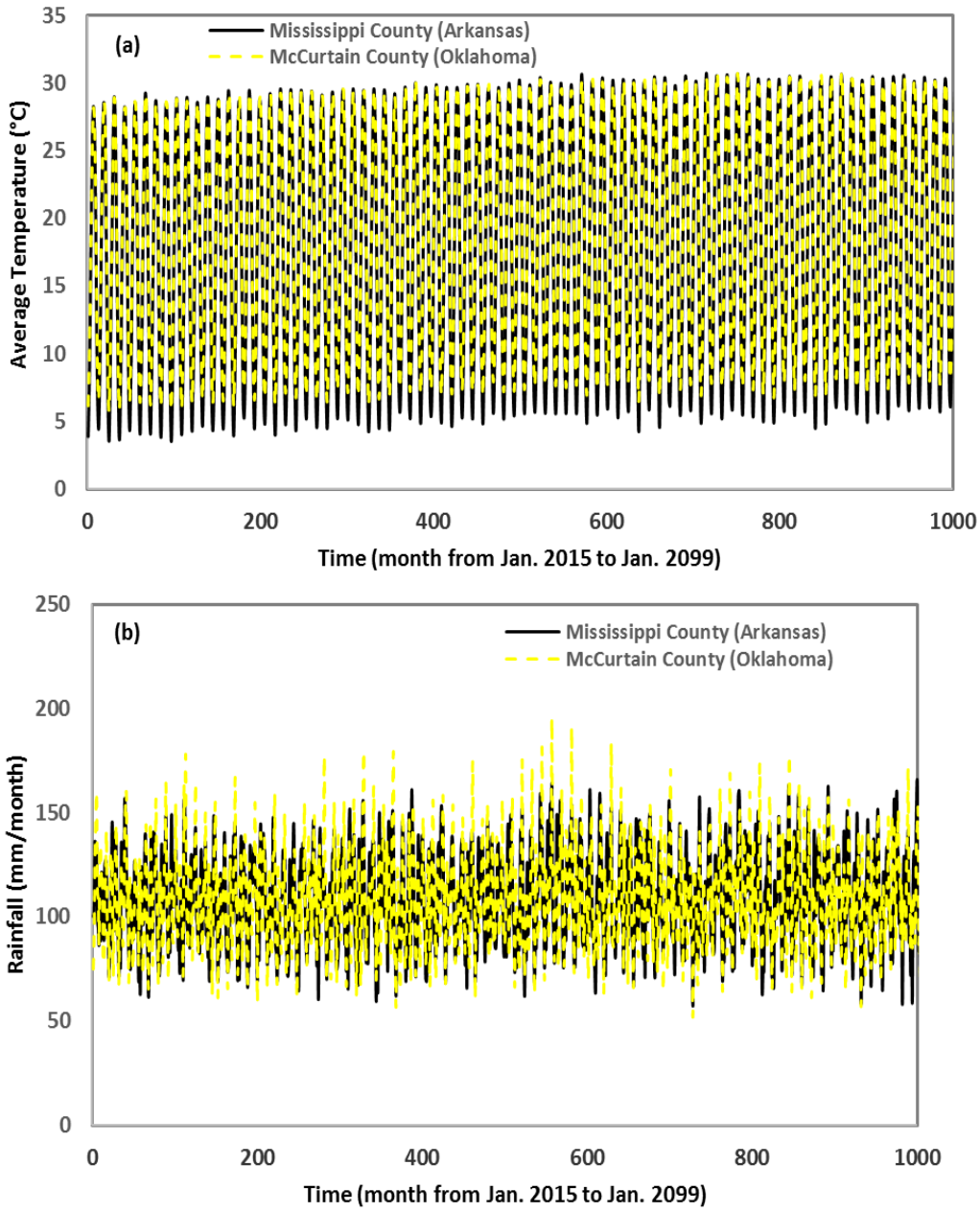

Figure 3.7. Average air temperature (a) and precipitation (b) comparison between Arkansas and Oklahoma (Mississippi and McCurtain counties)

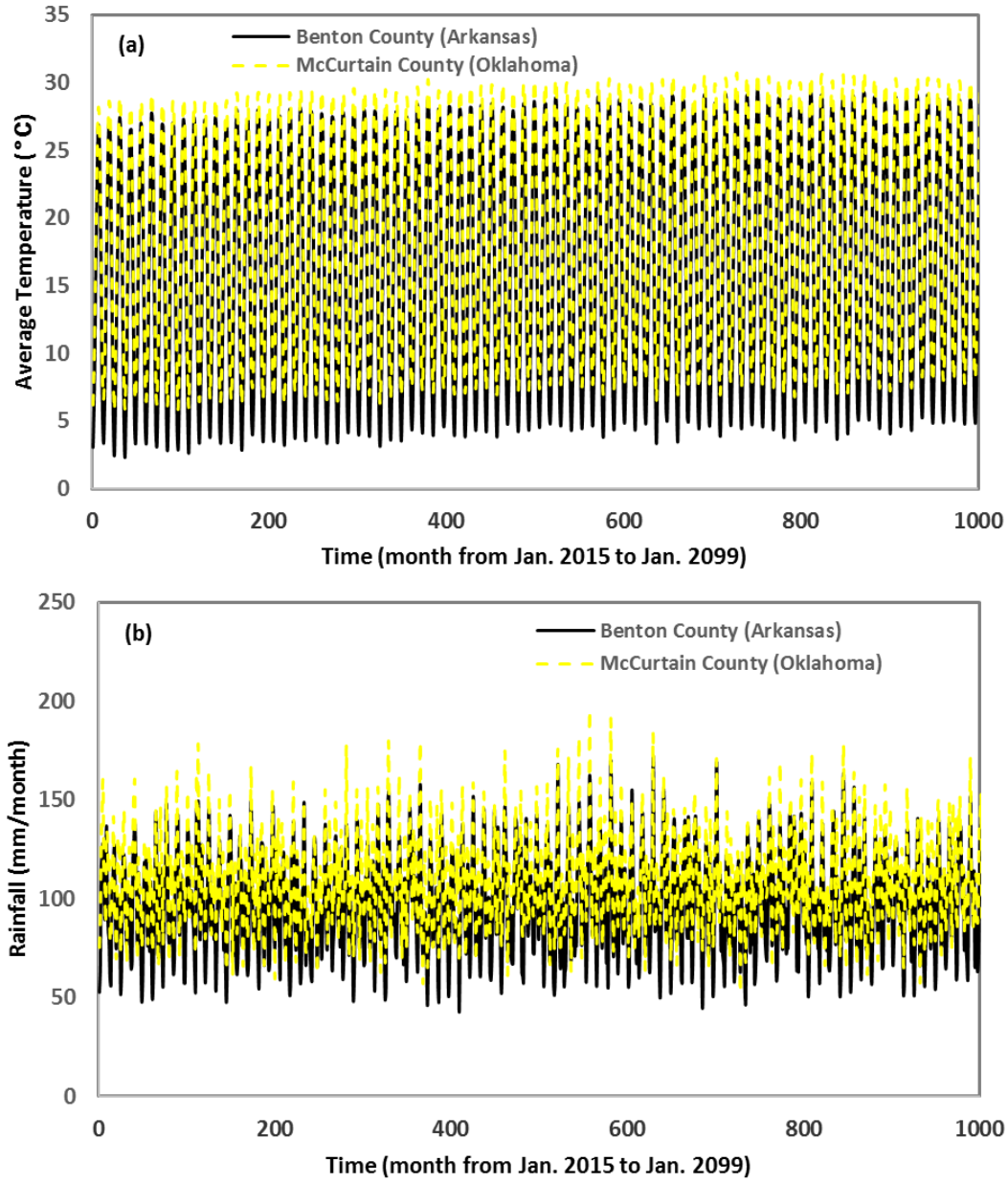

Figure 3.8. Average air temperature (a) and precipitation (b) comparison between Arkansas and Oklahoma (Benton and McCurtain counties)

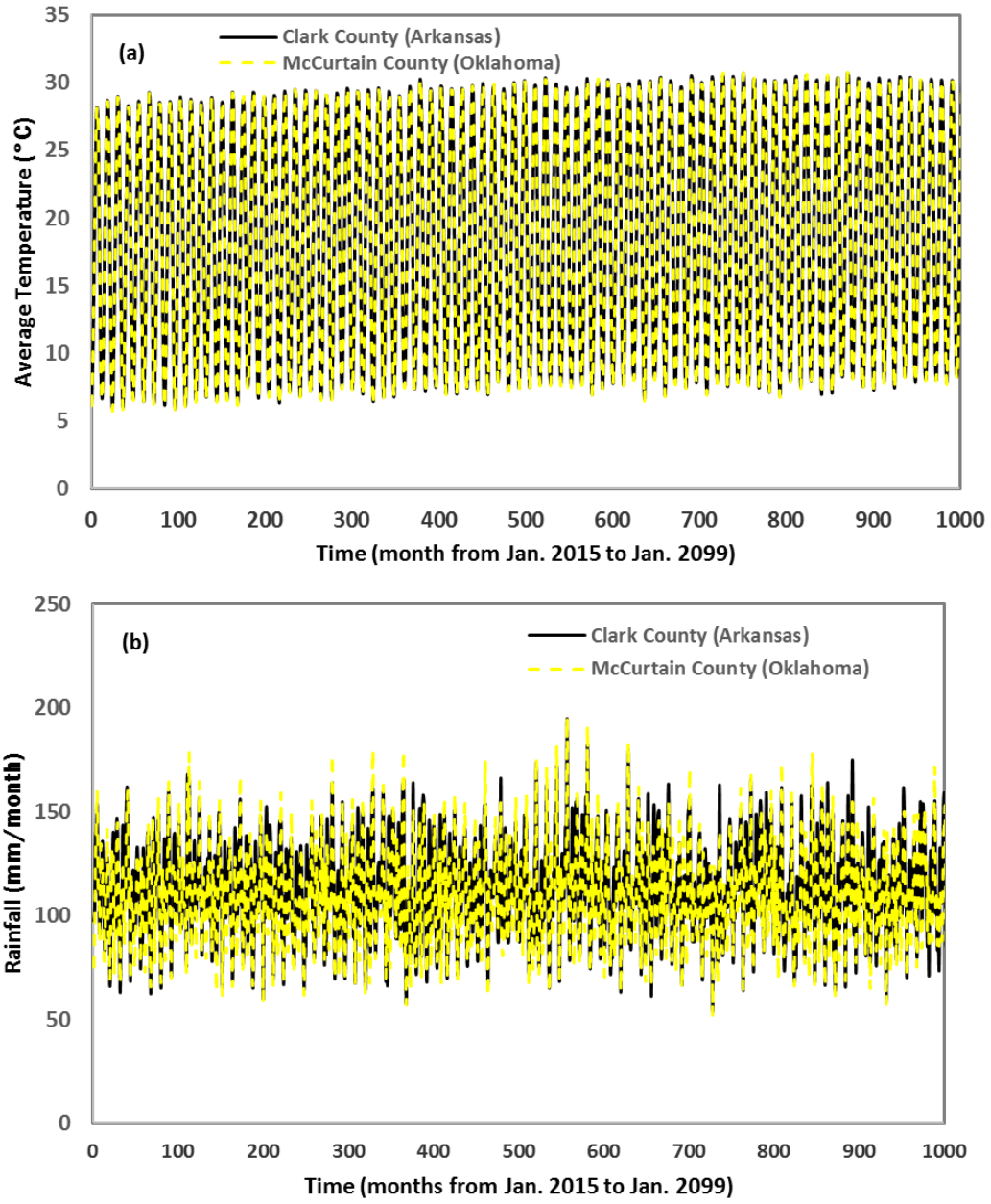

Figure 3.9. Average air temperature (a) and precipitation (b) comparison between Arkansas and Oklahoma (Clark and McCurtain counties)

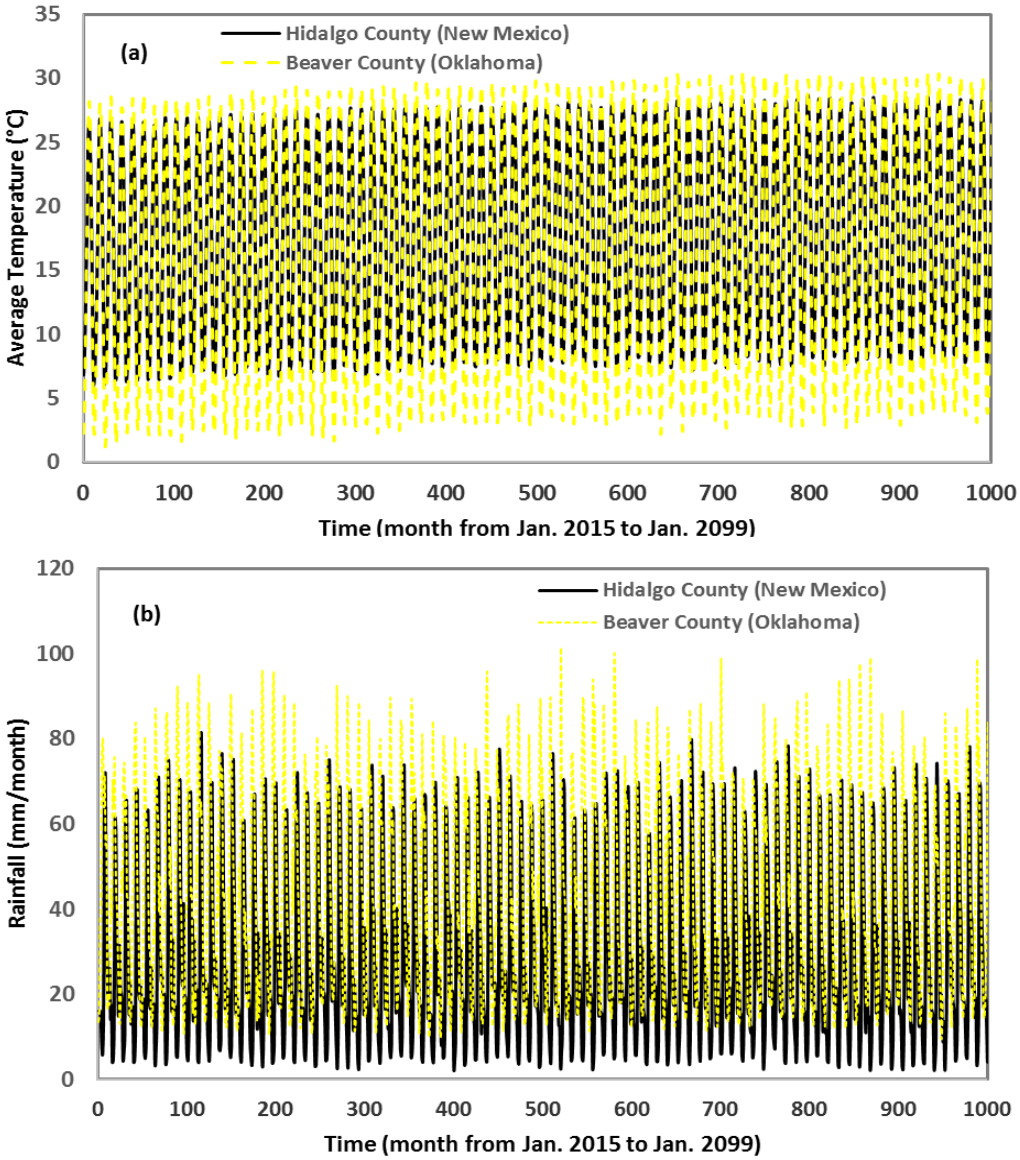

Figure 3.10. Average air temperature (a) and precipitation (b) comparison between New Mexico and Oklahoma (Hidalgo and Beaver counties)

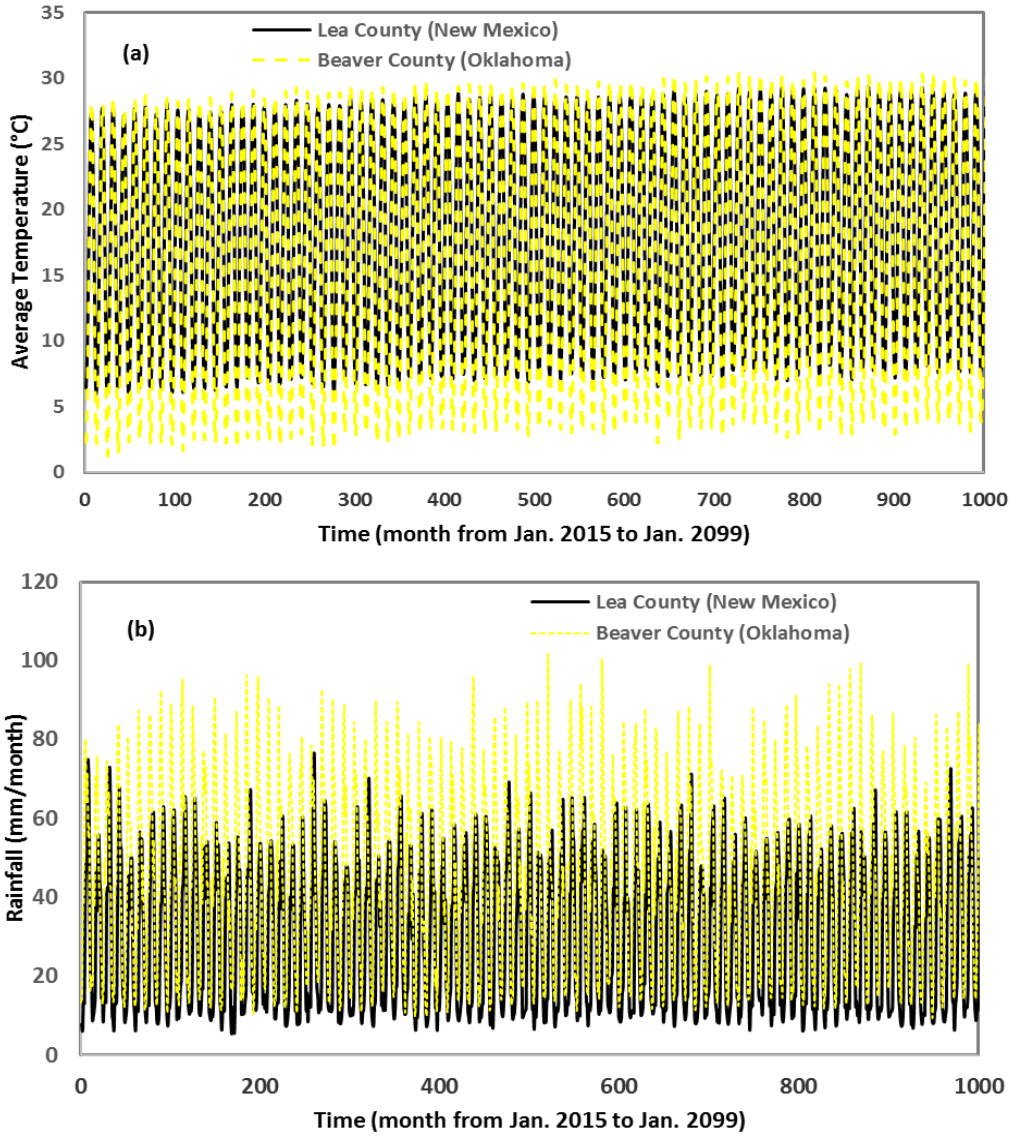

Figure 3.11. Average air temperature (a) and precipitation (b) comparison between New Mexico and Oklahoma (Lea and Beaver counties)

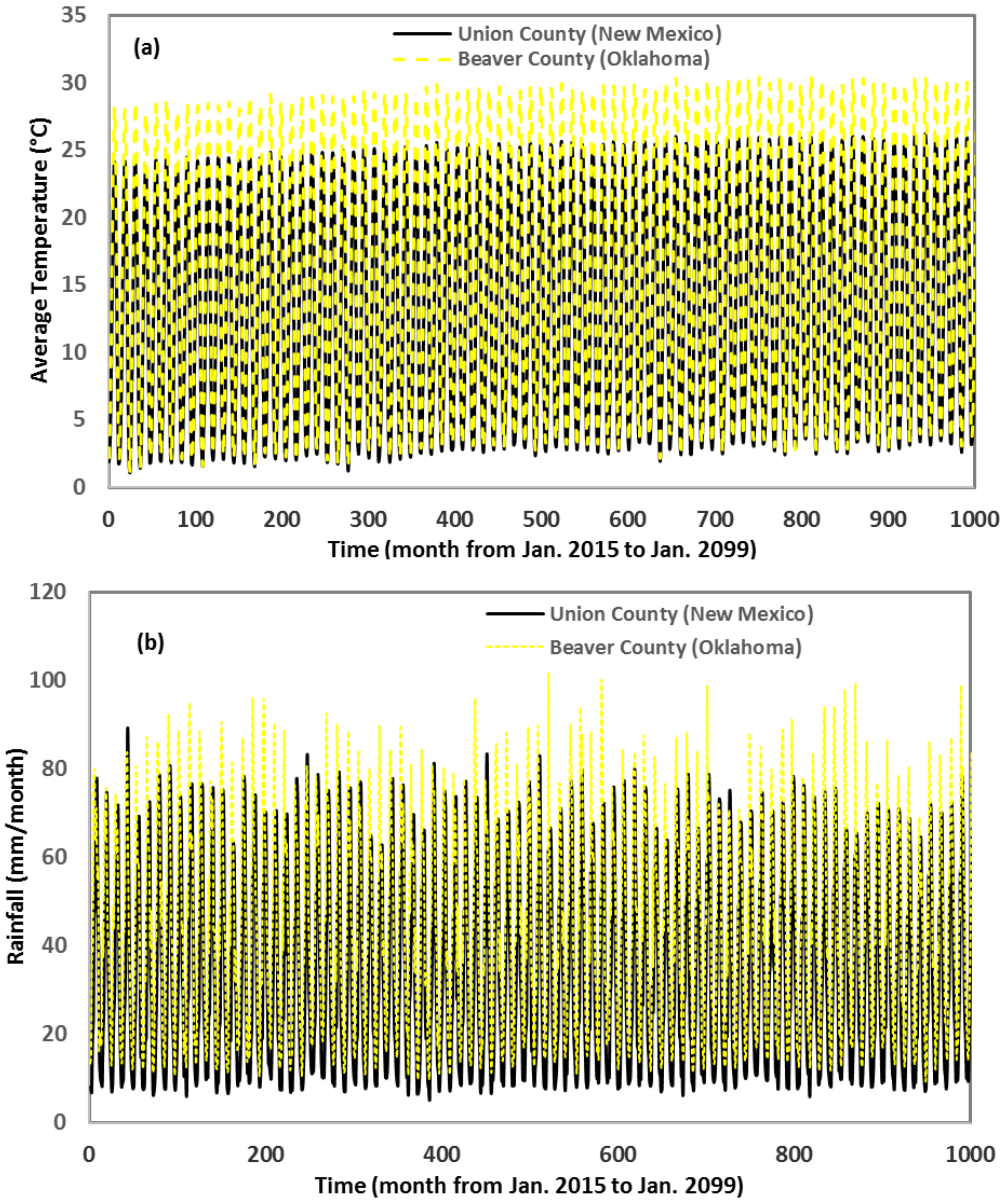

Figure 3.12. Average air temperature (a) and precipitation (b) comparison between New Mexico and Oklahoma (Union and Beaver counties)

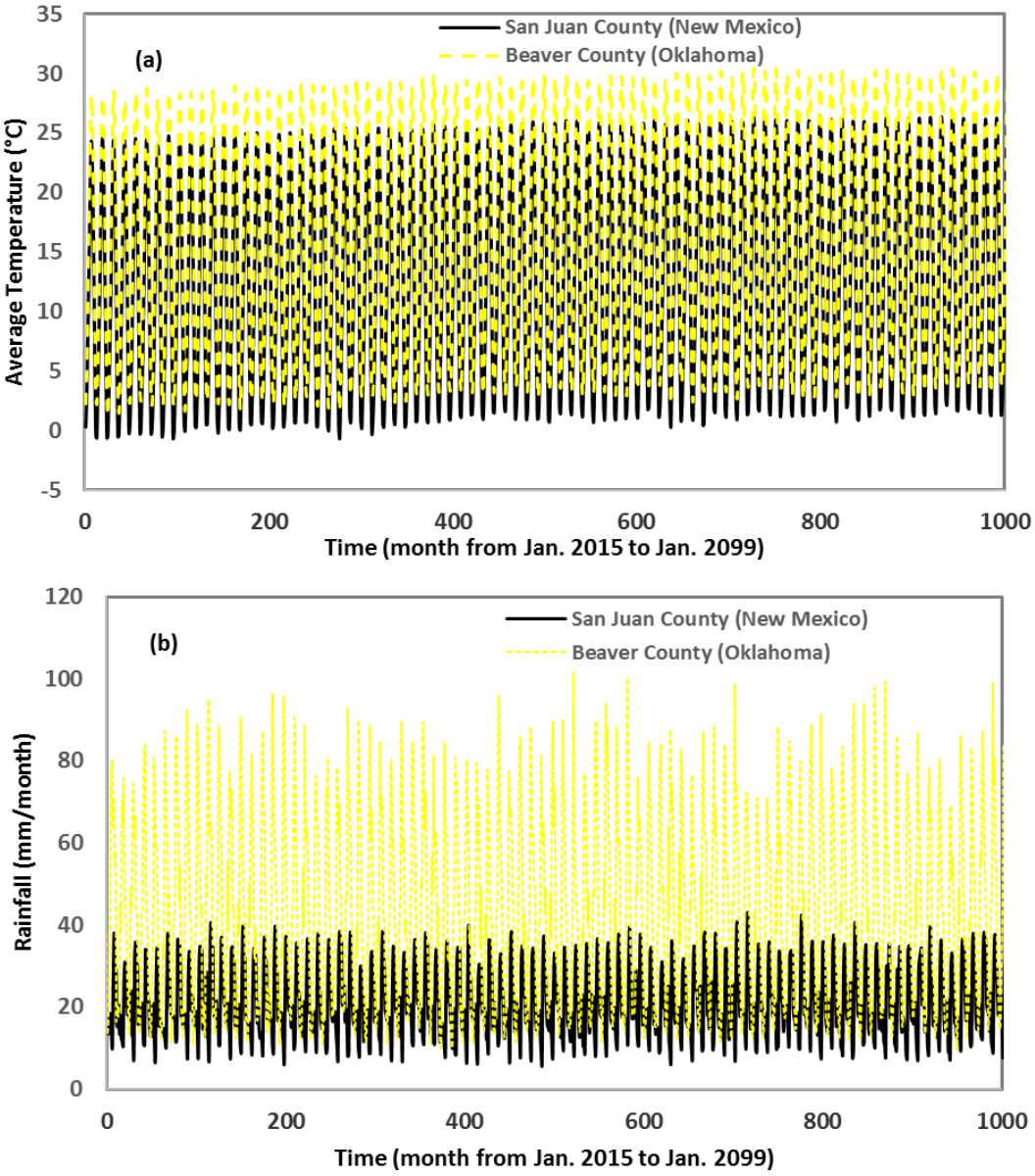

Figure 3.13. Average air temperature (a) and precipitation (b) comparison between New Mexico and Oklahoma (San Juan and Beaver counties)

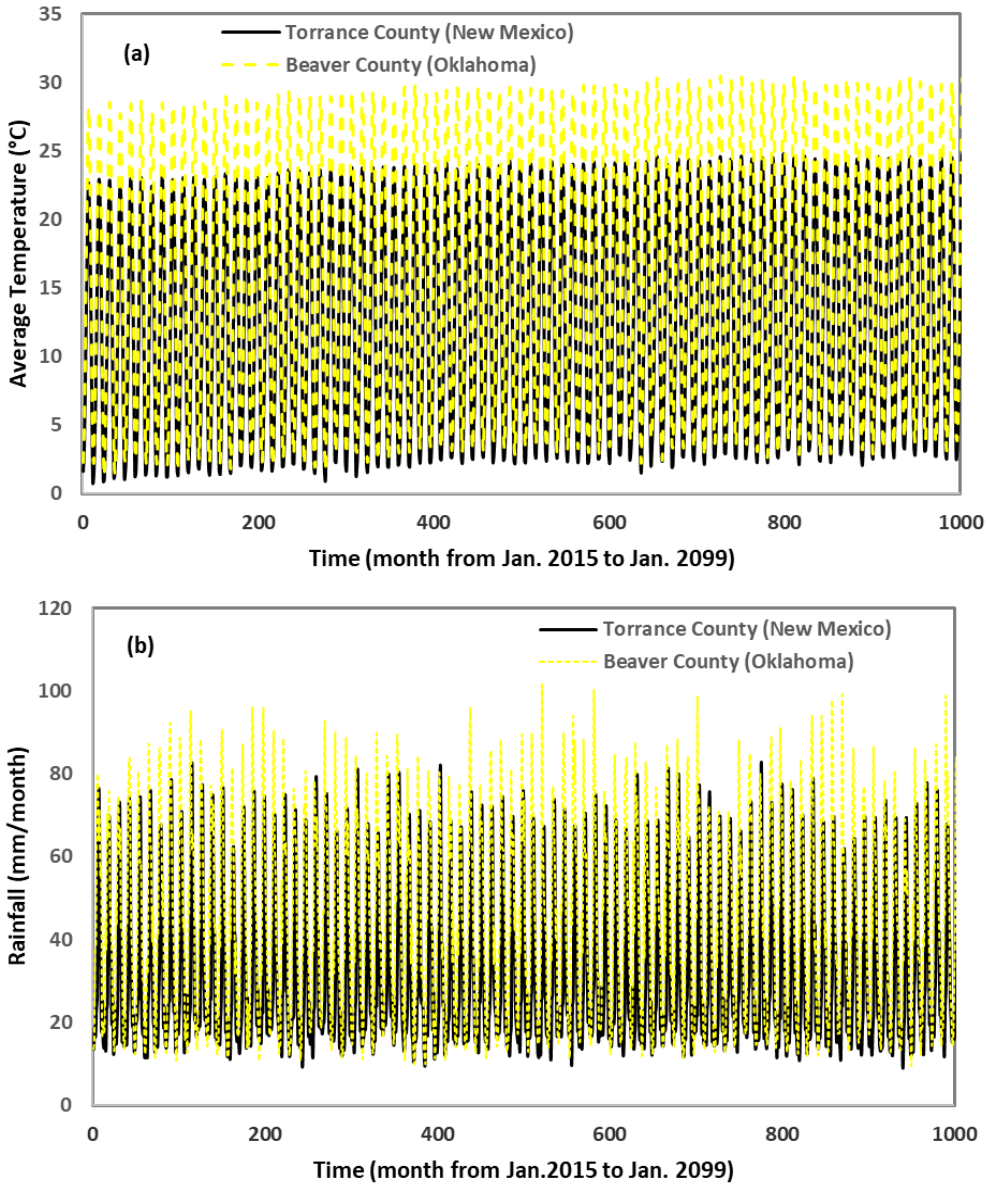

Figure 3.14. Average air temperature (a) and precipitation (b) comparison between New Mexico and Oklahoma (Torrance and Beaver counties)

4. SEEPAGE ANALYSIS FOR SOIL MOISTURE PREDICTION IN REGION 6

4.1. Soil Moisture Prediction around a Typical Pile

Seepage involving two-phase flow in unsaturated soil is characterized by non-linear partial differential equations. Among the soil properties required for unsaturated seepage analysis are the water coefficient of permeability and the water storage functions, which are highly non-linear. Both soil properties can be represented as a function of negative pore water pressure or suction. The water coefficient of permeability is a measure of ability of soils to conduct water. This coefficient is a function of the volumetric of water content, which is, in turn, a function of soil suction. The water storage is an index of amount of water absorbed or released by the change of pore water pressure in the soil and it is measured by the slope of soil water characteristic curve.

SVFlux, developed by SoilVision Systems Ltd. (2012), is a finite element program used to model transient flow of water, heat, and vapor in unsaturated soil. The program has been built around fundamental equations governing the exchange of water between the soil and atmosphere at the ground surface (e.g. Penman 1948, Wilson et al. 1994) and it can account for variations in the soil state (dry, frozen, saturated, unsaturated), soil type, soil temperature, extent, and type of vegetative cover among other things.

Basically, the user is required to input a number of different parameters that govern the movement and storage of water (in liquid and vapor forms) within a soil profile as well as information about the type and temporal variation of vegetative cover

at the site. In addition, the initial soil moisture conditions in the profile are required. The output generated from the program provides predicted moisture (and suction) profiles as a function of time.

The input parameters required for the analysis using the program are divided into four categories: precipitation data, evaporation data, vegetation data, and soil data. As for the output, the program is used to provide variations in volumetric water content over time at specific depths in the soil profiles. A geometry similar to the southern embankment for the I-44 Bridge in Oklahoma, including the soil foundation and backfill, adopted for the purpose of seepage modeling is shown in Figure 4.1. While this 2-D representation of the embankment and abutment does not capture the three-dimensional features of the pavement and sloped vegetated embankment surfaces next to the pavement, it provides a starting point for examining unsaturated seepage in the embankment and backfill behind the abutment. In the model, the ground surface behind the abutment to the left side of pile axis in Figure 4.1 was treated as the flux boundary that was subjected to atmospheric conditions based on real local weather data.

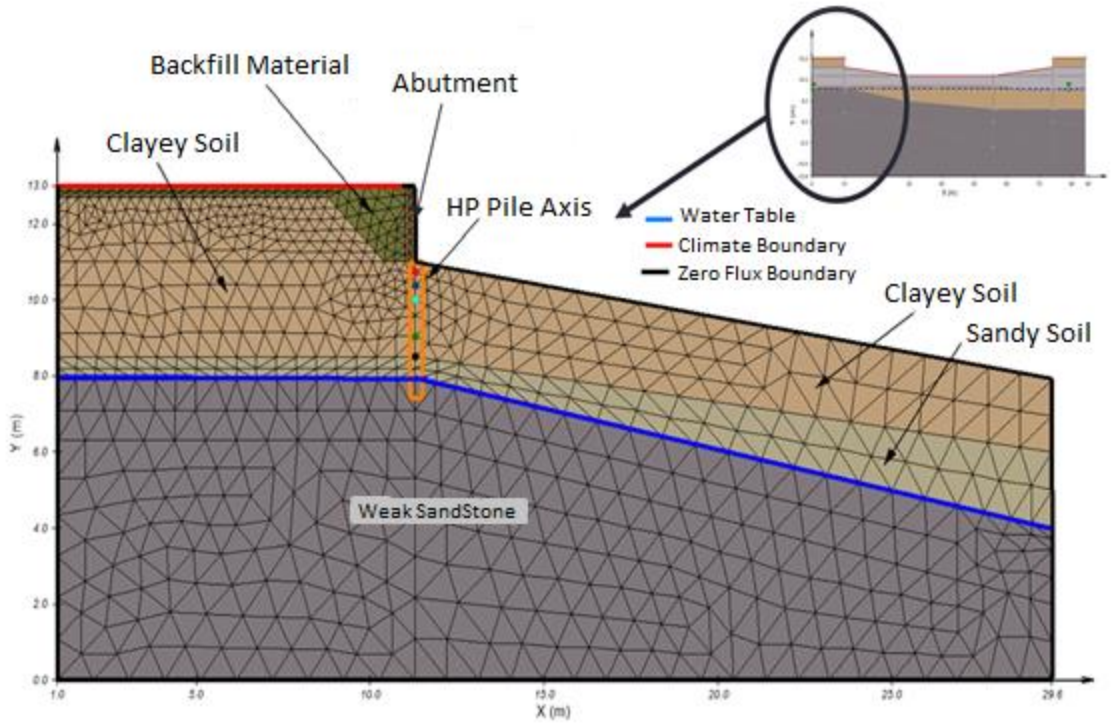

Figure 4.1. Finite element mesh and boundary conditions for the south abutment of I-44 Bridge in Oklahoma

Historical weather data available from the Mesonet for 1994 to 2001 (7 years) at Comanche County, Medicine Park, OK, which is close to the I-44 bridge, was downloaded to use as the atmospheric loading on the ground surface. As a starting point, the boundary condition on the sloped ground surface located to the right side of pile axis, under the bridge, was assumed to be impermeable. However, as this surface was under shaded conditions due to the bridge deck location a modified atmospheric loading can be defined in the parametric study. The soil water characteristic curve (SWCC) was assumed using Zapata's model (1999), which was based on the grain size

distribution (percent passing #200) and plasticity index (PI) as shown in Figure 4.2 for clayey layer.

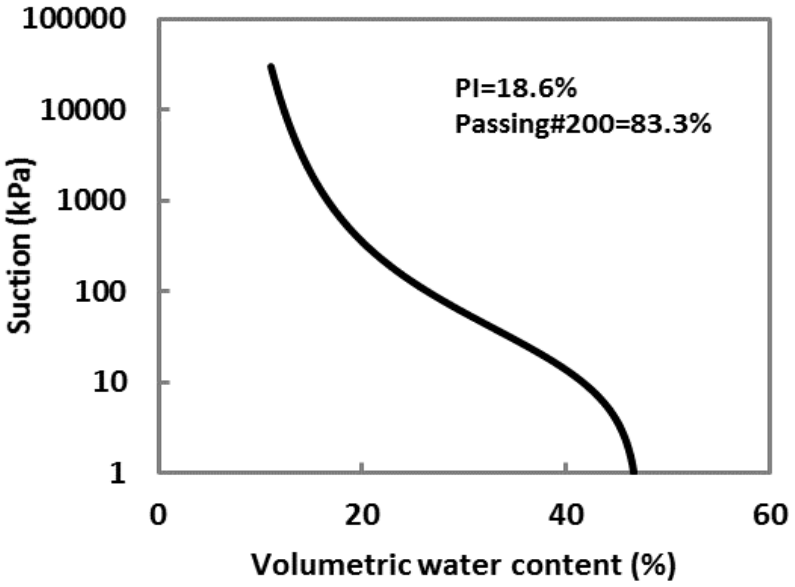

Figure 4.2. Soil Water Characteristic curve (SWCC) for clayey soil

The saturated permeability of backfill, sandy, and clayey layers were assumed to be $1x10^{-6}$, $1x10^{-7}$, and $1x10^{-8}$ m/s, respectively. These assumptions were made based on the classification of soils as moderate to very low degrees of permeability (Terzaghi and Peck 1967). The infiltration and evaporation components from the local weather station are shown in Figures 4.3 and 4.4. The estimated and computed transpiration components associated with vegetation are shown in Figure 4.5.

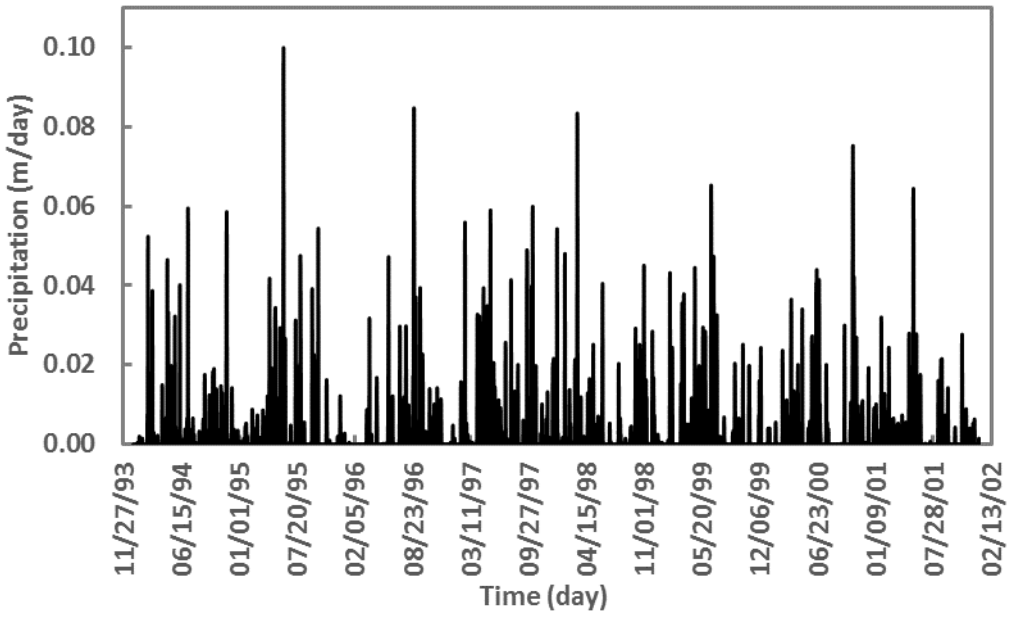

Figure 4.3. Daily Precipitation data from 1994 to 2001 (from Oklahoma Mesonet Station Medicine Park)

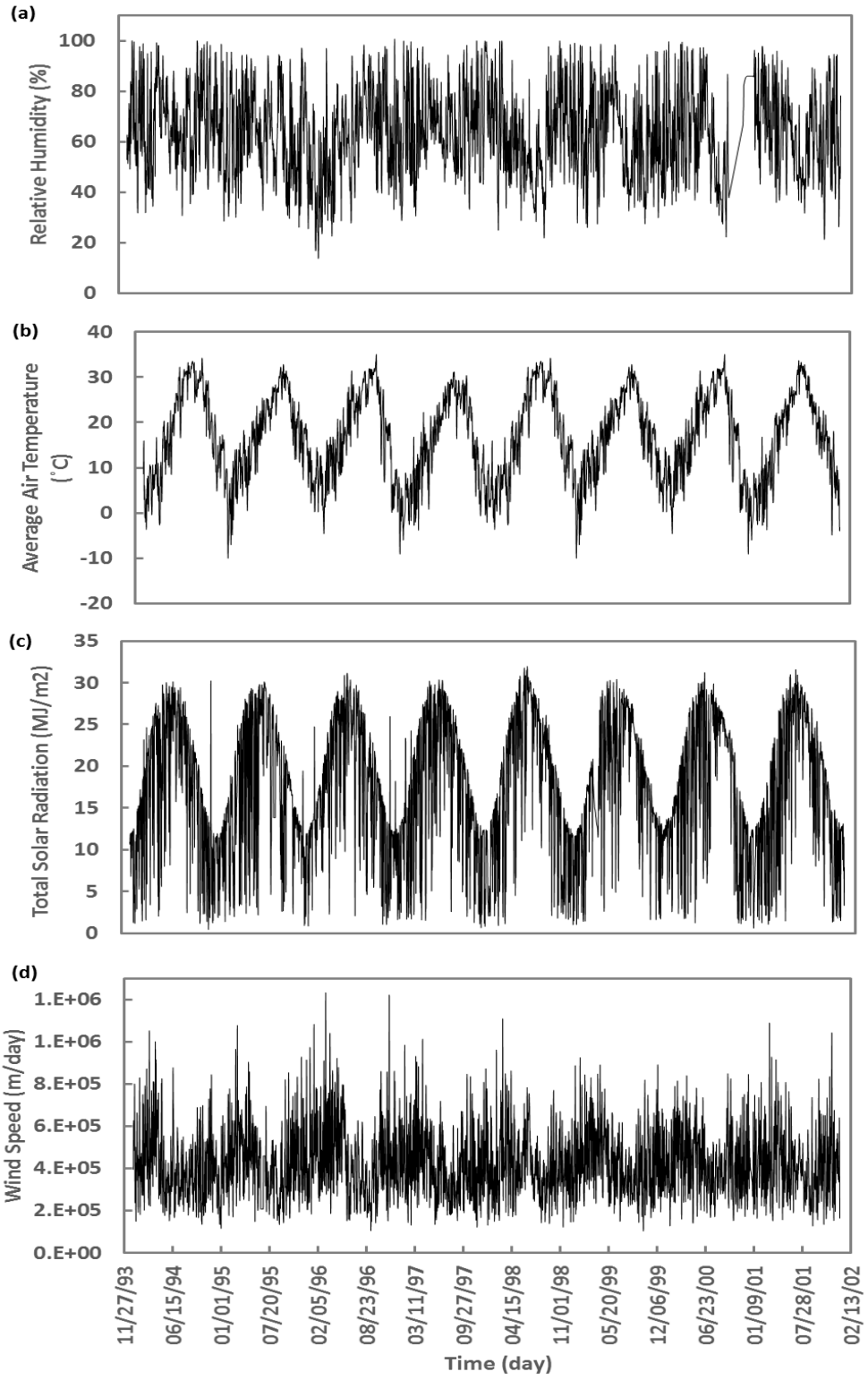

Figure 4.4. Daily Evaporation related data from 1994 to 2001: (a) relative humidity (b) average air temperature (c) total solar radiation (d) wind speed (from Oklahoma Mesonet Station Medicine Park)

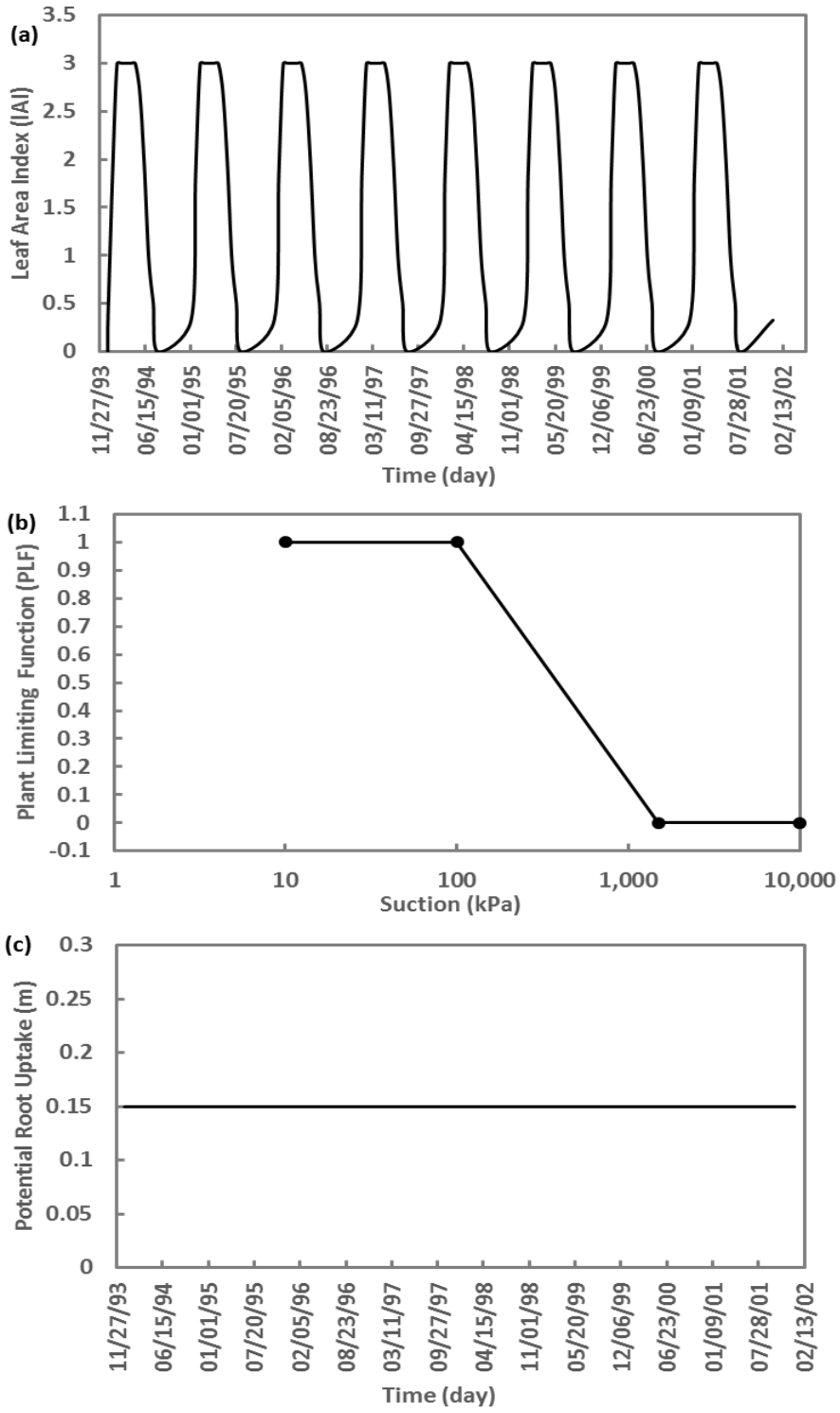

Figure 4.5. Daily transpiration related data from 1994 to 2001: (a) leaf area index (b) plant limiting function (c) potential root uptake

While it is possible to utilize the Penman Method to predict evaporative flux at the ground surface using historical climate data obtained from weather stations, the projected future climate data is limited to temperature and rainfall and does not include relative humidity, solar radiation, and wind speed. Thus, only the Thornthwaite Method can be applied for future years. The differences between these two methods are discussed in detail in Section 4.2. To overcome this limitation, finding logical ways to use historical data sets to develop a calibration procedure between the Penman and Thornthwaite methods was a primary purpose of this research. The calibration method developed is discussed in Section 4.3.

4.2. Atmospheric Boundary Condition

In addition to precipitation data, the potential evaporation and transpiration are required to predict the moisture variations in foundation soil and abutment backfill material in a typical IAB. The potential evaporation can be determined in different ways including use of measured data, or by calculation using available methods including: Penman's Equation (1948), or Thornthwaite's Equation (1948), or Priestley-Taylor's Equation (1972).

Among the above-mentioned equations, Thornthwaite's Equation (1948) is the only one that functions on a single parameter, the monthly air temperature and some empirical parameters as shown in Equation 4.1. Since available data for the future are limited to monthly maximum and minimum air temperature, Thornthwaite's equation (1948) was selected as the method to predict the moisture changes for the current research. The equation is,

$$\text{PET}=1.6\, L_d \left(\frac{10T}{I}\right)^a \qquad \textbf{(4.1)}$$

where: PET is the monthly potential evapotranspiration (cm), L_d is the daytime length or time from sunrise to sunset in multiples of 12 hours, T is the monthly mean air temperature(°C),

$$a = 6.75 \times 10^{-7}\, I^3 - 7.71 \times 10^{-5}\, I^2 + 0.01791 I^1 + 0.49239,$$

and *I* is the annual heat index, which is computed from the monthly heat indices.

$$I = \sum_{j=1}^{12} i_j, \quad i_j = \left(\frac{T_j}{5}\right)^{1.514} \qquad \textbf{(4.2)}$$

Tj is the mean air temperature in °C for month j for j = 1 to 12.

To compare and partially validate the results obtained using Thornthwaite's Method (1948), Penman's Method (1948) having more variables, such as relative humidity, solar radiation, and wind speed as well as air temperature was used to calculate the potential evaporation using historical data and compared to Thornthwaite based predictions. The Penman Model predicts potential evaporation as shown in the following equation,

$$\text{PE}= \frac{\Gamma Q_n + \eta E_a}{\Gamma + \eta} \qquad \textbf{(4.3)}$$

where: PE is potential evaporation in m/day, E_a is flux, which is calculated in m/day using Equation 4-4, Q_n is net radiation at the water surface in m/day, Γ is slope of saturation vapor pressure vs. temperature curve in kPa/°C, η is the psychrometric constant equal to 0.06733 kPa/°C.

$$E_a = 0.35(1+0.146\ W_w)\ C_f u_{v0}(1-h_r) \qquad \textbf{(4.4)}$$

where: W_w is wind speed in km/hr, C_f= conversion factor, u_{v0} is saturated vapor pressure in the mean air temperature with the units of kPa, and h_r is relative humidity in the air above the ground.

Evaporation associated with transpiration, which is a process of water migration through a plant results in evapotranspiration. The amount of water flux is controlled by transpiration through parameters such as bare soil potential evaporation, leaf-area index (LAI), plant limiting function (PLF), which is related to soil suction, and the root zone profile. Since these parameters were not routinely available for the sites considered, some assumptions were used to incorporate them in the numerical modeling.

There is an atmospheric moisture flux balance that must be satisfied at the ground surface when calculating actual evaporation. The water on the ground surface either infiltrates the soil (or runs off) or rises to the sky through the process called actual evaporation. Actual evaporation used in an atmospheric moisture flux balance for the

Thornthwaite (1948) Method was assumed to be equal to potential evaporation, which is a maximum amount of evaporation. In contrast, a modified Wilson-Penman's Method (1994) was used for calculation of actual evaporation in Penman's method (1948).

4.3. Calibration of soil moisture prediction models

The potential evapotranspiration obtained from Thornthwaite Equation is calibrated against results derived from the Penman Equation. To calibrate the equations, the slope of the regression between potential evapotranspiration derived from two methods was forced to pass through the origin for each month for the calibration period. This calibration procedure was discussed by Moeletsi et al. (2013). The calibration coefficient was then obtained by calculating the product of the slope of the regression lines (forced to pass at 0, 0) and the original coefficient.

$$C_T = Slope \times 1.6 \qquad \textbf{(4.5)}$$

where, C_T is a new constant for the Thornthwaite Equation, which is substituted for the constant number or 1.6 used in Equation 4.1. A monthly potential evapotranspiration estimated from two methods before calibration is shown in Figure 4.6 using the historical dataset from 1994 to 2001.

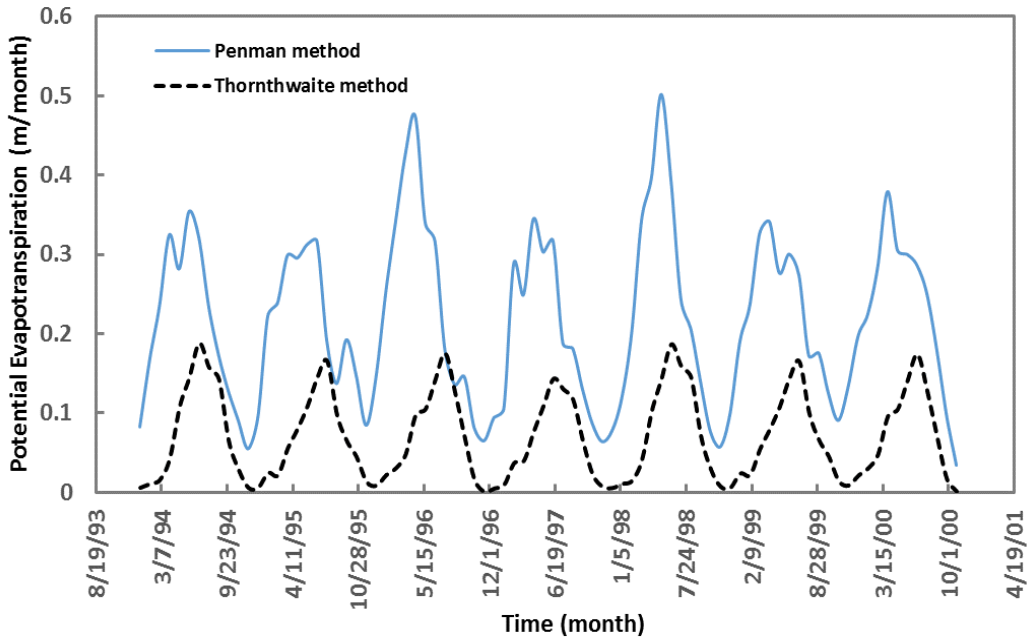

Figure 4.6. Thornthwaite potential evapotranspiration and Penman potential evapotranspiration from 1994-2001

The Thornthwaite potential evapotranspiration (TPET) calibrated with the slopes calculated from each month as shown in Figures 4.7 and 4.8 is in good agreement with Penman potential evapotranspiration (PPET) as shown in Figure 4.9. The actual evapotranspiration, which is a modified potential evapotranspiration, is required to contribute to the net infiltration as a soil-atmosphere boundary condition. Wilson-penman (1994) Equation was used for modifying Penman potential evapotranspiration. A method using transpiration (vegetation) parameters was proposed by the author of this research to calibrate the Thornthwaite actual evapotranspiration (TAET) with the Penman actual evapotranspiration (PAET). Three different Leaf Area Index (LAI) curves were designated as variables to obtain the actual evapotranspiration from the Thornthwaite potential evapotranspiration as shown in Figure 4.10. Three calibrated

curves of the TAET resulted from three different LAI alternatives; these are shown in Figure 4.11 and compared with the PAET. In Figure 4.12, results of unsaturated seepage modeling for the I-44 Bridge are presented based on the Penman and calibrated Thornthwaite actual evaporation.

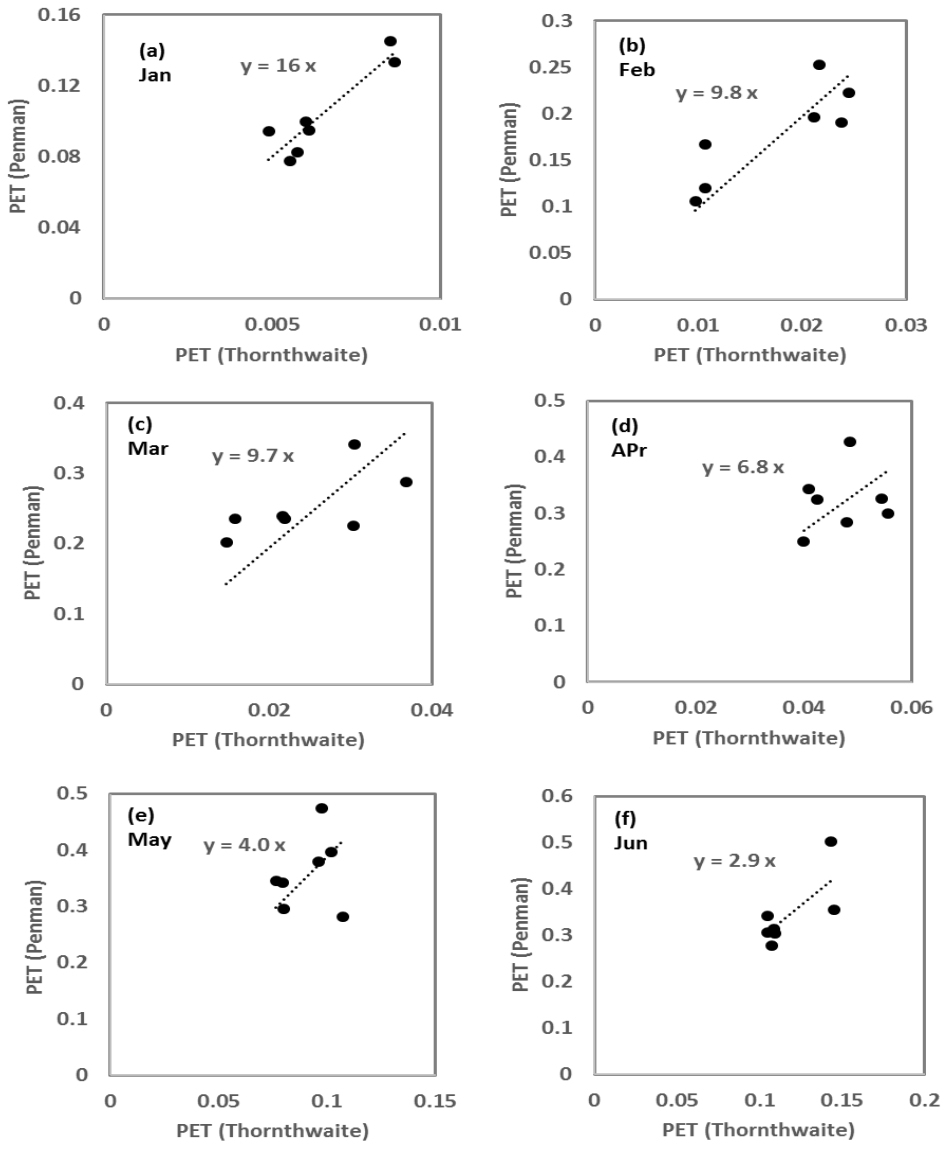

Figure 4.7. Calibration factors for monthly Thornthwaite potential evapotranspiration (m/month) from (a) January to (f) June

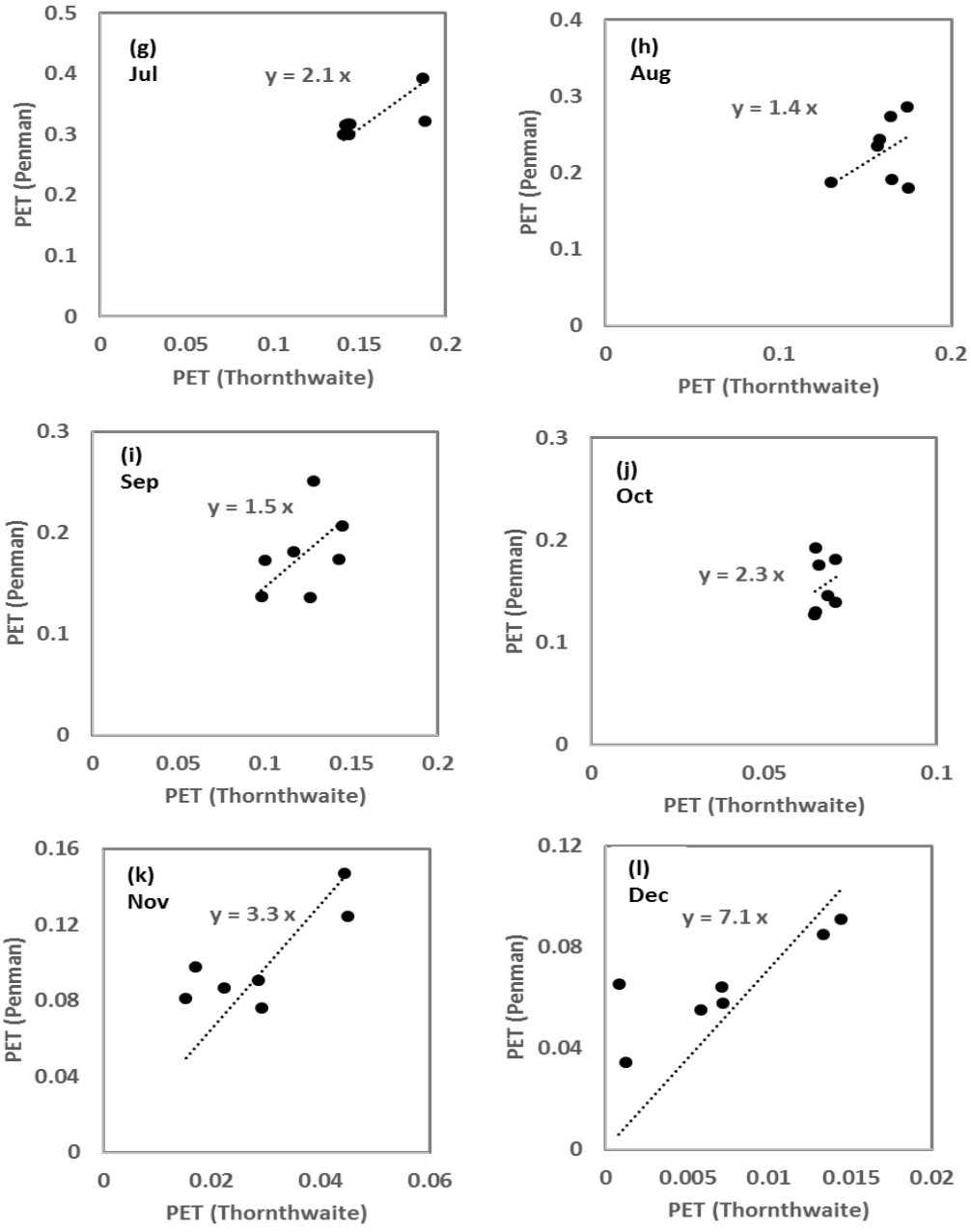

Figure 4.8. Calibrations factor for monthly Thornthwaite potential evapotranspiration (m/month) from (g) July to (l) December

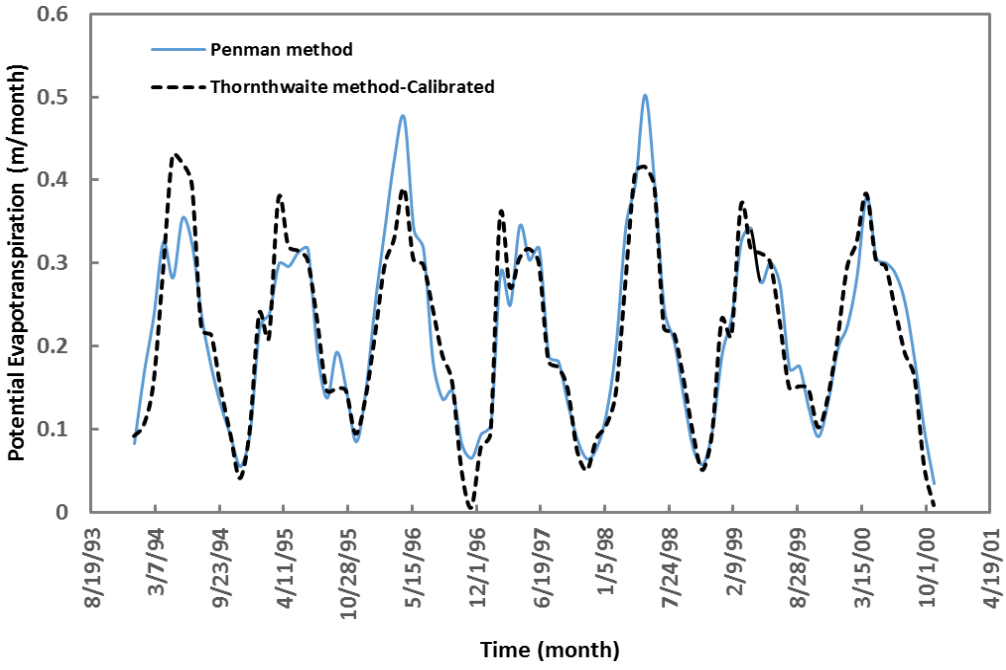

Figure 4.9. Calibrated Thornthwaite potential evapotranspiration and Penman potential evapotranspiration from 1994-2001

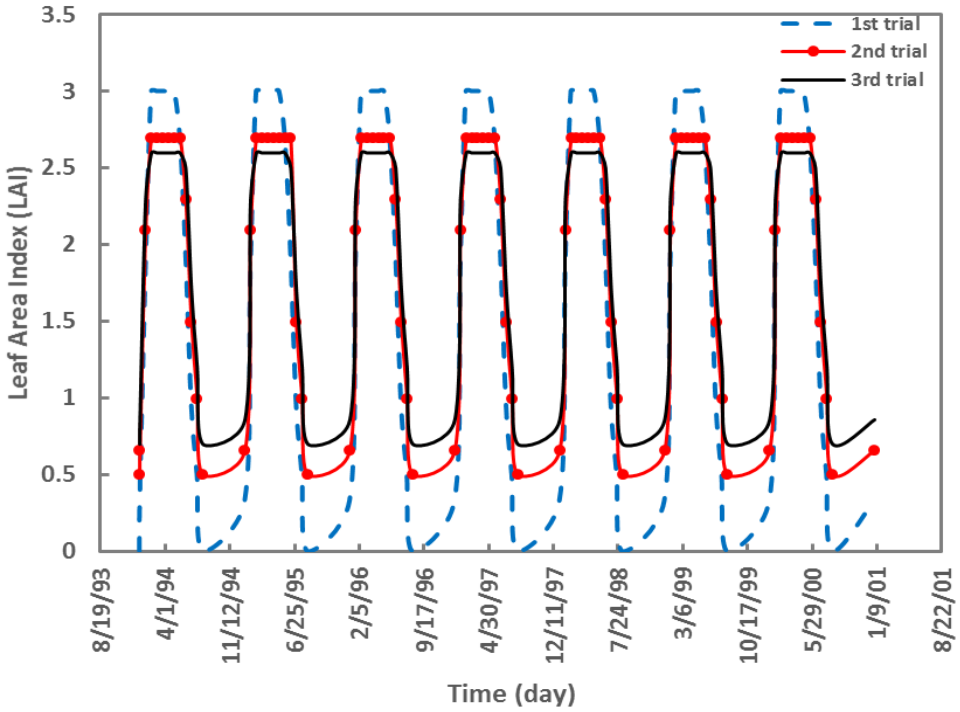

Figure 4.10. Leaf Area Index for different trials

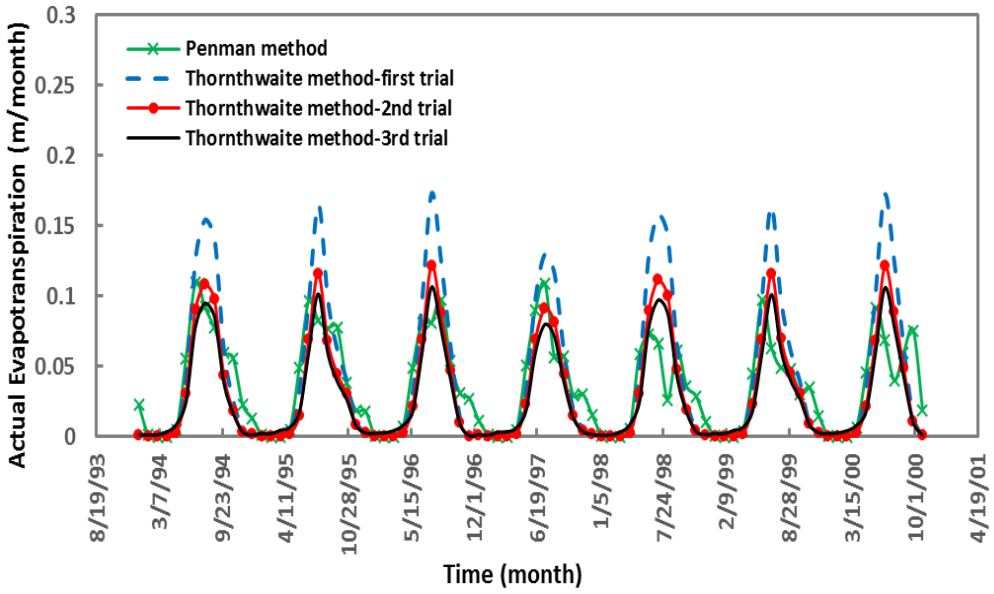

Figure 4.11. Calibrated Thornthwaite actual evapotranspiration and Penman actual evapotranspiration from 1994-2001

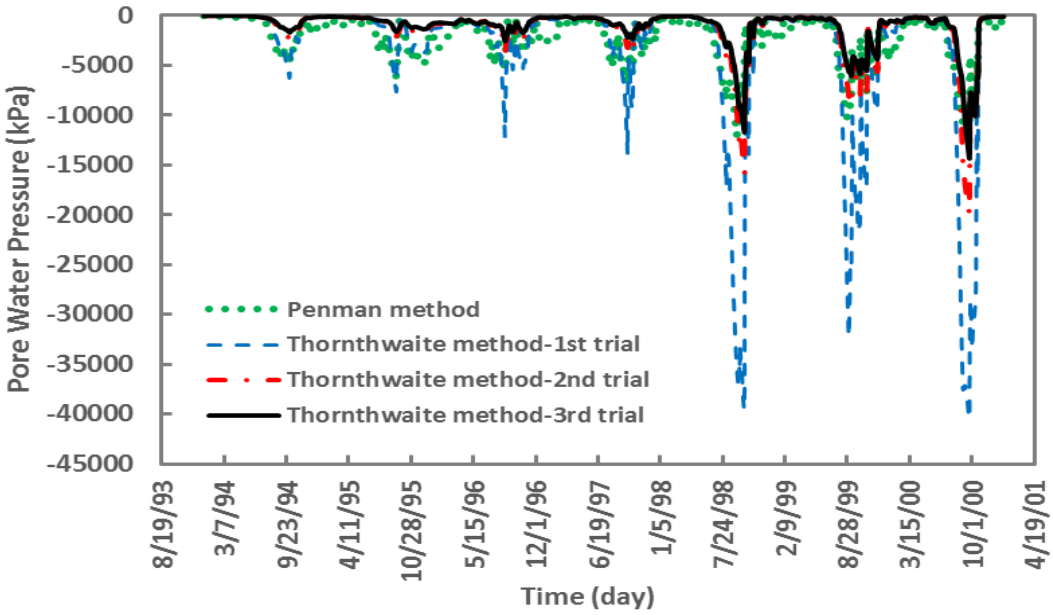

Figure 4.12. Pore water pressure change around soil surrounding the pile head from 1994-2001

The pore water pressure variations shown in Figure 4.12 for the calibration period indicate that the calibration using the leaf area index is a reasonable method for

adjusting the Thornthwaite Method to match Penman Method. Therefore, a pattern of leaf area index for 150 years from 1950 to 2099 analogous to the 3rd trial of calibration method was used to predict the pore water pressure changes at the top of the pile from past to future. It can be seen in Figure 4.13(a) that the negative pore water pressure (suction) increased with time and the calibrated suctions were less than the original amounts of suction predicted with the uncalibrated Thornthwaite Method. In addition, it can be seen in Figure 4.13(b) that the predicted profile of maximum suction from the calibrated Thornthwaite method was much lower than the uncalibrated model with a maximum difference of about 34,000 kPa at the pile head. These predictions based on the projected climate data are consistent with the projected increases in temperature during the 21st century under essentially constant projected rainfall amounts for the same period. While there is a great deal of uncertainty in climate projections, the preceding method provides a rational basis for examining the variations in soil moisture content, positive and negative pore water pressures, and hence soil stiffness resulting from different climate change scenarios. This allows for an analysis of changes in lateral loading behavior of the bridge abutment system due to projected variations in moisture conditions, as described in Chapter 5.

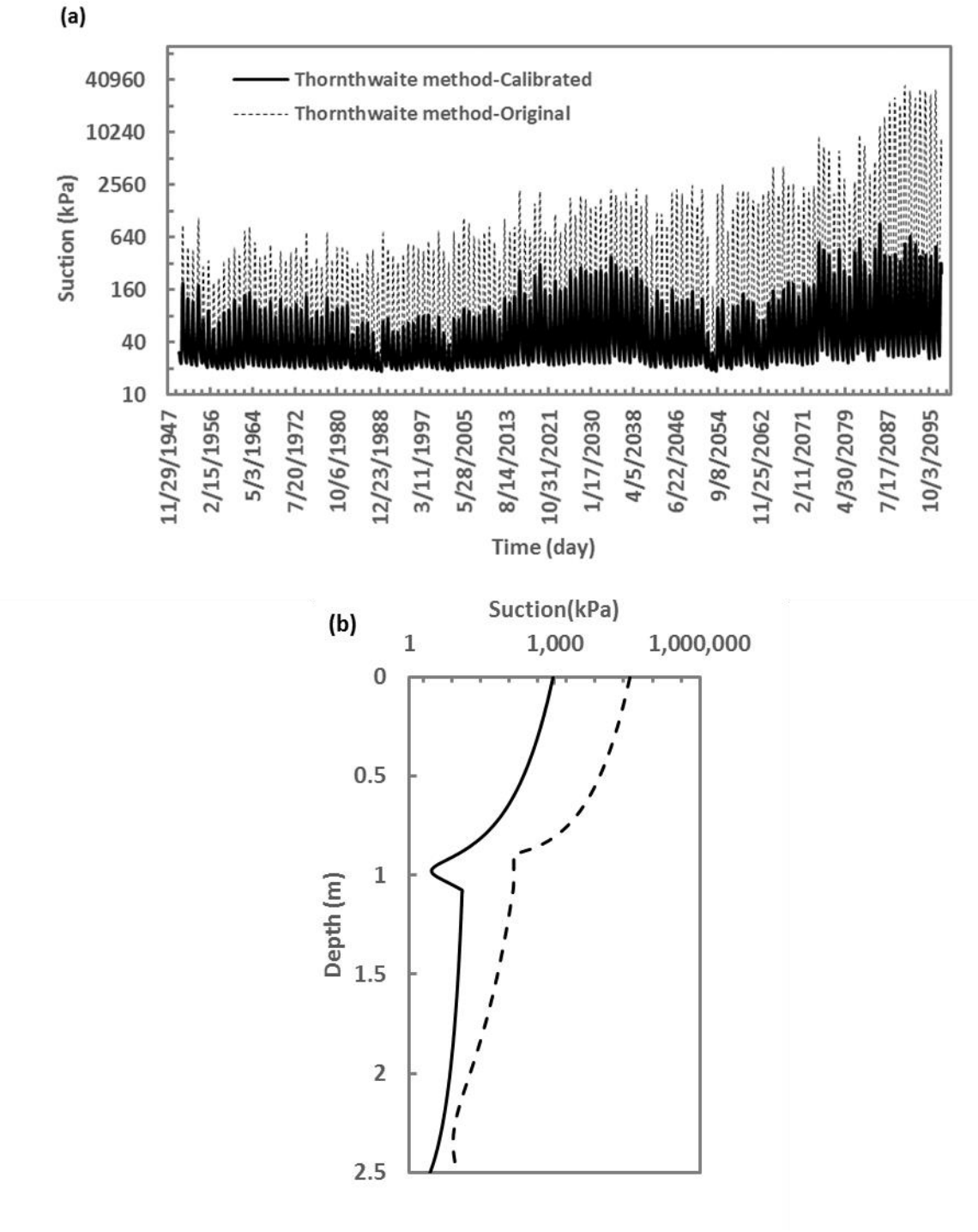

Figure 4.13. (a) Suction predictions from 1950 to 2099 for soil surrounding the pile head (b) Maximum suction profile in the clayey layer surrounding the pile from the pile head to 2.5 m below that (2 to 4.5 m from the ground surface)

4.3.1. 1-D and 2-D Seepage Modeling

In preceding discussions, the unsaturated seepage analysis results were based on the two-dimensional (2-D) bridge abutment model shown in Figure 4.1. It was decided for the purpose of the unsaturated seepage parametric study of moisture changes around a pile to utilize a one-dimensional (1-D) soil model instead of the 2-D model shown in Figure 4.1. This was done based on the following compelling reasons. 1) While geometrically the 2-D model in Figure 4.1 better resembles the true bridge abutment geometry, there are many three-dimensional aspects of the actual bridge abutment that are not accounted for, such as the overlying pavement structure, sloped embankment surface, flux boundary conditions under the bridge, variable ground water conditions, etc. Thus, there is considerable uncertainty regarding whether the 2-D model would be better than a 1-D model in representing the actual 3-D seepage conditions. 2) There is great uncertainty in the predicted future weather data associated with the climate modeling in the NCCV tool. 3) 1-D modeling is much more computationally efficient compared to 2-D modeling. 4) Comparisons of results of 1-D and 2-D models, shown subsequently, are reasonably similar in light of other sources of uncertainty in the soil moisture predictions. Thus, it was decided that the 1-D modeling would serve the purpose of the research in investigating how future changes in weather and soil moisture around a pile will impact the pile behavior. The additional modeling complexity of a 2-D model is not warranted in light of other sources of uncertainty.

For comparison, 1-D and 2-D seepage modeling was conducted using the historical weather dataset from Comanche County (Oklahoma) from 1994 to 2003. A

sketch of the 1-D model geometry simulating the soil layers around the abutment and the pile in Figure 4.1, is shown in Figure 4.14. Figures 4.15 and 4.16 show the 2-D and 1-D pore water pressure variations with respect to time at a point around the pile head based on the Penman and the Thornthwaite methods, respectively.

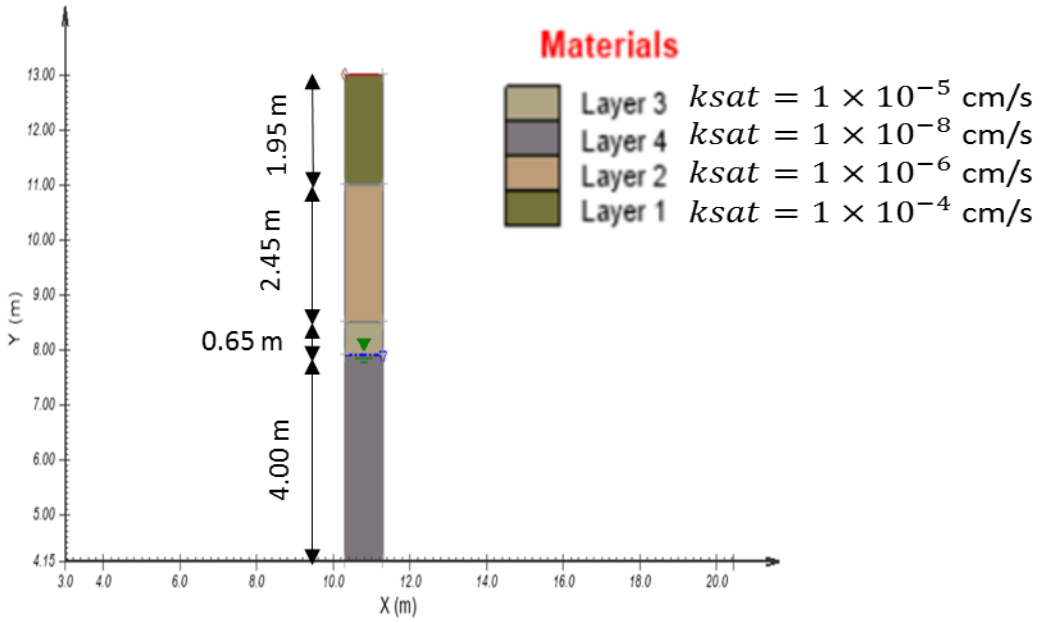

Figure 4.14. 1-D model geometry and properties

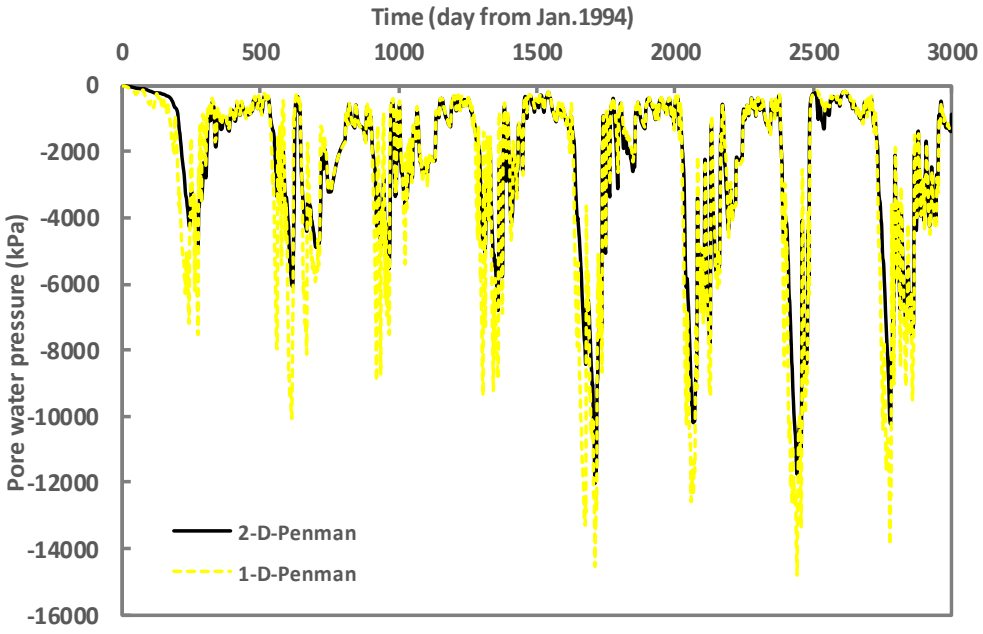

Figure 4.15. 1-D and 2-D seepage analysis conducted using Penman's method

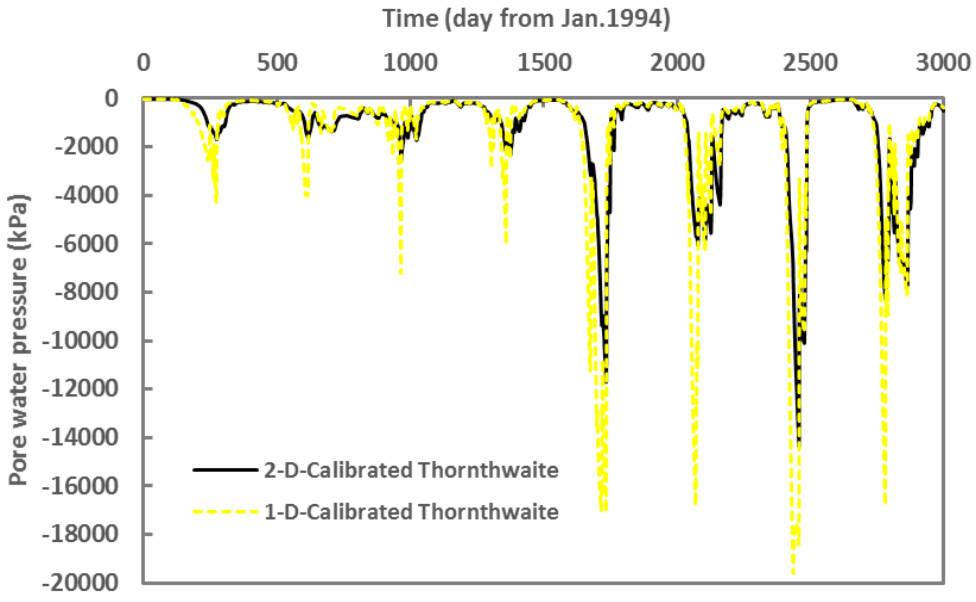

Figure 4.16. 1-D and 2-D seepage analysis conducted using calibrated Thornthwaite's method

The same 1-D model was used for the selected counties in the state of Oklahoma and seepage results obtained are shown in Figures 4.17 through 4.19, which display the pore water pressure variation with time for a point around the pile head. The weather conditions for Beaver county resulted in higher suction (negative pore water pressure) compared to other counties in Oklahoma.

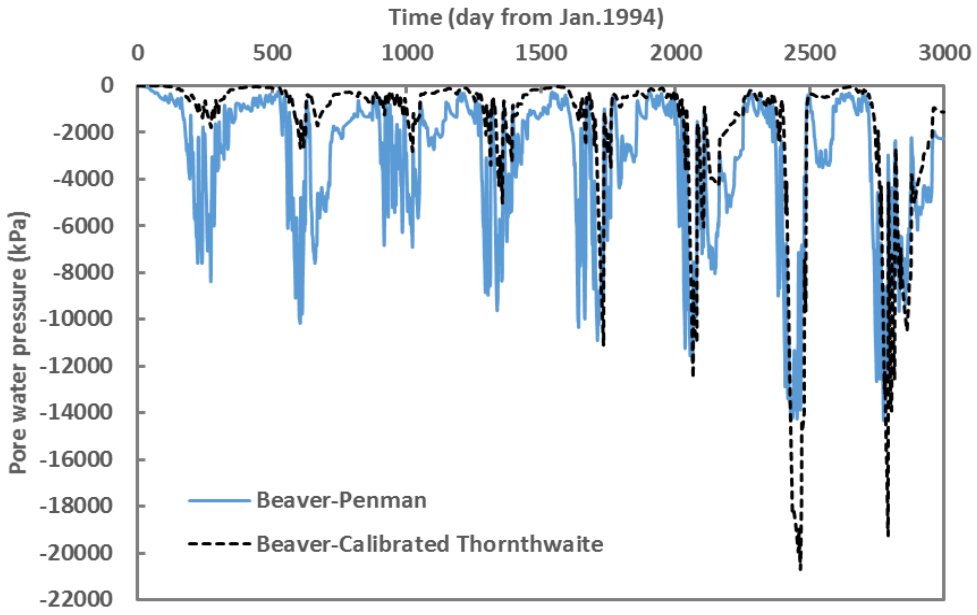

Figure 4.17. 1-D seepage analysis in Beaver County, Oklahoma, conducted using Penman's and calibrated Thornthwaite's methods

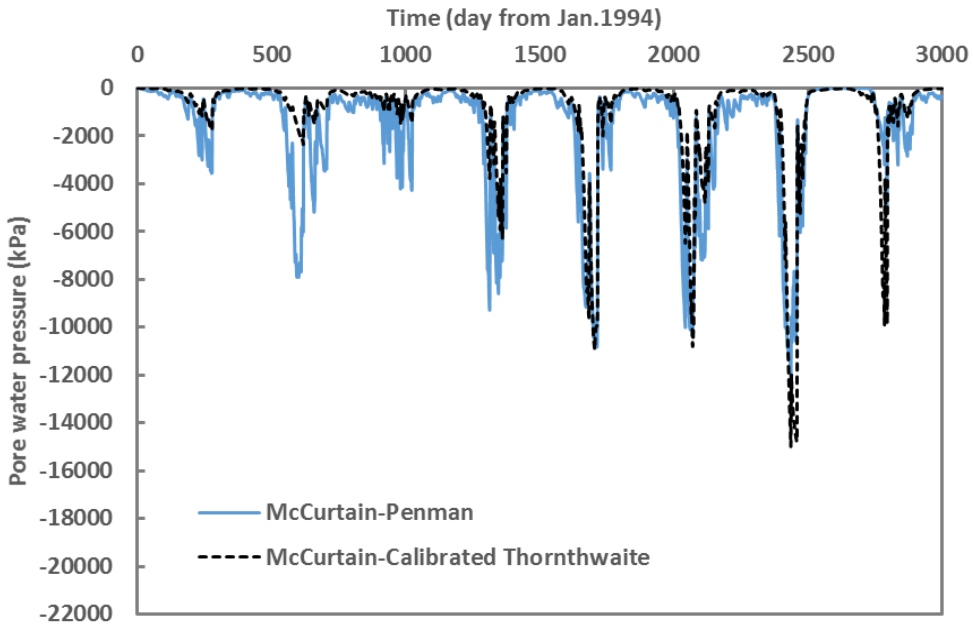

Figure 4.18. 1-D seepage analysis in McCurtain County, Oklahoma, conducted using Penman's and calibrated Thornthwaite's methods

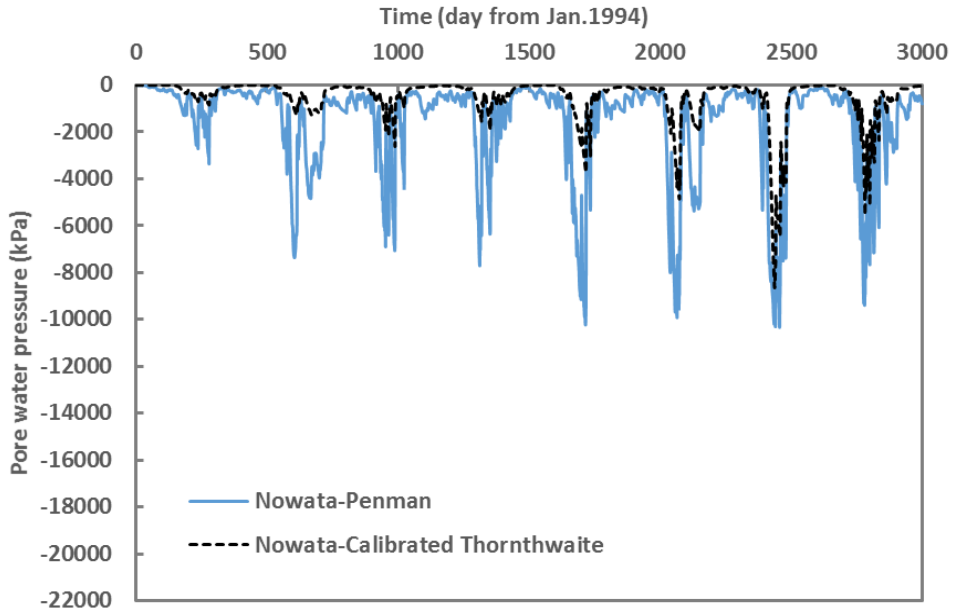

Figure 4.19. 1-D seepage analysis in Nowata County, Oklahoma, conducted using Penman's and calibrated Thornthwaite's methods

5. NUMERICAL MODELING OF INTEGRAL ABUTMENT PILES IN UNSATURATED SOIL

5.1. Finite Difference Modeling using LPILE

LPILE was utilized to investigate the pile-soil interaction for abutment piles in soil under unsaturated conditions. Since LPILE was not developed for specific application to the unsaturated soil condition, the concept of apparent cohesion proposed by Fredlund and Rahardjo (1993) and Vanapalli (1996) were used in the modeling. Stiffness variations in soil around an abutment pile may result from changes in moisture content in the soil. To investigate the abutment pile behavior caused by soil moisture changes, the predicted suction corresponding to different moisture contents obtained from the unsaturated seepage analysis was used to determine the apparent cohesion. The apparent cohesion depends on suction and the unsaturated shear strength parameters. The apparent cohesion and unsaturated strength parameters are used to define p-y curves in LPILE. Clayey soils are more vulnerable to the moisture related mechanical property changes than sandy soils, so only the clayey soil layers used in the model were assigned soil properties dependent on suction.

In LPILE, soil response to pile lateral displacement at a particular point on the pile depends on the p-y curve, which is a function of soil shear strength parameters among other things. The p-y curves for LPILE were developed using the equations proposed by Evans and Duncan (1982) and Mokwa et al. (2000) for unsaturated soils as shown in Figures 5.1 and 5.2. The p-y curve for c-ϕ soil proposed by Evans and Duncan (1982) and as incorporated in LPILE consists of combining soil resistance from the Reese

et al. (1974) sand p-y curve and Matlock (1970) clay p-y curve. The early portion of the p-y curve is obtained by the soil modulus at small displacements. The soil modulus is the product of the modulus coefficient, k, and the depth below the ground surface. The modulus coefficient for sand and clay are based on friction angle and cohesion, respectively. To draw a p-y curve using this method, two restricted points on the displacement axis are defined in which the peak soil resistance and the residual soil resistance take place. The displacement coordinates of y=b/60 and y=3b/80 (b= foundation diameter) are where the peak and residual soil resistance occur, respectively. It is also assumed that the soil resistance decreases from the peak to the residual linearly.

Mokwa et al. (2000) proposed the following equation using a cubic parabola:

$$p = 0.5 p_{ult} \left[\frac{y}{A \epsilon_{50} D}\right]^{0.33} \quad \textbf{(5.1)}$$

where p is the soil resistance, p_{ult} is the ultimate resistance, y is the lateral foundation displacement at a particular depth, A is an empirical coefficient, ε_{50} is the strain at 50% of the ultimate soil strength obtained from a triaxial shear test, and D is the foundation diameter. The ultimate soil resistance, p_{ult}, is calculated using Brinch-Hansen's theory (1961) and modified based on results from full-scale tests. The equation of p_{ult} is as follows:

$$p_{ult} = M \gamma_m D z K_q + M c D K_c \quad \textbf{(5.2)}$$

where M is an empirical modification factor = 0.85, γ_m is the soil moist unit weight, D is the foundation diameter, z is the depth below the ground surface, K_q is a coefficient for the frictional component of the soil resistance, c is the soil cohesion and K_c is a coefficient for the cohesive component of the soil resistance. Five load tests conducted on relatively short drilled shaft foundations embedded in unsaturated silty (ML and MH) and clayey (CL and CH) soils were used to back-calculate the parameters required for the above equations.

Both p-y curves exhibited a similar linear trend at very low displacements. Softening and hardening behaviors were captured using the former and the latter equations. These behaviors were more pronounced at higher suction. A simple linear extended Mohr-Coulomb failure model was used with these methods, and soil properties for the unsaturated clay were assumed based on experimental tests. For the purpose of developing p-y curves for the c-ϕ soil using the LPILE program, the effect of suction was incorporated into the cohesion intercept using the following equations from Fredlund and Rahardjo (1993) and Vanapalli (1996), respectively. It should be noted that the Equations 5.3 and 5.4 were used for the case study and parametric study, respectively.

$$c = c' + (u_a - u_a)\tan\emptyset^b \qquad \textbf{(5.3)}$$

where: c' is the effective stress cohesion intercept and represents the saturated soil condition, (u_a-u_w) is suction, and ϕ^b is the friction angle with respect to suction. For the saturated condition, c=c'.

$$c = c' + (u_a - u_a)\tan\emptyset'[\frac{(\theta-\theta_r)}{(\theta_s-\theta_r)}] \qquad \textbf{(5.4)}$$

where: c' is the effective stress cohesion intercept and represents the saturated soil condition, (u_a-u_w) is suction, ϕ' is the effective friction angle, and θ_r & θ_s are the residual and saturated volumetric water contents, respectively. For a saturated condition, c=c'.

A model of the previously mentioned bridge abutment next to Medicine Bluff Creek along I-44 in Lawton, OK was developed for use with LPILE. The geotechnical properties of the soil layers obtained from SPT and CPT correlations and laboratory testing and compatible with typical soil properties available in LPILE are listed in Table 5.1 (Reese et al. 1974, 1976; Detournay and Cheng 1993).

Table 5.1. Properties of typical soli layers

Soil layer	Soil thickness (m)	Total unit weight (kN/m^3)	Soil lateral stiffness, k, (kN/m^3)	Effective stress cohesion intercept, c' (kN/m^2)	Effective stress friction angle, ϕ' (°)	Friction angle with respect to suction, ϕ^b (°)
Loose sand backfill-first layer	2.00	15.63	6790	-	30	-
Stiff lean clay-second layer	2.00	21.5	-	0	30	10
Dense silty sand-third layer	0.6	20.72	61,000	-	35	-
Weak laminated sandstone interbedded with shale seams	6.00	24.35	-	-	-	-

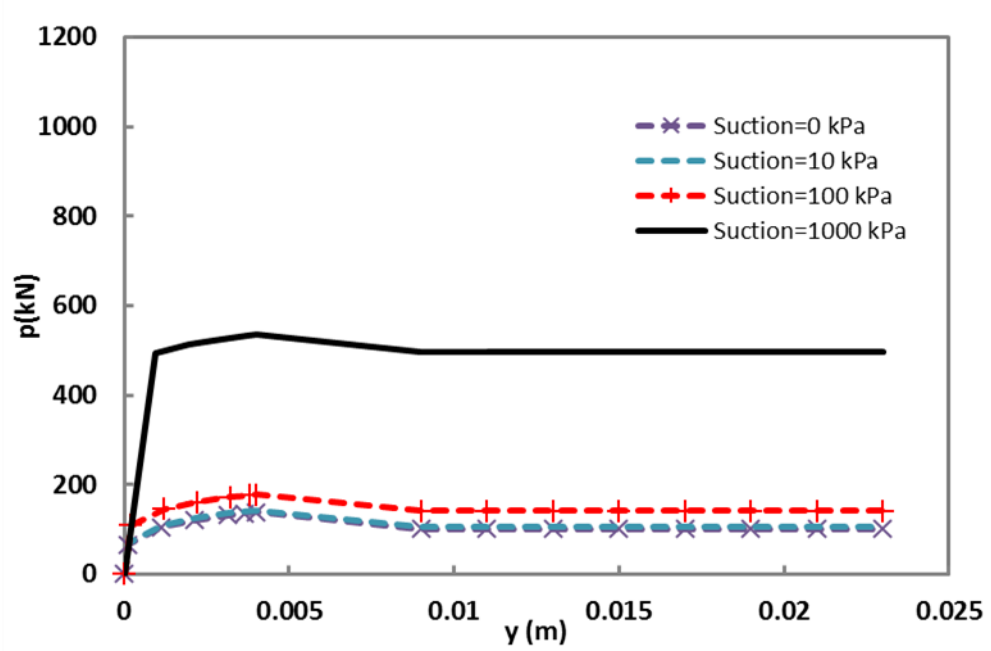

Figure 5.1. p-y curves for the clay layer obtained from Evans and Duncan (1982) equation

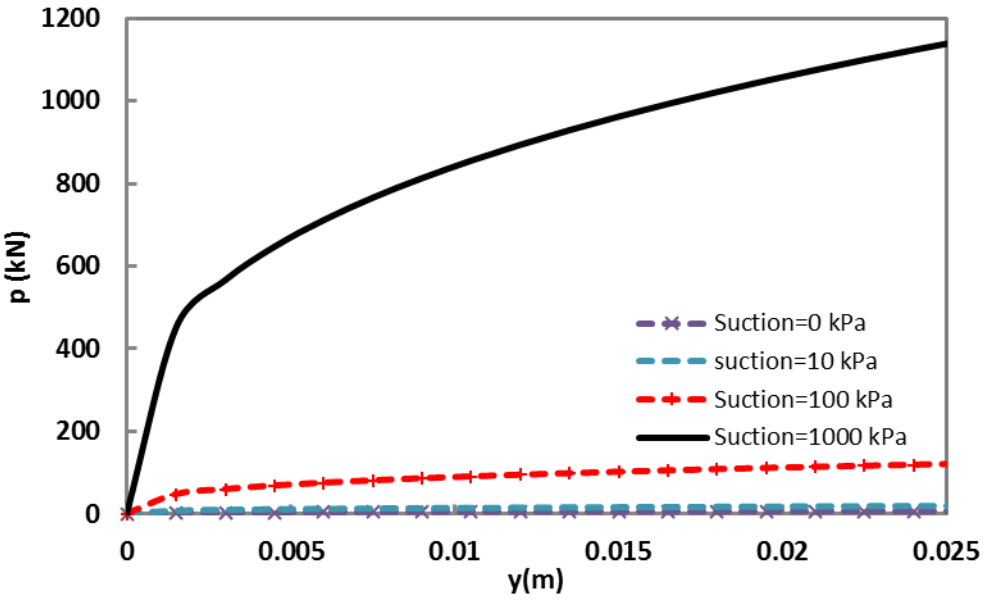

Figure 5.2. p-y curves for the clay layer obtained from Mokwa et al. (2000) equation

5.2. Comparison of pile response using Evans and Duncan (1982) and Mokwa et al. (2000) p-y curves

According to a study conducted by Kirupakaran (2013), the I-44 bridge deck was subjected to an average temperature variation of 95˚F (35 ˚C) over a six-month period. Assuming the thermal deformation of the bridge was symmetric to the center of the bridge, the thermally induced deformation of the superstructure at the abutment due to the change in temperature of the superstructure can be calculated by Equation 5.5.

$$\delta = \alpha \times \Delta T \times L/2 \qquad \textbf{(5.5)}$$

where, α is the coefficient of thermal expansion, ΔT is the change in temperature and L is the total length of the bridge. Thermal expansion coefficient of the reinforced concrete superstructure was considered as 11.21×10^{-6}/˚C. Therefore, thermally induced deformation of the superstructure based on Equation (5.5) at the abutment will be 0.019 m. The average movement of the superstructure based on crack meter readings was 0.022 m. Since the calculated superstructure movement was in the range of the measured readings from the crack meter, thermally induced deformation at the abutment was assumed to be 0.022 m. The displacement of the abutment was directly applied as the boundary condition at the top of abutment in LPILE modeling. The connection between the abutment and the bridge deck was assumed to be fixed. The boundary condition of having a displacement without any rotation at the top of the abutment was compatible with the performance of IABs both in practice and theory.

The axial load on the pile due to the superstructure was considered as 136.6 kN (Kirupakaran 1983).

The results of the LPILE analysis revealed that bending moments obtained using the Evans and Duncan (1982) model were less than those obtained using the Mokwa et al. (2000) model at high suctions. The hardening behavior of soil in the high suction range observed in the p-y curves of Mokwa et al. (2000) in Figure 5.2 can lead to increase in bending moments at large displacements compared to those obtained from the Evans and Duncan (1982) model in Figure 5.1. On the other hand, Evans and Duncan (1982) p-y curves give slightly larger bending moments at low suction values. The response of an abutment pile in a soil with high stiffness results in higher bending moments as shown in Figures 5.3 and 5.4. The lateral deflections at the pile head showed that a soil layer with higher suction and stiffness provides greater resistance to lateral displacement at the top of the pile, which resulted in more abrupt curvature changes and greater bending moment.

The bending moments and the lateral deflections only in the piles are shown in Figure 5.5 and 5.6. Note that in these Figures the depth is measured from the top of the pile at the bottom of the abutment. It is important to note that for the both models, even at low or zero suction, the bending moments at the top of the pile exceed the theoretical yielding moment of the pile. This is attributed to the soil stiffness and extreme curvature that occurs where the pile enters the bottom of the abutment. This finding suggest that a soft soil would be beneficial at reducing bending moments near

the top of the pile, which could be accomplished by placing the piles in predrilled holes around the upper portion of the pile and backfilling them with a compressible material.

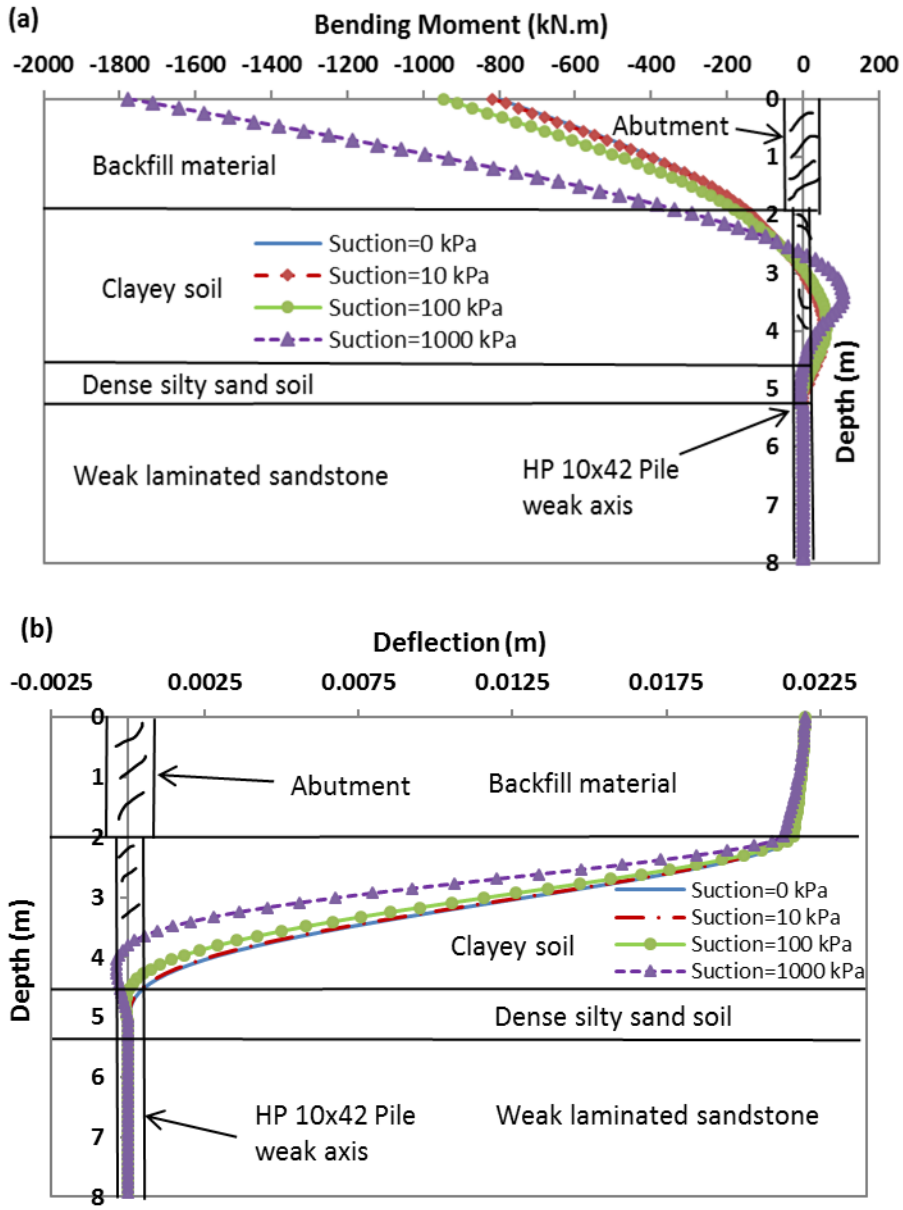

Figure 5.3. (a) Bending moments and (b) lateral deflections in the abutment and the pile using p-y curves from Evans and Duncan (1982)

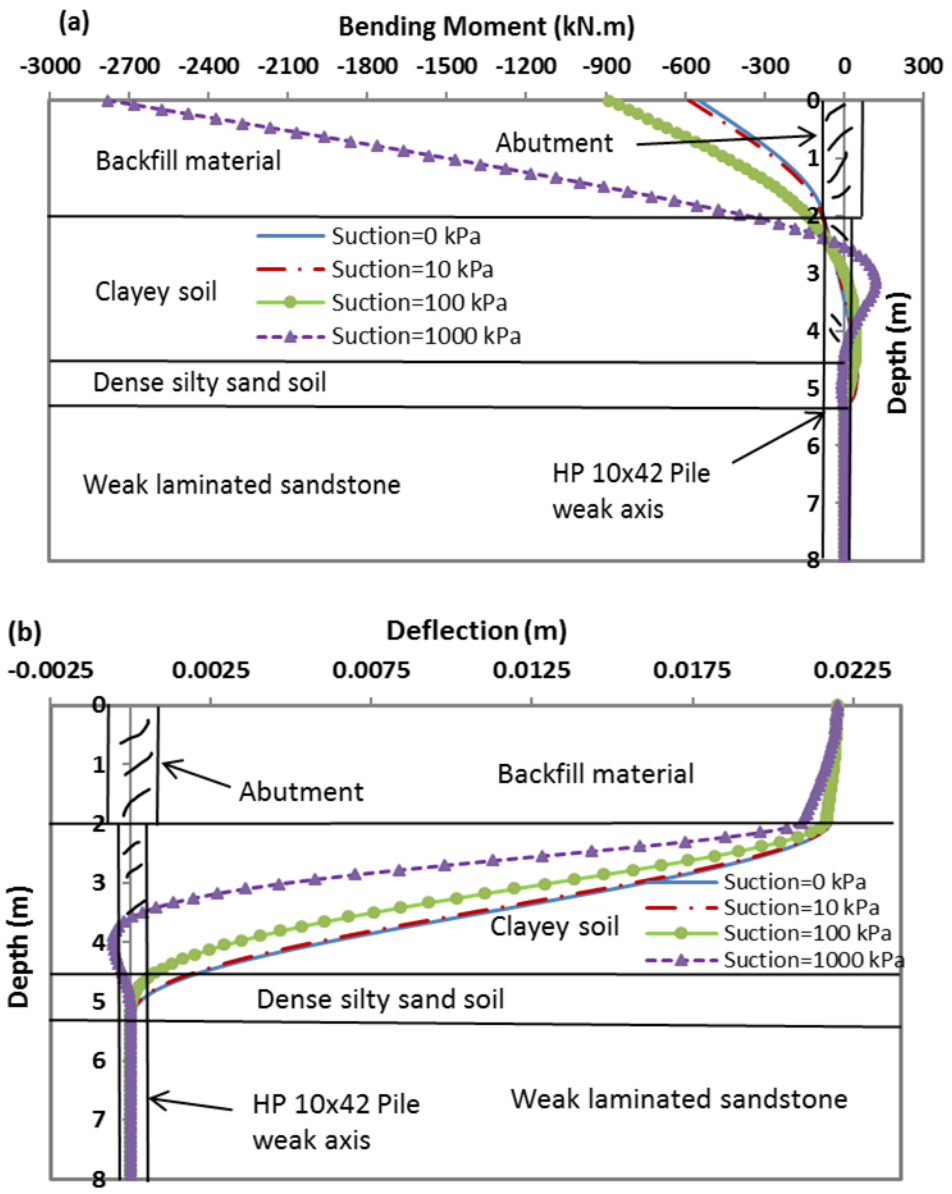

Figure 5.4. (a) Bending moments and (b) lateral deflections in the abutment and the pile using p-y curves from Mokwa et al. (2000)

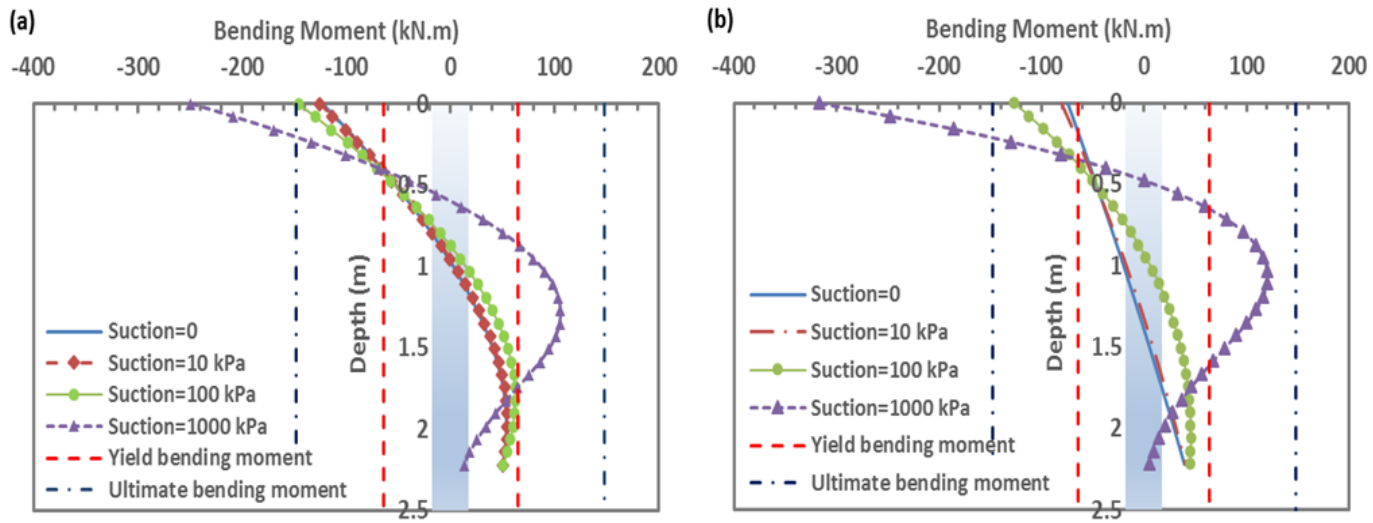

Figure 5.5. Bending moment variations for the top of the pile using (a) Evans and Duncan (1982)and (b) Mokwa et al. (2000) p-y curves

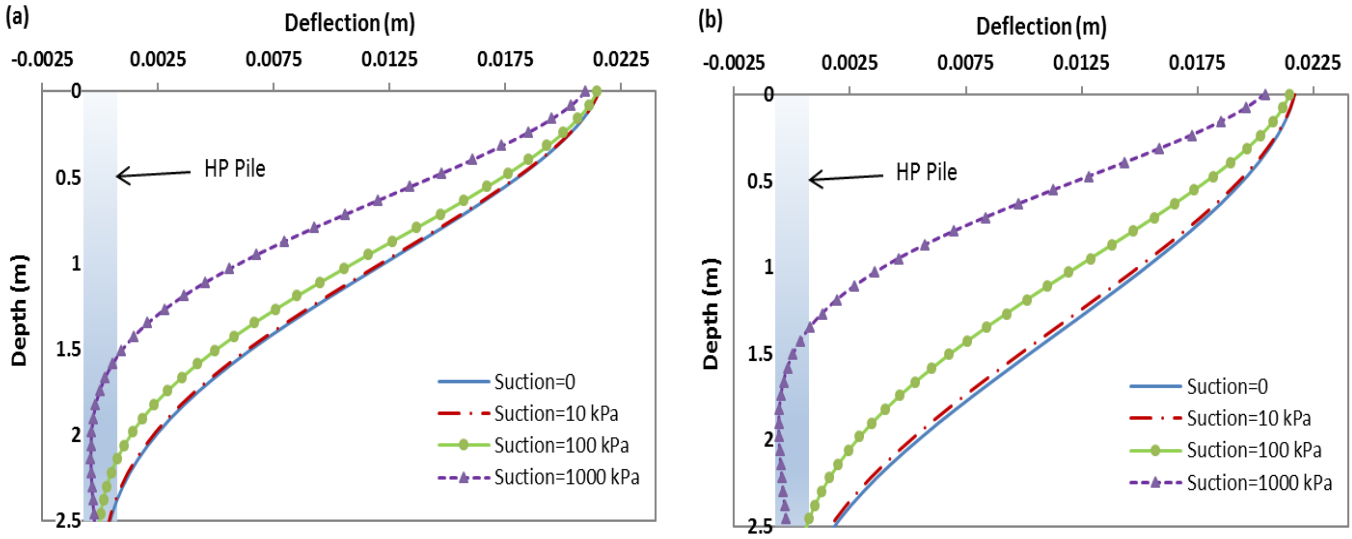

Figure 5.6. Lateral deflection variations for the top of the pile using (a) Evans and Duncan (1982) and (b) Mokwa et al. (2000) p-y curves

6. PARAMETRIC ANALYSIS OF ABUTMENT PILE LATERAL LOADING

6.1. Introduction

The parametric analysis of piles involved two separate parametric studies. The first utilized the unsaturated seepage modeling using SVFlux to evaluate the unsaturated flow of moisture in different soil profiles to establish the suction distributions to be used in LPILE modeling. The second involved LPILE to examine the response of abutment piles for different soil and pile conditions. The variables considered for the parametric studies were based on some basic information from the states in Region 6 as shown in Table 6.1. Based on the information in Table 6.1, some basic parameters used for the sensitivity analysis are summarized in Table 6.2. Generally, relatively short and long piles with lengths of 10 m and 20 m were considered in the parametric studies. The relatively short piles were surrounded by 5 m of soil and 5 m of rock to restrain the piles at the bottom. The relatively long piles were surrounded by different soil layers. The studies related to the seepage analysis involved a combination of different hydraulic properties and depth of soil layers. The soil water characteristic curves (SWCC) for a typical fine-grained and coarse-grained soil used for the seepage analysis were obtained based on the Zapata's model as shown in Figure 6.1. The atmospheric boundary condition for all cases was identical and included the relatively driest condition, resulting in high suctions. The lateral displacement used for the mechanical analyses of piles was based on the maximum calibrated temperature differences experienced in the counties.

Table 6.1. General information of IABs built in Region 6

Case Study from Different States	Pile Type	Pile Length (m)	Bridge Length (m)	Soil Profile (USCS/layer thickness in m)			
				1st Layer	2nd Layer	3th Layer	4th Layer
Oklahoma	HP 10x42	7.9	64.0	CL/2.4	SM/0.6	Sand Stone/4.85	----
Texas	HP 12x53	12.5	67.6	Sand/12.5	-----	-----	----
Louisiana	HP 14x89	29.9	91.4	CL/3.65	SC/0.75	CL/9.1	SM/25.5
New Mexico	HP 14x89	21.3	54.8	SM/12	CL/3	SC/3	CL/3.2

Table 6.2. Pile and soil variables

Parameter	Variable-1	Variable-2	Variable-3	Variable-4
Pile Type	HP 10x42	HP 12x53	HP 14X89	----
Pile Orientation	Weak axis	Strong axis	----	----
Pile Length(m)	10	20	----	----
Bridge Length (m)	50	70	90	----
Backfill Thickness (m)	1.5	3	----	----
Soil Profile (USCS)-Thickness (m)	CL-5	SM-5	CL-15	SM-15
Backfill Permeability (m/s)	$1x10^{-3}$	$1x10^{-4}$	$1x10^{-5}$	----
Soil Profile (USCS)-Permeability (m/s)	CL - $1x10^{-8}$	SM - $1x10^{-6}$	----	----

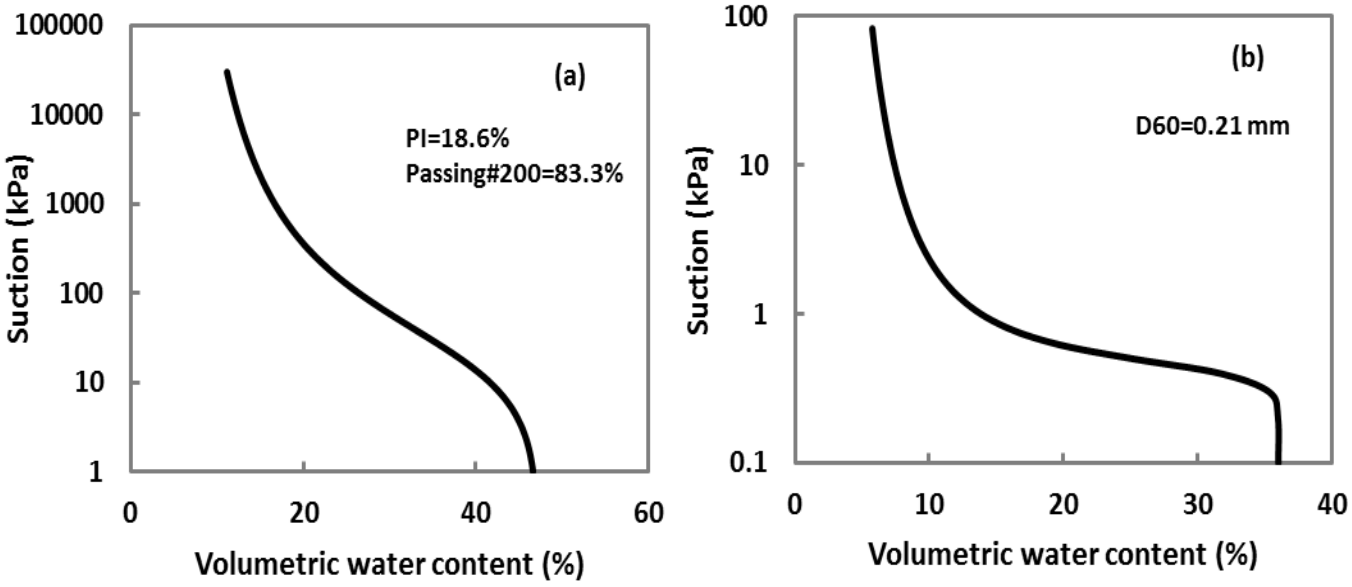

Figure 6.1. SWCC for (a) fine-grained soil and (b) coarse-grained soil

6.2. Seepage Parametric Analysis

6.2.1. Relatively Short Pile

Two main parameters, depth and hydraulic conductivity of different soils were variables in this parametric study. The first layer of the model included three different backfill materials with two different thicknesses (1.5 and 3 m). The second layer was clayey or sandy soil with a thickness of 5 m. The atmospheric boundary condition derived from Beaver County was considered for the transient seepage analyses. The weather data from Jan. 2015 to Jan. 2099 were used. The calibrated Thornthwaite's method was utilized for all cases. A typical pore water pressure variation on the ground surface during the given time as plotted in Figure 6.2 shows that the negative pore water pressure reached the peak value in a period time between 2090 and 2095. The maximum negative pore water pressure distributions are shown in Figures 6.3 through 6.6. The changes of pore water pressure in the clay layers were approximately bilinear, whereas the sand layers showed relatively uniform changes of pore water pressure. The high negative pore water pressures in the sand layers indicate the sand is in a relatively dry condition and in the residual moisture regime of the soil water characteristic curve.

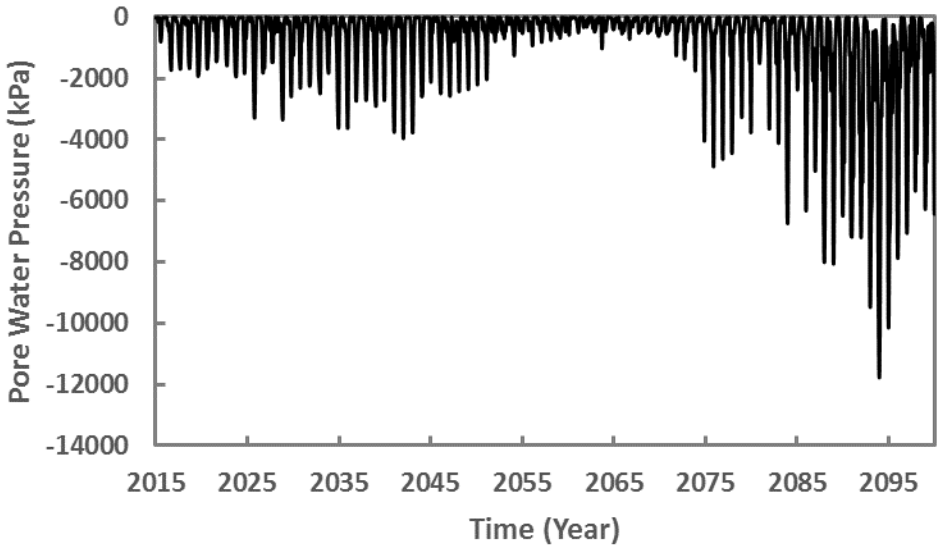

Figure 6.2. Pore water pressure variation on the ground surface from 2015-2099

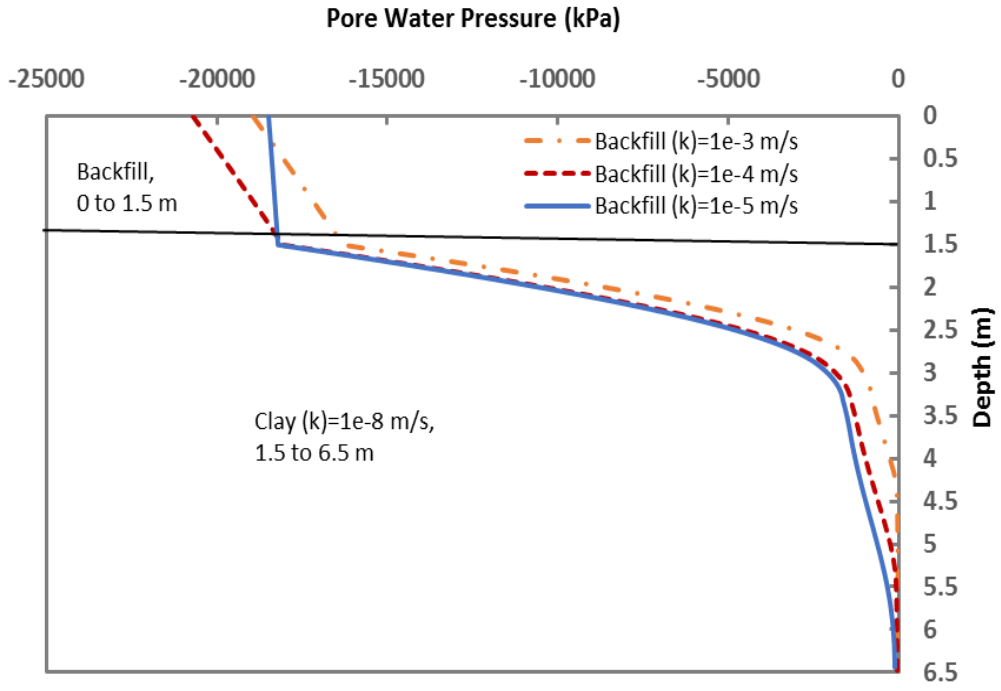

Figure 6.3. Case-1 pore pressure profiles: clay layer beneath different backfill materials with a thickness of 1.5 m

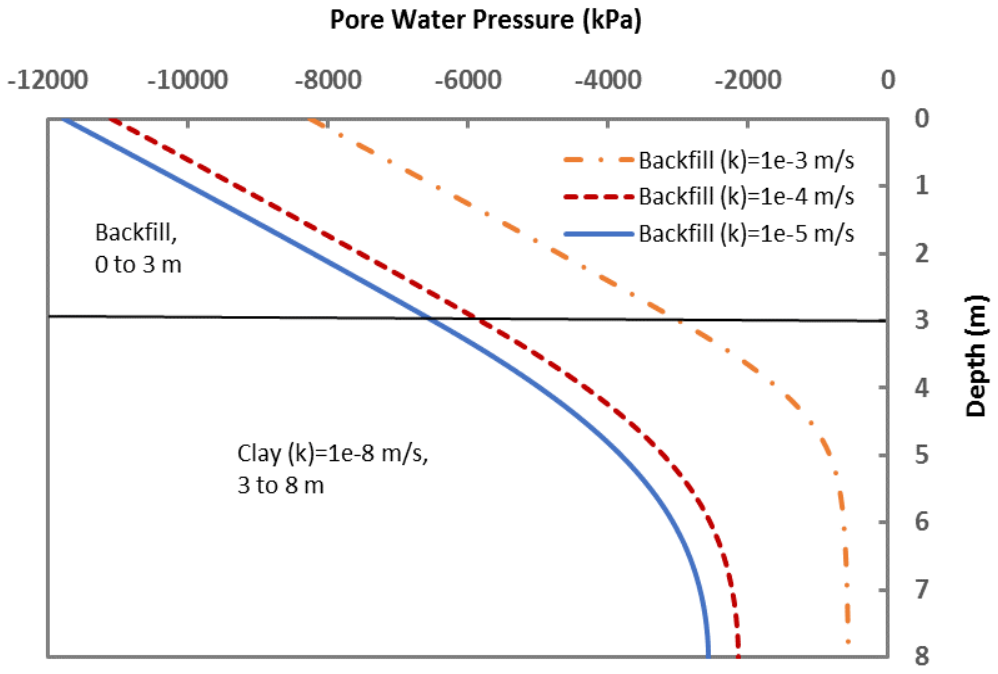

Figure 6.4. Case-2 pore pressure profiles: clay layer beneath different backfill materials with a thickness of 3 m

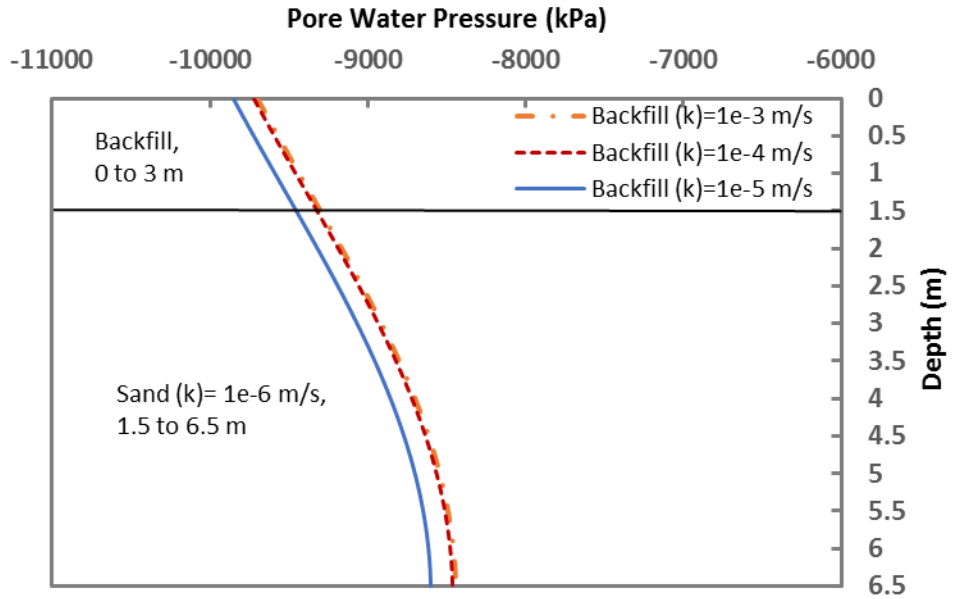

Figure 6.5. Case-3 pore pressure profiles: sand layer beneath different backfill materials with a thickness of 1.5 m

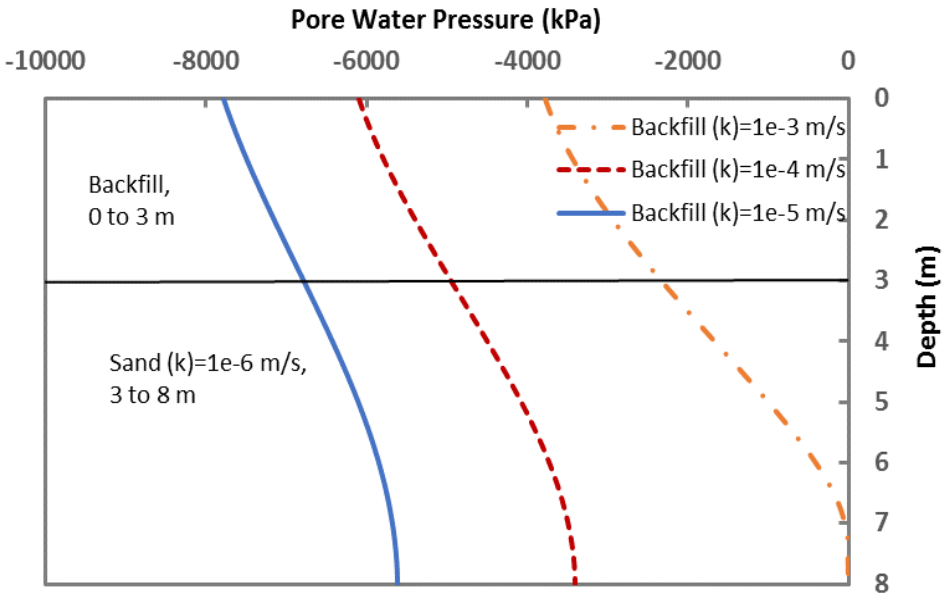

Figure 6.6. Case-4 pore pressure profiles: sand layer beneath different backfill materials with a thickness of 3 m

6.2.3. Relatively Long Pile

The relatively long pile was assumed to be 20 m long. The first layer of the model surrounding the abutment included three different backfill materials with two different thicknesses (1.5 and 3 m). The second layer of soil surrounding the pile was either one single layer with a thickness of 20 m as a first alternative or was divided in two different layers with a thickness of 5 m and 15 m as a second alternative. Again, the atmospheric boundary condition derived from Beaver County was applied for the transient seepage analyses. The weather data from Jan. 2015 to Jan. 2099 were used. The calibrated Thornthwaite's method was utilized for all cases. The negative pore water pressure reached the peak value in a time period similar to the case studies conducted for the relatively short piles.

Figures 6.7 through 6.14 show the maximum negative pore water pressure distributions. The change of pore water pressure or moisture reached a depth of approximately 16 m and 12 m for the single clay and the single sand layers, respectively. However, the extent of influence of changes for the cases having two different layers (sand-clay and clay-sand) were approximately at the same depth with different magnitudes of pore water pressures.

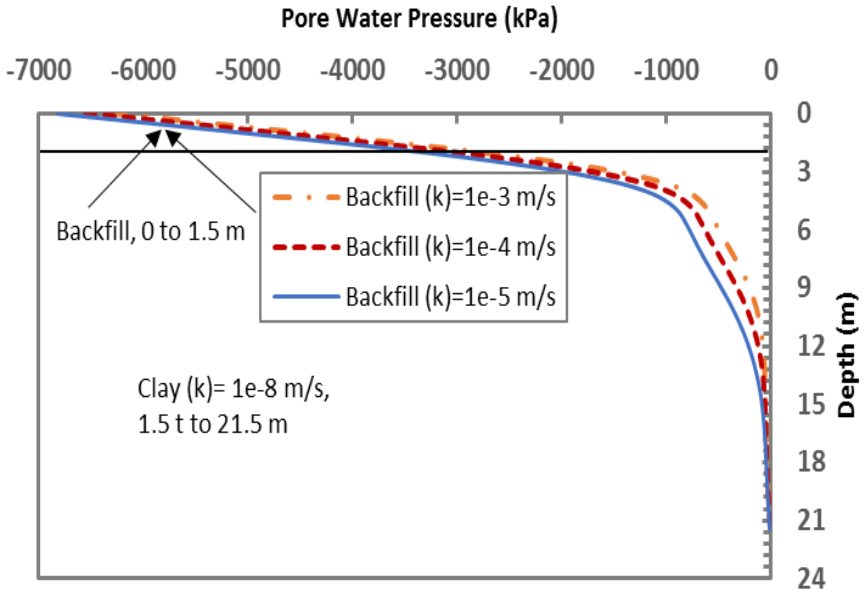

Figure 6.7. Case-5 pore pressure profiles: clay layer beneath different backfill materials with a thickness of 1.5 m

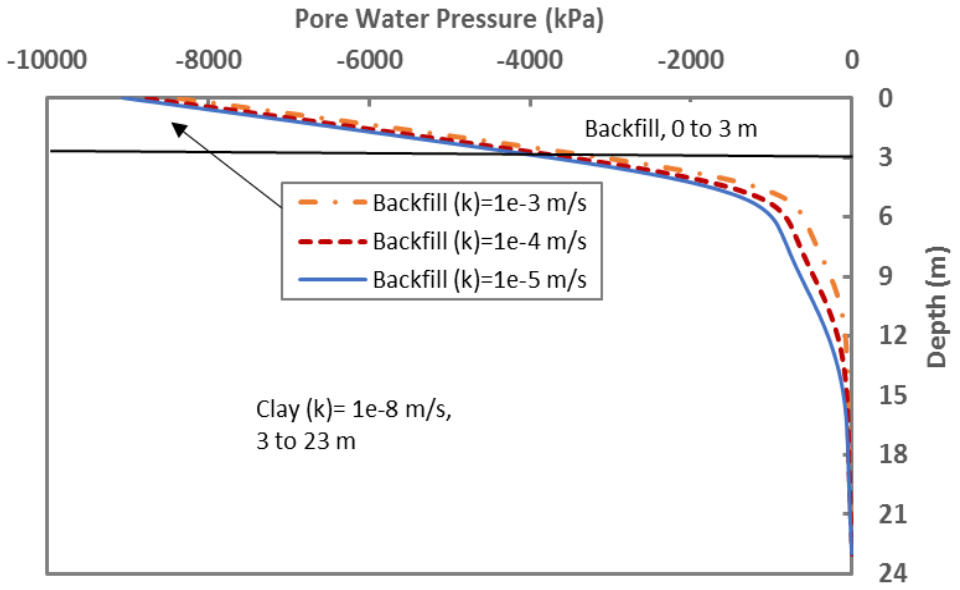

Figure 6.8. Case-6 pore pressure profiles: clay layer beneath different backfill materials with a thickness of 3 m

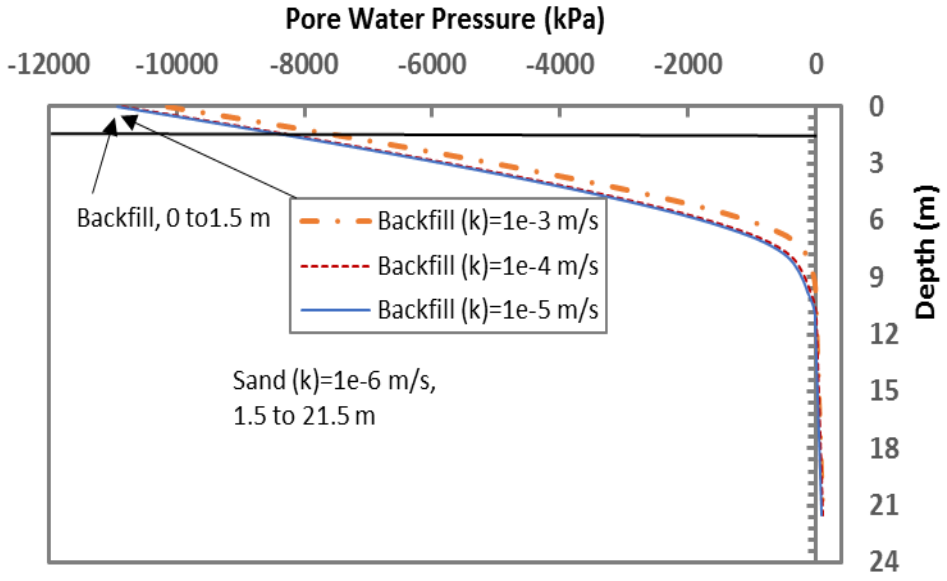

Figure 6.9. Case-7 pore pressure profiles: sand layer beneath different backfill materials with a thickness of 1.5 m

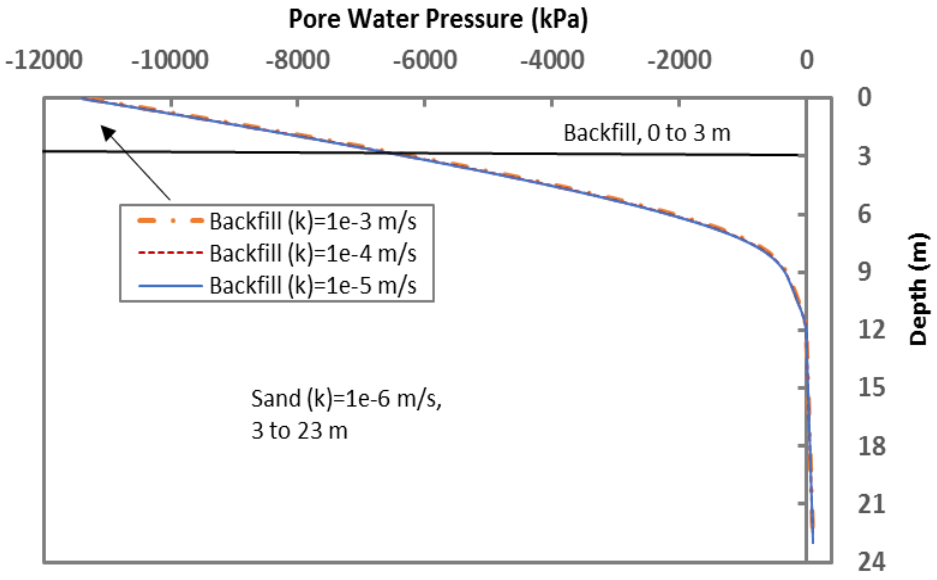

Figure 6.10. Case-8 pore pressure profiles: sand layer beneath different backfill materials with a thickness of 3 m

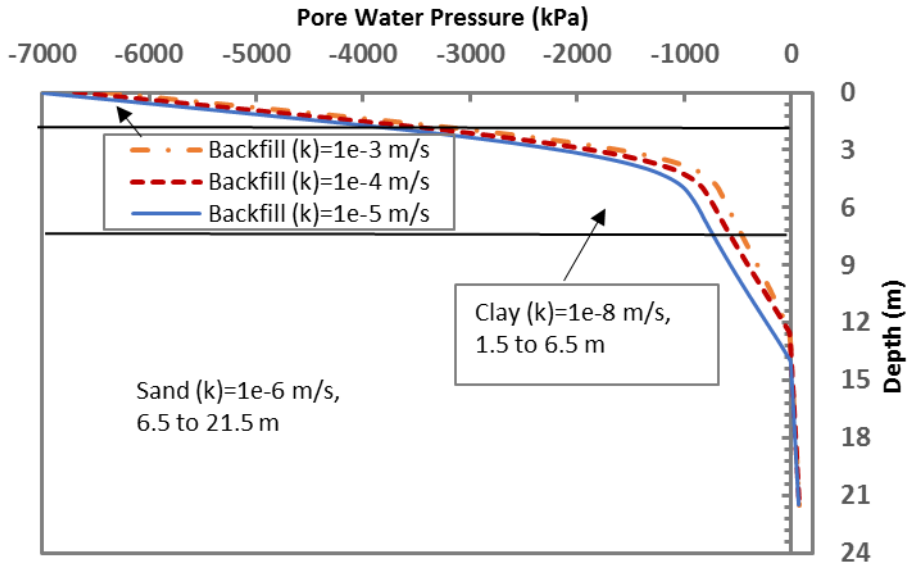

Figure 6.11. Case-9 pore pressure profiles: clay and sand layers beneath different backfill materials with a thickness of 1.5 m

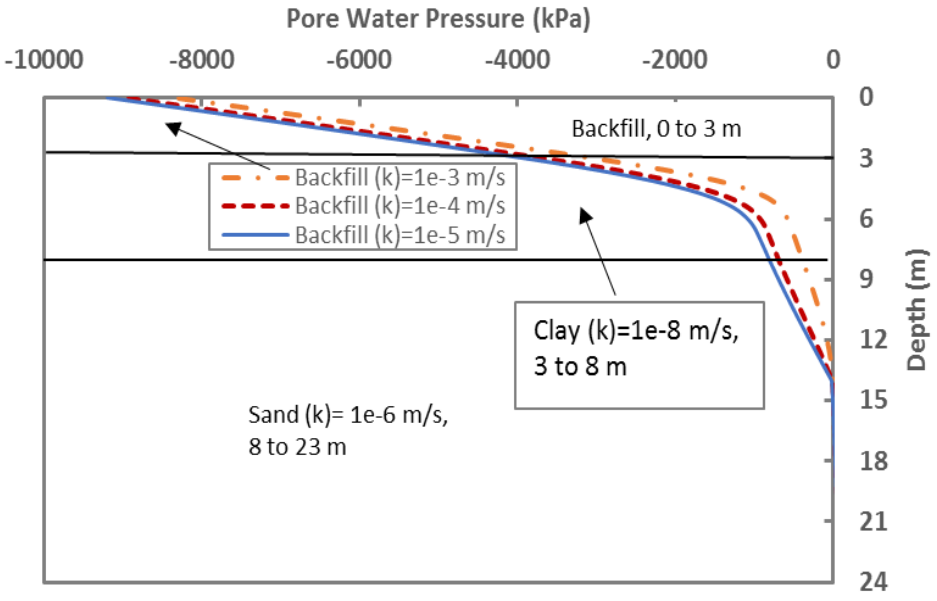

Figure 6.12. Case-10 pore pressure profiles: clay and sand layers beneath different backfill materials with a thickness of 3 m

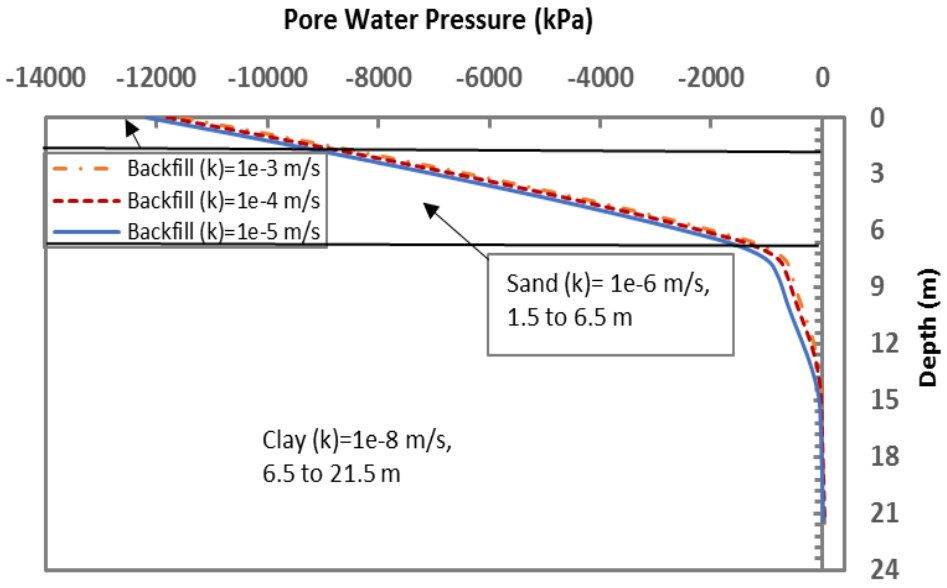

Figure 6.13. Case-11 pore pressure profiles: sand and clay layers beneath different backfill materials with a thickness of 1.5 m

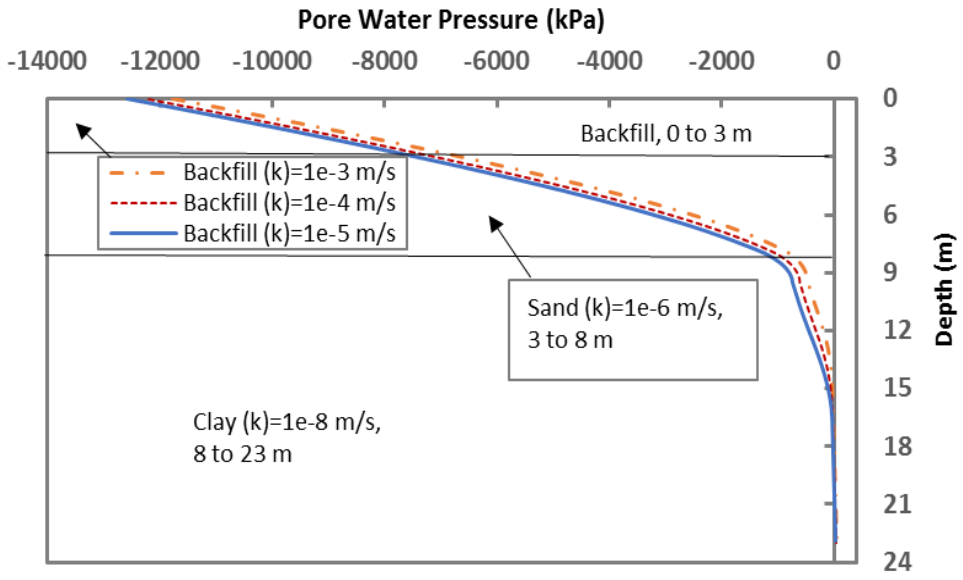

Figure 6.14. Case-12 pore pressure profiles: sand and clay layers beneath different backfill materials with a thickness of 3 m

6.3. Soil-Pile Interaction Parametric Analysis

The relatively short and long piles with different properties and orientations were considered for the parametric studies as shown in Table 6.2. To produce the p-y curves using LPILE and the proposed method (e.g. Mokwa et al. 2000), the effect of suction was considered through using the concept of apparent cohesion from the Equation 5.4 for the driest condition. The saturated condition (i.e. suction=0) was considered as the wettest condition. The average temperature change was obtained from temperature variations in Beaver County as a representative county for the driest condition. This temperature change was calibrated using the temperatures measured on a typical bridge (i.e., Lawton Bridge) and the weather station close to the bridge as shown in Figures 6.15 and 6.16. The calibration factor was calculated

as the ratio of seasonal maximum bridge temperature change to the seasonal maximum weather station temperature change. Using the information in Figures 6.15 and 6.16, a calibration factor of 1.08 was used to convert the weather station temperature change to the average bridge temperature change. The effective stress strength parameters used for the soil layers are summarized in Table 6.3.

Table 6.3. Effective Stress Properties

Soil Type	Effective Cohesion (c') (kPa)	Effective Friction Angle with respect to Net Normal Stress (ϕ')
Backfill material	0	35
Clay	10	25
Sand	0	30

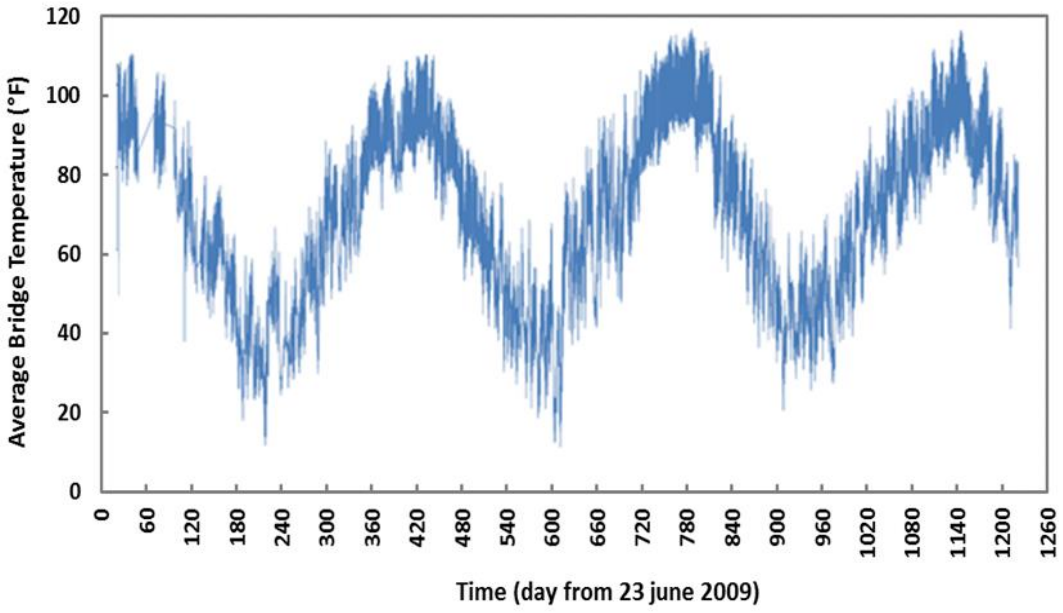

Figure 6.15. Temperature variations measured on the bridge (obtained from Kirupakaran 2013)

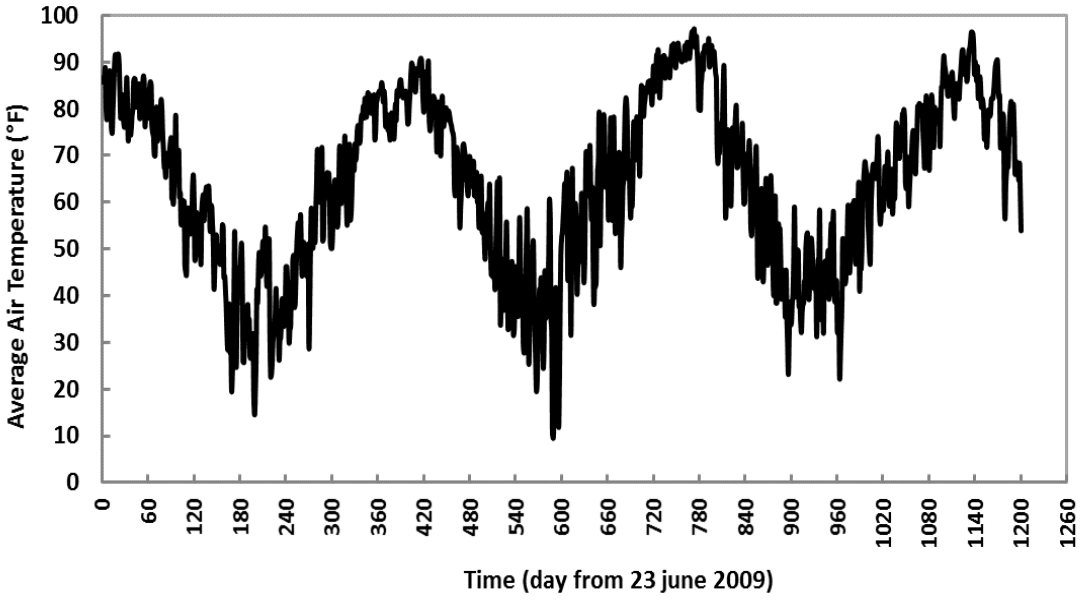

Figure 6.16. Temperature variations measured at the weather station close to the bridge

The apparent cohesion was derived based on the driest condition or the highest suction distribution along the soil layer for each case from the seepage analyses. The suction was assumed to be zero for the backfill material for all lateral load modeling cases. This assumption was reasonable based on the following factors: 1) the relatively high stiffness of the abutment relative to the backfill sand, 2) the fact that fixed displacement was applied to the top of the relatively rigid abutment, and 3) the relative insensitivity of the sand to suction changes. The apparent cohesion developed in each of the model soil layers is shown in Figures 6.17 through 6.22. The "X" symbols in these figures indicate the predicted apparent cohesion at points where significant changes in the slope of the trends was observed at the top and bottom of each layer. Apparent cohesion values used to develop the p-y curves at

specific depths along the pile were found by linear interpolation between these points.

The results of LPILE parametric analyses are summarized in Tables 6.4, 6.5 and 6.6. For each analysis scenario described above, the tables include the bridge length, lateral displacement applied to the top of the abutment, and the ratio of the maximum bending moment in the pile to the yield moment for different HP piles with weak and strong axis bending orientations. The ratios of maximum bending moments to the yield bending moments of different HP piles are summarized in Tables 6.4, 6.5, and 6.6. It should be noted that the yield bending moment of steel piles were calculated from the following equation:

$$M_y = f_y \times S \qquad \textbf{(6.1)}$$

where, *S* is elastic section modulus for bending about the axis considered (weak or strong axis), and f_y is yield strength of steel, which is equal to 0.276 GPa. The yield bending moment for weak axis (strong axis), M_y, of steel HP 10x42, HP 12x53, and HP 14x89 piles were calculated as 64.30 (196.20), 95.50 (301.70), and 200.40 (592.60) kN.m, respectively.

A comprehensive review of the results presented in Tables 6.4 through 6.6 results in several important observations as follows:

1) Larger cross-section piles performed better than smaller piles in terms of resisting bending moments. Of the 72 scenarios investigated for the largest pile cross-section (HP14x89), 52 out of 72 resulted in bending moments less than the yield moment for strong axis bending and 23 out 72 for weak axis bending. For the

smallest pile cross-section (HP10x42) the corresponding values were 31 and 15 for strong and weak axis bending.

2) As noted above, piles in strong axis bending developed bending moments less than the yield moments more often than piles in weak axis bending. Of the 216 strong axis bending scenarios summarized in Tables 6.4 to 6.6, 119 out of 216 resulted in maximum bending moments less than the yield moments; however, for the weak axis bending scenarios the corresponding value was 57 out of 216. While this may suggest that piles might be better oriented for strong axis bending, one must consider since the analysis was performed with a fixed lateral displacement applied to the top of the abutment, significantly greater forces will be developed in the bridge structure and abutment due to the bending resistance of the larger piles and stiffer bending direction. This must be considered in the overall analysis since excessive forces due to an overly stiff pile system may lead to damage to abutment backwall, deck, and girders. The overall goal is to have a relatively flexible pile system with bending moments less than yield moments.

3) Overall, short piles performed slightly better than long piles with respect to maximum bending moments. Of the 144 scenarios involving short piles in single layers of sand or clay, 62 resulted in bending moments less than the yield moments, while for long piles the number was 54 out 144. Long piles performed marginally better than short piles in the saturated single soil layer scenarios; 47 out of the 72 scenarios resulted in bending moments less than the yield moment while for short piles the number was 45 out of 72. However, for the unsaturated scenarios the short

piles outperformed the long piles with 17 out of 72 scenarios resulting in bending moments less than the yield moments compared to 7 out of 72 for the long piles. These results show that the pile response is not dependent on only the length of the piles but also the nature of the soil and changes in the soil due to moisture variations.

4) For the soil properties assigned to clay and sand layers used in the analysis, the pile bending in the sand layers resulted in lower bending moments compared to the clay layers. These results cannot be considered as the norm since sand and clay layers can have widely varying strength and stiffness characteristics depending on the relative density of sand, stress history, and undrained strength of clay among other factors. However, these results do show that stiffer soils will result in higher bending moments depending on the assumed soil properties.

5) The presence of significant matric suction in the soil profile results in significant increases in bending moments in laterally loaded piles in clay but relatively much lower increases in bending moments for piles in sand. This is attributed to the large increases in apparent cohesion in the clayey soils compared to the sandy soils as shown in Figures 6.17 to 6.22.

6) For many of the cases involving saturated soil, maximum bending moments exceeded the yield moments of the piles. This is an important observation because the saturated case is a “best case” scenario where soils offer less bending resistance resulting in more gentle curvature of piles and lower maximum bending moments. This observation suggests that careful attention should be given to reducing the soil

stiffness around the top of the pile for all soil conditions, even those of modest strength and stiffness.

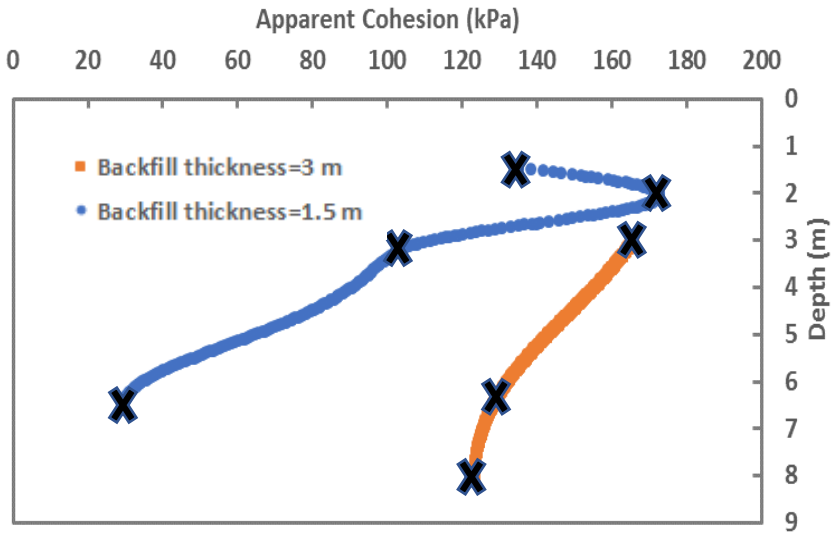

Figure 6.17. Case-1 and 2 for relatively short pile: Clay layer beneath different thicknesses of backfill materials

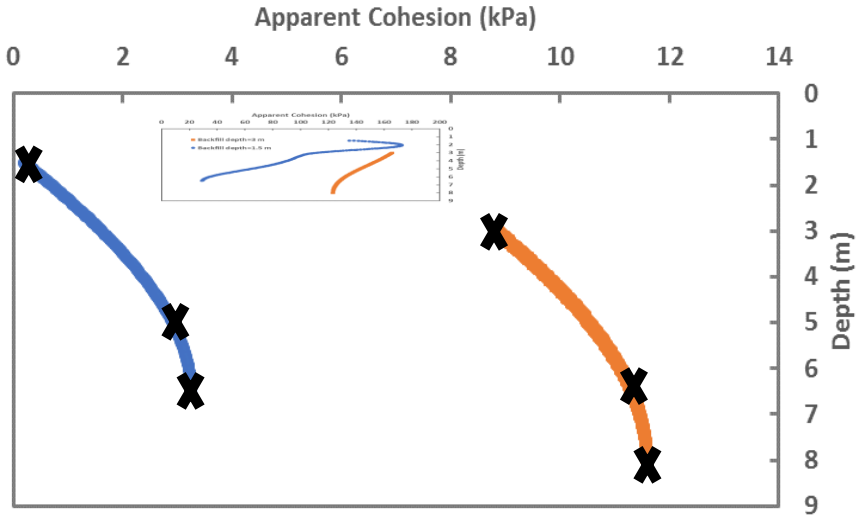

Figure 6.18. Case-3 and 4 for relatively short pile: Sand layer beneath different thicknesses of backfill materials

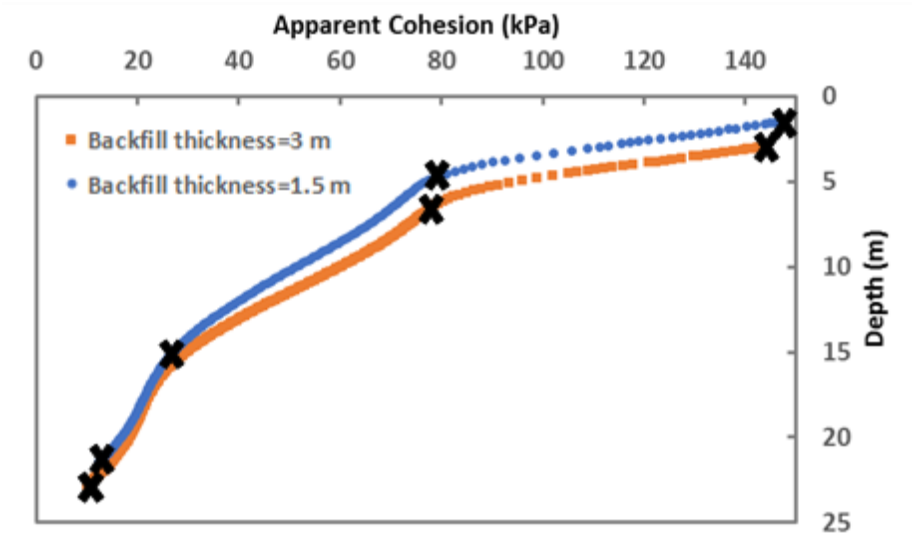

Figure 6.19. Case-5 and 6 for relatively long pile: Clay layer beneath different thicknesses of backfill materials

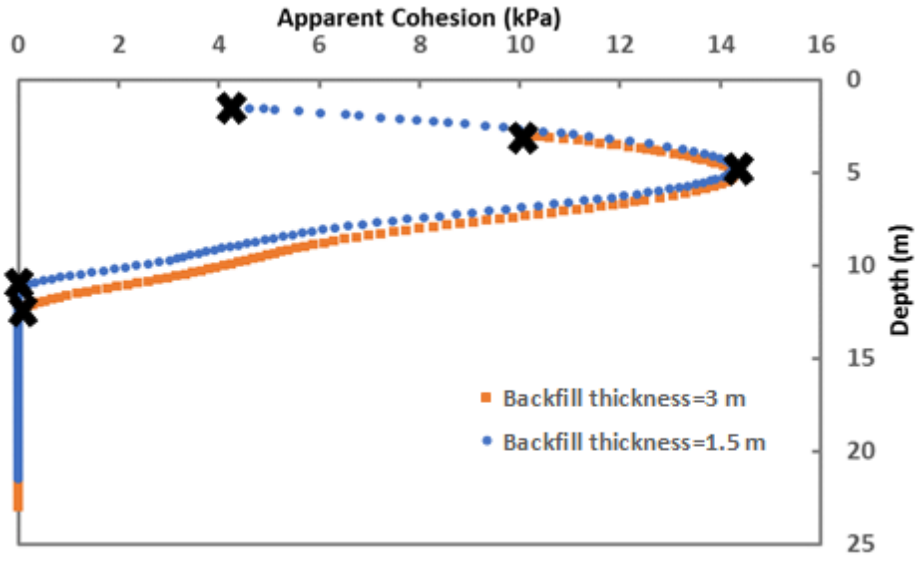

Figure 6.20. Case-7 and 8 for relatively long pile: Sand layer beneath different thicknesses of backfill materials

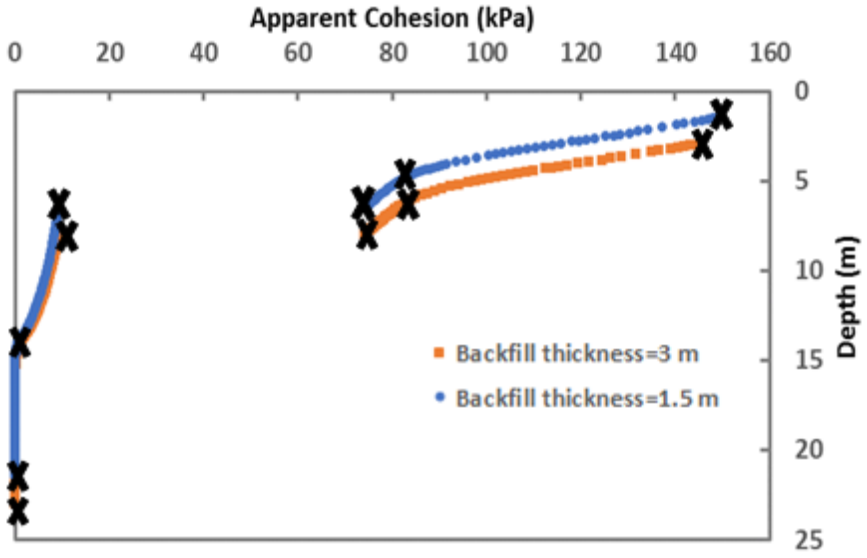

Figure 6.21. Case-9 and 10 for relatively long pile: Clay and Sand layers, respectively beneath different thicknesses of backfill materials

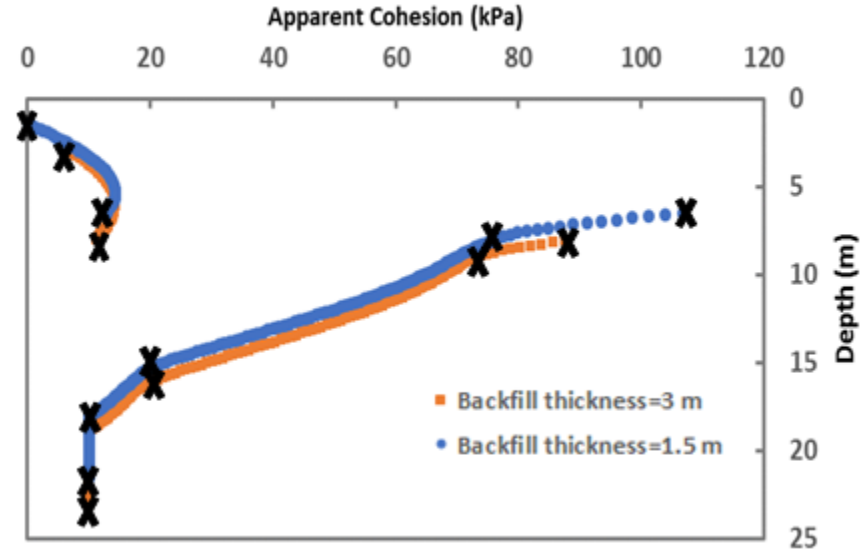

Figure 6.22. Case-11 and 12 for relatively long pile: Sand and Clay layers, respectively beneath different thicknesses of backfill materials

Table 6.4. Ratio of Maximum Bending Moment of Pile Head to Yield Bending Moment-Relatively Short Pile (5 m-single soil layer)

Short Pile (Backfill thickness=1.5 m)-Saturated-Single Clay Layer							
Bridge Length(m)	Lateral displacement (m)	HP10*42 (S)	HP10*42 (W)	HP12*53 (S)	HP12*53 (W)	HP14*89 (S)	HP14*89 (W)
50	0.013	0.94	1.72	0.82	1.53	0.28	1.13
70	0.018	1.17	2.14	1.03	1.89	0.35	1.41
90	0.023	1.38	2.52	1.22	2.23	0.42	1.67
Short Pile (Backfill thickness=3 m)-Saturated-Single Clay Layer							
Bridge Length(m)	Lateral displacement (m)	HP10*42 (S)	HP10*42 (W)	HP12*53 (S)	HP12*53 (W)	HP14*89 (S)	HP14*89 (W)
50	0.013	0.89	1.68	0.76	1.46	0.56	1.06
70	0.018	1.12	2.09	0.96	1.83	0.71	1.33
90	0.023	1.33	2.47	1.14	2.17	0.86	1.58
Short Pile (Backfill thickness=1.5 m) -Saturated-Single Sand Layer							
Bridge Length(m)	Lateral displacement (m)	HP10*42 (S)	HP10*42 (W)	HP12*53 (S)	HP12*53 (W)	HP14*89 (S)	HP14*89 (W)
50	0.013	0.43	0.74	0.42	0.67	0.39	0.56
70	0.018	0.55	0.92	0.55	0.84	0.52	0.72
90	0.023	0.67	1.08	0.67	0.99	0.65	0.88
Short Pile (Backfill thickness=3 m) -Saturated-Single Sand Layer							
Bridge Length(m)	Lateral displacement (m)	HP10*42 (S)	HP10*42 (W)	HP12*53 (S)	HP12*53 (W)	HP14*89 (S)	HP14*89 (W)
50	0.013	0.42	0.73	0.40	0.65	0.36	0.54
70	0.018	0.54	0.91	0.53	0.82	0.48	0.69
90	0.023	0.65	1.08	0.65	0.98	0.59	0.85
Short Pile (Backfill thickness=1.5 m)-Unsaturated-Single Clay Layer							
Bridge Length(m)	Lateral displacement (m)	HP10*42 (S)	HP10*42 (W)	HP12*53 (S)	HP12*53 (W)	HP14*89 (S)	HP14*89 (W)
50	0.013	3.20	6.20	2.68	5.32	1.89	3.74
70	0.018	3.96	7.68	3.33	6.59	2.36	4.65
90	0.023	4.65	9.00	3.92	7.73	2.78	5.47
Short Pile (Backfill thickness=3 m)-Unsaturated-Single Clay Layer							
Bridge Length(m)	Lateral displacement (m)	HP10*42 (S)	HP10*42 (W)	HP12*53 (S)	HP12*53 (W)	HP14*89 (S)	HP14*89 (W)
50	0.013	2.68	5.66	2.11	4.66	1.32	3.00
70	0.018	3.47	7.21	2.76	5.98	1.76	3.92
90	0.023	4.19	8.62	3.36	7.19	2.17	4.76
Short Pile (Backfill thickness=1.5 m)-Unsaturated- Single Sand Layer							

Bridge Length(m)	Lateral displacement (m)	HP10*42 (S)	HP10*42 (W)	HP12*53 (S)	HP12*53 (W)	HP14*89 (S)	HP14*89 (W)
50	0.013	0.55	0.96	0.51	0.87	0.45	0.69
70	0.018	0.69	1.20	0.66	1.09	0.58	0.88
90	0.023	0.83	1.42	0.79	1.29	0.72	1.06
Short Pile (Backfill thickness=3 m)-Unsaturated- Single Sand Layer							
Bridge Length(m)	Lateral displacement (m)	HP10*42 (S)	HP10*42 (W)	HP12*53 (S)	HP12*53 (W)	HP14*89 (S)	HP14*89 (W)
50	0.013	1.04	1.95	0.88	1.69	0.64	1.23
70	0.018	1.30	2.44	1.12	2.13	0.81	1.55
90	0.023	1.55	2.88	1.33	2.53	0.98	1.85

Table 6.5. Ratio of Maximum Bending Moment of Pile Head to Yield Bending Moment-Relatively Long Pile (20 m-one soil layer)

Long Pile-(Backfill thickness=1.5 m)-Saturated-Single Clay Layer							
Bridge Length(m)	Lateral displacement (m)	HP10*42 (S)	HP10*42 (W)	HP12*53 (S)	HP12*53 (W)	HP14*89 (S)	HP14*89 (W)
50	0.013	1.04	1.35	0.70	1.23	0.54	0.96
70	0.018	0.98	1.70	0.88	1.55	0.68	1.21
90	0.023	1.17	2.03	1.05	1.84	0.81	1.43
Long Pile-(Backfill thickness=3 m)-Saturated-Single Clay Layer							
Bridge Length(m)	Lateral displacement (m)	HP10*42 (S)	HP10*42 (W)	HP12*53 (S)	HP12*53 (W)	HP14*89 (S)	HP14*89 (W)
50	0.013	0.94	1.79	0.79	1.55	0.57	1.11
70	0.018	1.18	2.24	1.00	1.94	0.72	1.39
90	0.023	1.39	2.64	1.19	2.29	0.86	1.65
Long Pile-(Backfill thickness=1.5 m)-Saturated-Single Sand Layer							
Bridge Length(m)	Lateral displacement (m)	HP10*42 (S)	HP10*42 (W)	HP12*53 (S)	HP12*53 (W)	HP14*89 (S)	HP14*89 (W)
50	0.013	0.36	0.63	0.32	0.57	0.25	0.44
70	0.018	0.45	0.79	0.41	0.72	0.31	0.56
90	0.023	0.53	0.94	0.48	0.85	0.37	0.66
Long Pile-(Backfill thickness=3 m)-Saturated-Single Sand Layer							
Bridge Length(m)	Lateral displacement (m)	HP10*42 (S)	HP10*42 (W)	HP12*53 (S)	HP12*53 (W)	HP14*89 (S)	HP14*89 (W)
50	0.013	0.41	0.77	0.36	0.67	0.26	0.49
70	0.018	0.51	0.95	0.45	0.83	0.33	0.62
90	0.023	0.61	1.12	0.53	0.98	0.39	0.73
Long Pile-(Backfill thickness=1.5 m)-Unsaturated-Single Clay Layer							

Bridge Length(m)	Lateral displacement (m)	HP10*42 (S)	HP10*42 (W)	HP12*53 (S)	HP12*53 (W)	HP14*89 (S)	HP14*89 (W)
50	0.013	2.28	3.93	2.03	3.60	1.53	2.79
70	0.018	2.89	4.99	2.58	4.57	1.94	3.54
90	0.023	3.45	5.97	3.07	5.46	2.32	4.22
Long Pile-(Backfill thickness=3 m)-Unsaturated- Single Clay Layer							
Bridge Length(m)	Lateral displacement (m)	HP10*42 (S)	HP10*42 (W)	HP12*53 (S)	HP12*53 (W)	HP14*89 (S)	HP14*89 (W)
50	0.013	2.75	5.93	2.14	4.81	1.33	3.05
70	0.018	3.51	7.45	2.76	6.09	1.75	3.93
90	0.023	4.19	8.85	3.33	7.27	2.13	4.73
Long Pile-(Backfill thickness=1.5 m)-Unsaturated-Single Sand Layer							
Bridge Length(m)	Lateral displacement (m)	HP10*42 (S)	HP10*42 (W)	HP12*53 (S)	HP12*53 (W)	HP14*89 (S)	HP14*89 (W)
50	0.013	0.85	1.41	0.79	1.32	0.55	1.07
70	0.018	1.08	1.79	1.00	1.67	0.79	1.36
90	0.023	1.29	2.15	1.19	2.00	0.95	1.62
Long Pile-(Backfill thickness=3 m)-Unsaturated-Single Sand Layer							
Bridge Length(m)	Lateral displacement (m)	HP10*42 (S)	HP10*42 (W)	HP12*53 (S)	HP12*53 (W)	HP14*89 (S)	HP14*89 (W)
50	0.013	1.22	2.33	1.03	2.01	0.72	1.43
70	0.018	1.53	2.91	1.30	2.52	0.92	1.81
90	0.023	1.82	3.43	1.54	2.99	1.09	2.15

Table 6.6. Ratio of Maximum Bending Moment of Pile Head to Yield Bending Moment-Relatively Long Pile, (20 m-two different soil layers)

Long Pile-(Backfill thickness=1.5 m)-Saturated-5 m Clay and 15 m Sand Layers							
Bridge Length(m)	Lateral displacement (m)	HP10*42 (S)	HP10*42 (W)	HP12*53 (S)	HP12*53 (W)	HP14*89 (S)	HP14*89 (W)
50	0.013	0.78	1.35	0.69	1.23	0.54	0.96
70	0.018	0.98	1.70	0.88	1.55	0.68	1.21
90	0.023	1.16	2.03	1.04	1.84	0.81	1.43
Long Pile-(Backfill thickness=3 m)-Saturated-5 m Clay and 15 m Sand Layers							
Bridge Length(m)	Lateral displacement (m)	HP10*42 (S)	HP10*42 (W)	HP12*53 (S)	HP12*53 (W)	HP14*89 (S)	HP14*89 (W)
50	0.013	0.93	1.80	0.79	1.55	0.57	1.11
70	0.018	1.17	2.24	0.99	1.94	0.72	1.39
90	0.023	1.39	2.64	1.18	2.28	0.86	1.64
Long Pile-(Backfill thickness=1.5 m) -Saturated-5 m Sand and 15 m Clay Layers							

Bridge Length(m)	Lateral displacement (m)	HP10*42 (S)	HP10*42 (W)	HP12*53 (S)	HP12*53 (W)	HP14*89 (S)	HP14*89 (W)
50	0.013	0.36	0.63	0.33	0.57	0.27	0.45
70	0.018	0.46	0.79	0.42	0.72	0.35	0.57
90	0.023	0.54	0.94	0.51	0.85	0.43	0.68
Long Pile-(Backfill thickness=3 m)-Saturated-5 m Sand and 15 m Clay Layers							
Bridge Length(m)	Lateral displacement (m)	HP10*42 (S)	HP10*42 (W)	HP12*53 (S)	HP12*53 (W)	HP14*89 (S)	HP14*89 (W)
50	0.013	0.41	0.77	0.37	0.67	0.29	0.50
70	0.018	0.52	0.95	0.47	0.84	0.38	0.64
90	0.023	0.62	1.12	0.57	0.99	0.46	0.77
Long Pile-(Backfill thickness=1.5 m)-Unsaturated-5 m Clay and 15 m Sand Layers							
Bridge Length(m)	Lateral displacement (m)	HP10*42 (S)	HP10*42 (W)	HP12*53 (S)	HP12*53 (W)	HP14*89 (S)	HP14*89 (W)
50	0.013	2.29	3.96	2.04	3.61	1.54	2.80
70	0.018	2.90	5.01	2.58	4.59	1.95	3.55
90	0.023	3.46	5.99	3.08	5.47	2.32	4.23
Long Pile-(Backfill thickness=3 m)-Unsaturated-5 m Clay and 15 m Sand Layers							
Bridge Length(m)	Lateral displacement (m)	HP10*42 (S)	HP10*42 (W)	HP12*53 (S)	HP12*53 (W)	HP14*89 (S)	HP14*89 (W)
50	0.013	2.74	5.93	2.13	4.79	1.33	3.04
70	0.018	3.49	7.43	2.74	6.08	1.74	3.91
90	0.023	4.17	8.83	3.31	7.24	2.12	4.70
Long Pile-(Backfill thickness=1.5 m)-Unsaturated-5 m Sand and 15 m Clay Layers							
Bridge Length(m)	Lateral displacement (m)	HP10*42 (S)	HP10*42 (W)	HP12*53 (S)	HP12*53 (W)	HP14*89 (S)	HP14*89 (W)
50	0.013	0.73	1.18	0.69	1.12	0.56	0.93
70	0.018	0.94	1.51	0.88	1.43	0.72	1.19
90	0.023	1.12	1.81	1.06	1.71	0.87	1.43
Long Pile-(Backfill thickness=3 m)-Unsaturated-5 m Sand and 15 m Clay Layers							
Bridge Length(m)	Lateral displacement (m)	HP10*42 (S)	HP10*42 (W)	HP12*53 (S)	HP12*53 (W)	HP14*89 (S)	HP14*89 (W)
50	0.013	1.12	2.09	0.96	1.83	0.69	1.33
70	0.018	1.41	2.62	1.22	2.29	0.88	1.68
90	0.023	1.68	3.10	1.45	2.73	1.05	2.00

7. CONCLUSIONS AND RECOMMENDATIONS

7.1 Summary

Research presented in this report explored the impact of variable soil saturation on the lateral load behavior of integral abutment piles. In particular, the research used unsaturated seepage modelling to predict the variations in soil moisture content using climate forecasts of weather through the end of this century. To do this, a technique for calibrating the future weather predictions was developed using historical weather data. Then, the calibrated weather information was used in the unsaturated seepage modeling to predict future moisture content variations and the associated matric suction profiles surrounding abutment piles. Next, techniques were used to incorporate matric suction into the lateral load analysis of abutment piles. In this way, the impact of suction variations over time on lateral load behavior of piles was investigated. Finally, a sensitivity analysis of other parameters affecting the lateral load behavior of integral abutment piles was conducted. The sensitivity analysis involved considerations of climate patterns and integral abutment bridge construction methods in Oklahoma and other Region 6 states. The following sections present some conclusions and recommendations on lateral load analysis of integral abutment piles in a changing climate.

7.2 Conclusions

1. A historical weather survey for selected counties in Oklahoma using Mesonet data showed that Beaver and McCurtain counties located at the northwestern and the southeastern parts of Oklahoma, respectively, reasonably represent the driest and

the wettest counties, especially based on the amounts of precipitation for a given period.

2. A future weather survey of Region 6 demonstrated that selected counties representing the State of New Mexico had a climate pattern close to that of Beaver County and the counties selected in the States of Arkansas and Louisiana had a climate pattern analogous to the McCurtain County. The variety of climate patterns observed for the State of Texas were similar to the State of Oklahoma. Thus, Beaver County weather and projected climate was used in the parametric analysis to establish the maximum future suction conditions.
3. Historical potential evapotranspiration obtained from Thornthwaite's equation was calibrated using correction factors developed for each month using Penman's equation for a case study in Oklahoma. The correction factors were observed to vary for each month.
4. Actual evapotranspiration was modified by Leaf Area Index (LAI) for the Thornthwaite method. Variations of LAI from 0.8 for first and last quarter of the year and 2.6 for the rest of the year created reasonable calibrated results in comparison with the Penman method.
5. 1-D and 2-D seepage analyses conducted using Penman's and calibrated Thornthwaite's methods showed that the 1-D model overestimated the drying condition resulting in more suction changes compared to the 2-D model.
6. The pile-soil interaction analysis for an IAB subjected to temperature and moisture variations indicated that the pile bending behavior during lateral loading was sensitive

to suction changes of the foundation soil. The bending moment increased when the suction increased due to an increase of soil stiffness.

7. In the parametric study involving pile lateral loading analysis, piles in strong axis bending experienced bending moments less than the yield moments more often than piles in weak axis bending. However, since the analysis was performed with an applied displacement at the top of the abutment that was the same in both cases, the forces developed in the bridge abutment, deck, and girders will be much greater for strong axis bending.
8. Generally, the parametric study in this report showed that the pile orientations and soil foundation stiffness due to suction changes have a significant effect on the bending moment and lateral displacement behavior of abutment piles.
9. Of particular note, is that for many of the piles and soil scenarios investigated through the parametric analysis, yielding moments in the piles were exceeded by the predicted bending moments even for the saturated conditions. The saturated condition represents the softest soil response and is expected to produce the least amount of curvature and reduced bending moments relative to stiffer soils. It should also be noted that the soil properties assumed in the analysis are quite typical and don't represent overly strong or weak soils in the saturated condition. This finding indicates that a soft soil near the top of the pile is desirable to reduce bending moments. This could be achieved through predrilling a hole around the top of pile and backfilling it with compressible material.

7.3 Recommendations

Generally, results of this work show that changing climate over the long term may result in net drying of soil profiles and increased matric suction around the top of the piles. Increases in matric suction in soil around the piles increases the strength and stiffness around the piles, which results in increased resistance to pile bending and greater curvature near the top of the pile where it enters the abutment. This in turn, increases the maximum bending moments near the top of the pile. However, even for soils in the saturated condition, the soil resistance can be significant enough to cause excessive curvature and bending moments near the top of the pile where it enters the abutment. The excessive curvature at the pile top results from the contrast between the very rigid abutment and relatively flexible pile. The analysis shows that there is relatively little rotation and bending curvature in the abutment due to the bridge movement, which translates to minimal rotation at the top of the pile. This in turn leads to significant bending in the pile over a relatively short distance below the top of the pile. Some recommendations for practice and additional research follow.

Recommendations for Practice:

1. For integral abutment bridges, engineers should perform lateral loading analysis of abutment piles in light of the expected soil conditions and changes in soil conditions (i.e. moisture content variations) around the piles, pile length and properties, abutment and backfill conditions, and expected abutment displacements due to thermal loading. If bending moments are expected to be excessive, additional analyses

should be performed incorporating methods to reduce the soil stiffness around the top of the piles or incorporating different pile configurations.

2. To reduce induced forces in the abutment and bridge structure, the bending resistance of the abutment pile system should be addressed. If added flexibility is needed, piles for integral abutment bridges can be oriented for weak axis bending.
3. To improve the performance of abutment piles, engineers may consider using different piles with greater bending resistance or consider using soil (or other material) surrounding the top of the pile that is relatively compressible over a sufficient depth to reduce the abrupt curvature that can lead to excessive bending moments. The latter may be more cost effective and result in lower forces in the abutment and bridge structure as compared to using larger piles. Possibly a combination of the two approaches may be desirable. The use of predrilled holes with a compressible material around the top of the piles is a viable approach.

Recommendations for future research:

1. For the lateral load analysis, the connection between the top of the abutment and bridge was assumed to be rigid. This is a conservative assumption in that it limits the rotation of the abutment. While this assumption is more realistic than a pinned connection given the fact that the bridge girders are integral with the abutment, it would beneficial to investigate other boundary conditions such a rotational spring to see the influence of this assumption. In this way, the influence of abutment backfill properties may become more apparent. For example, one could examine more closely the question of how a compressible elastic material between the backfill and

abutment affects the abutment rotation and pile behavior. To answer this question, a more sophisticated finite element modeling approach may be needed to develop the interaction of the bridge, abutment and backfill components.

2. A detailed investigation of the forces developed in the abutment and bridge structure would provide greater insight into the about of flexibility needed in the abutment-backfill-pile system. Such an investigation would necessarily include a comprehensive finite element analysis of the entire system.
3. The seepage and soil-pile interaction analyses were conducted separately in this report. The Winkler foundation finite difference solution incorporated in LPile for pile-soil interaction analysis in unsaturated conditions can be compared with a continuum mechanics based solution such as those found in finite element programs TeraDysac and Code Bright, where hydro-mechanical coupling problems are solved simultaneously.
4. A pile group analysis considering suction changes of soil surrounding a pile group using 3-D seepage analysis is recommended for future work to compare with a single pile analysis conducted in this research.

8. REFERENCES

Abendroth, R.E., and Greimann, L.F., (2005), “Field testing of integral abutments”, Final Rep. No. HR-399, Iowa State Univ., Iowa Dept. of Transportation, Ames, Ia.

Alder, J.R., and Hostetler, S.W., (2013), “USGS National Climate Change Viewer”, US Geological Survey, https://www2.usgs.gov/climate_landuse/clu_rd/nccv.asp.

Arockiasamy, M., Butrieng, N., and Sivakumar, M., (2004) “State-of-the-Art of Integral Abutment Bridges: Design and Practice”, Journal of Bridge Engineering (ASCE), 9 (5).

Arsoy, S., Barker, R.M., and Duncan, J.M., (1999), “The Behavior of Integral Abutment Bridges”, Charlottesville: Virginia Transportation Research Council.

Benson, C.H., Bohnhoff, G.L., Ogorzalek, A.S., Shackelford, C.D., Apiwantragoon, P., and Albright, W.H., (2005), “Field Data and Model Predictions for a Monolithic Alternative Cover”, GSP 142 Waste Containment and Remediation (ASCE).

Broms, B.B., (1964a), “Lateral Resistance of Piles in Cohesive Soils”, Journal of the Soil Mechanics and Foundations Division, Proceedings of the American Society of Civil Engineers, Vol. 90, No. SM2, 27-63.

Broms, B.B., (1964b), “Lateral Resistance of Piles in Cohesionless Soils”, Journal of the Soil Mechanics and Foundations Division, Proceedings of the American Society of Civil Engineers, Vol. 90, No. SM3, 123-156.

Chao, K., Overton, D.D., and Nelson, J.D., (2010), "Effect of Water Sources on Water Migration in the Vadose Zone. In Experimental and Applied Modeling of Unsaturated Soils." ASCE.

Civjan, S.A., Bonczar, C., Brena, S.F., Dejong, J., and Crovo, D., (2007), “Integral Abutment Bridge Behavior: Parametric Analysis of a Massachusetts Bridge”, Journal of Bridge Engineering, 12, 64-71.

Collins, B.D., Znidarcic, D., (2004), "Stability Analyses of Rainfall Induced landslides", Journal of Geotechnical and Geoenvironmental Engineering.

Detournay, E., and Cheng, A.H.-D., (1993), “Fundamentals of poroelasticity.” Comprehensive rock engineering principles, practice and projects, analysis and design methods (Fairhurst, C. ed), Pergamon, Oxford, 113-171 (Chapter 5).

Dicleli, M. (2005), “Integral Abutment-Backfill Behaviour on Sand Soil-Pushover Analysis Approach”, Journal of Bridge Engineering, 10, 354-364.

Dicleli, M., and Albhaisi, S. M. (2004a), “Performance of abutment–backfill system under thermal variations in integral bridges built on clay”, *Engineering Structures,* 26, 949-962.

Dicleli, M. & Albhaisi, S. M. (2004b), “Estimation of Length Limits for Integral Bridges Built on Clay”, Journal of Bridge Engineering, 9**,** 572-581.

Dicleli, M. & Albhaisi, S. M. (2005), “Analytical formulation of maximum length limits of integral bridges on cohesive soils”, Canadian Journal of Civil Engineering, 32**,** 726-38.

Ensoft, Inc. (2007). "LPILE Plus Version 5.0." Computer Code, Austin, TX.

Evans, L. T., and Duncan, J. M., (1982), “Simplified analysis of laterally loaded piles”, Report No. UCB/GT/82-04, Geotechnical Engineering, Department of Civil Engineering, University of California, Berkeley, USA.

Faraji, S., Ting, J.M., Crovo, D.S., and Ernst, H., (2001), “Nonlinear Analysis of Integral Bridges: Finite-Element model”, Journal of Geotechnical and Geoenvironmental Engineering, Vol. 127.

Frosch, R., and Lovell, M., (2011), “Long-Term Behavior of Intregral Abutment Bridges”, Purdue University, doi:10.5703/1288284314640.

Gitrana, G.Jr., Fredlund, M.D., and Fredlund, D.G., (2006), “Numerical Modeling of Soil-atmosphere Interaction for Unsaturated Surfaces”, International Conference on Unsaturated Soils, USA.

Kamel, M.R., Benak, J. V., Tadros, M.K., and Jamshidi, M., (1996), “Prestressed concrete piles in jointless bridges”, PCI Journal, 41, 56-67.

Kang, J.B., Chao, K.C., and Overton, D.D. (2014), “Comparison of 1-D, 2-D, and 3-D Water Migration Study in Expansive Soils”, USA.

Khodair, Y., and Abdel-Mohti, A. (2014), “Numerical Analysis of Pile-Soil Interaction under Axial and Lateral Loads”, International Journal of Concrete Structures and Materials, 8(3), 239-249.

Khodair, Y.A., and Hassiotis, S., (2005), “Analysis of Soil-Pile Interaction in Integral Abutment”, Computer and Geotechnics, 32, 201-209.

Klaiber, F.W., White, D.J., Wipf, T.J., Phares, B.M., Robbins, V.W., (2004), “Development of Abutment Design Standards for Local Bridge Designs”, Iowa DOT Project TR-486, Final Report.

Kirupakaran, K., (2013), "Soil-structure interaction studies for understanding the behavior of integral abutment bridges", Ph.D. dissertation, School of Civil Engineering and Environmental Science, University of Oklahoma, Norman, Oklahoma, USA.

Knickerbocker, D., Basu, P.K., and Wasserman, E.P., (2005), “Behavior of two-span integral bridges unsymmetrical about the pier line.” Proc., FHWA Conf., Integral Abutment and Jointless Bridges (IAJB 2005), FHWA, Washington, D.C., 244-253.

Kunin, J. and Alampalli, S., (2000), “Integral abutment bridges: current practice in the United States and Canada.” Journal of Performance of Constructed Facilities, American Society of Civil Engineers 14 (3), 104-111.

Matlock, H., (1970), “Correlations for design of laterally loaded piles in soft clay”, Proceedings of 2nd Offshore Technology Conference, Houston, Texas, 1, 577-588.

Miller, G. A., Muraleetharan, K. K., Lim, Y. Y., (2001), “Wetting-induced settlement of compacted fill embankments”, Transportation Research Board, 1755, Geology and Properties of Earth Materials.

Muraleetharan, K.K., Miller, G., Kirupakaran, K., Krier, D., and Hanlon, B.R., (2012), "Soil-structure interaction studies for understanding the behavior of integral abutment bridges", Technical Report (No. OTCREOS7.1-37-F), Oklahoma Transportation Center, March

Muraleetharan, K.K., Ravichandran, N., and Taylor, L.M., (2003), "TeraDysac: TeraScale dynamic soil analysis code", Computer Code, School of Civil Engineering and Environmental Science, University of Oklahoma, Norman, Oklahoma.

Moeletsi M. E., Walker S., Hamandawana H., (2013), “Comparison of the hargreaves and samani equation and the thornthwaite equation for estimating dekadal evapotranspiration in the free state province”, South Africa. Phys Chem Earth, 66, 4-15.

Mokwa, R., Duncan, J., and Helmers, M., (2000), “Development of p-y curves for partly saturated silts and clays”, New Technological and Design Developments in Deep Foundations, 224-239.

New Mexico Department of Transportation (NMDOT), (2013), “Bridge Procedures and Design Guide”.

Park, K.D., and Fleming, I.R., (2006), “Evaluation of a geosynthetic capillary barrier”, Geotextiles and Geomembranes, 24(1), 64-71.

Penman, H. L., (1948), “Natural evapotranspiration from open water, bare soil and grass”, Proc. R. Soc. London Ser. A. 193, 120-145.

Rajeev, P., Chan, D., and Kodikara, J., (2012), “Ground-atmosphere interaction modelling for long-term prediction of soil moisture and temperature”, Canadian Geotechnical Journal, 49(9), 1059-1073.

Reese, L. C., Cox, W. R. and Koop, F. D., (1974), “Analysis of lateral loaded piles in sand”, Offshore technical conference, Dallas, Texas.

Reese, L. C., Touma, F. T. and O’Neill, M. W., (1976), “Behavior of driven piers under axial loading”, Journal of the geotechnical engineering division, proceedings of ASCE, 102(GT5), 493-510.

Scott, R.L., Shuttleworth, W.J., Keefer, T.O., and Warrick, A.W., (2000), “Modeling multiyear observations of soil moisture recharge in the semiarid American Southwest”, Water Resources Research, 36(8), 2233-2247.

SoilVision Systems Ltd. (2012), “SVFlux 2D Pro.”, Computer Code, Saskatoon, Saskatchewan, Canada.

SoilVision Systems Ltd. (2012), “SVSlope 2D Pro.”, Computer Code, Saskatoon, Saskatchewan, Canada.

Terzaghi, K., and Peck, R.B., (1967), “Soil Mechanics in Engineering Practice”, 2nd Edition, John Wiley and Sons, New York, USA.

Thornthwaite, C. W. (1948). "An approach toward a rational classification of climate", Geographical Review, 38 (1), 55-94

Weaver, T., and Grandi, O., (2009), “Lateral load analysis of deep foundations in unsaturated soils”, Contemporary Topics in In Situ Testing, Analysis, and Reliability of Foundations, 552-559.

Wilson, G. W., Fredlund, D.G., and Barbour, S.L., (1994), “Coupled soil-atmosphere modeling for soil evaporation”, Canadian Geotechnical Journal, 31, 151-161.

Vanapalli, S.K., Fredlund, D.G., Pufahl, D.E., and Clifton, A.W. (1996), “Model for the prediction of shear strength with respect to soil suction”, Canadian Geotechnical Journal, 33(3), 379-392.

Vanapalli, SK, and Oh, WT, (2010), “A Model for Predicting the Modulus of Elasticity of Unsaturated Soils Using the Soil-Water Characteristic Curve”, International Journal of Geotechnical Engineering, USA.

Voyiadjis, G.Z., Cai, S., Alshibli, K., Faghihi, D., Kong, B., Yang, Y., (2016), “Integral Abutment Bridge for Louisiana’s Soft and Stiff Soils”, Final Report, LTRC Project Number: 07-4ST, SIO Number: 30000131.

Zapata, C.E., (1999). “Uncertainty in soil–water characteristic curve and impacts on unsaturated shear strength predictions.” *Ph.D. Dissertation*, Arizona State University, Tempe, USA.

Zornberg, J.G., (2016), “Development of Integral / Semi-integral Abutments for TxDOT bridges”, Texas Department of Transportation (TxDOT) Research Project, Report number: 0-6936.

APPENDIX A

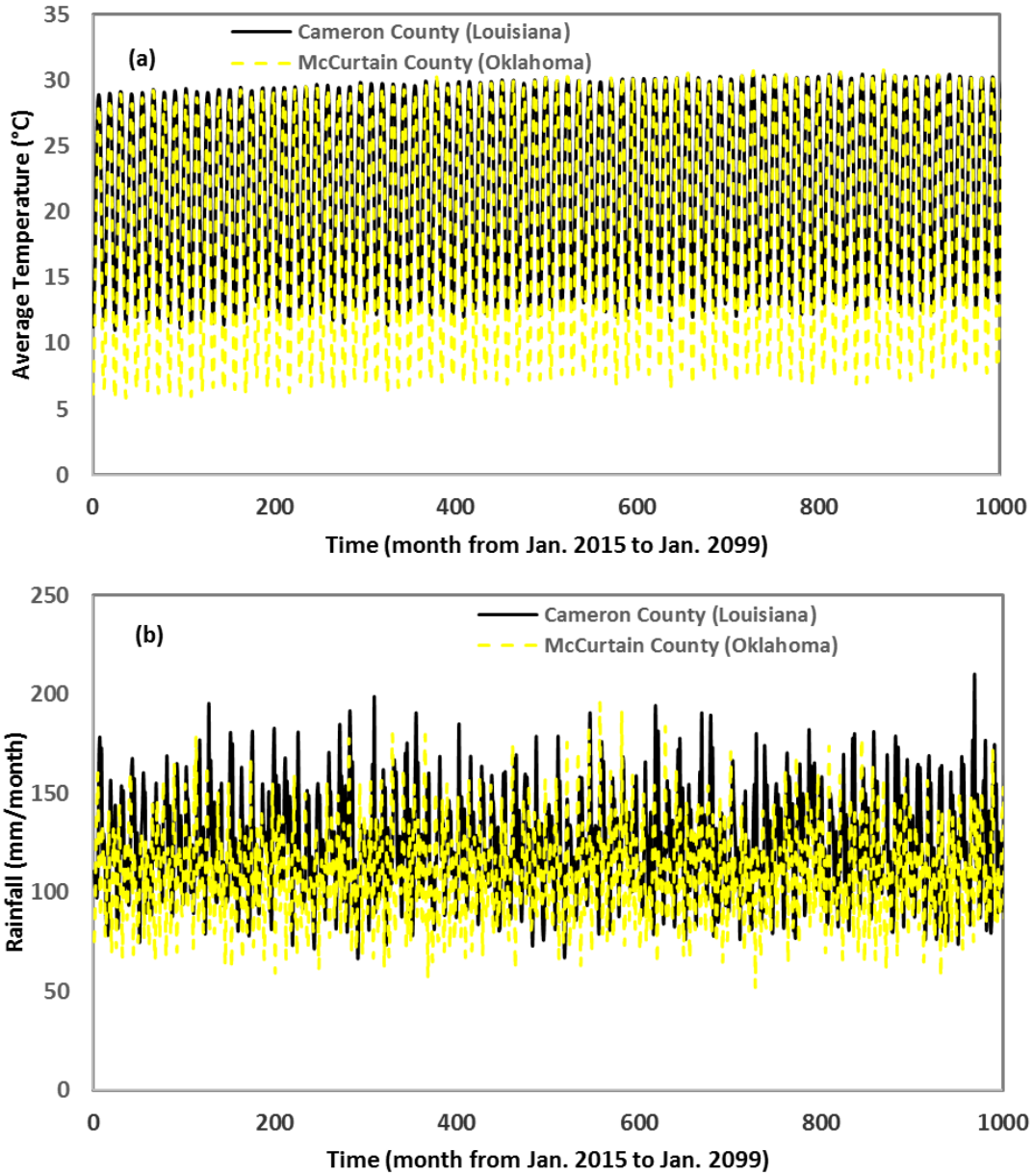

Figure A.1. Average air temperature (a) and precipitation (b) comparison between Louisiana and Oklahoma (Cameron and McCurtain counties)

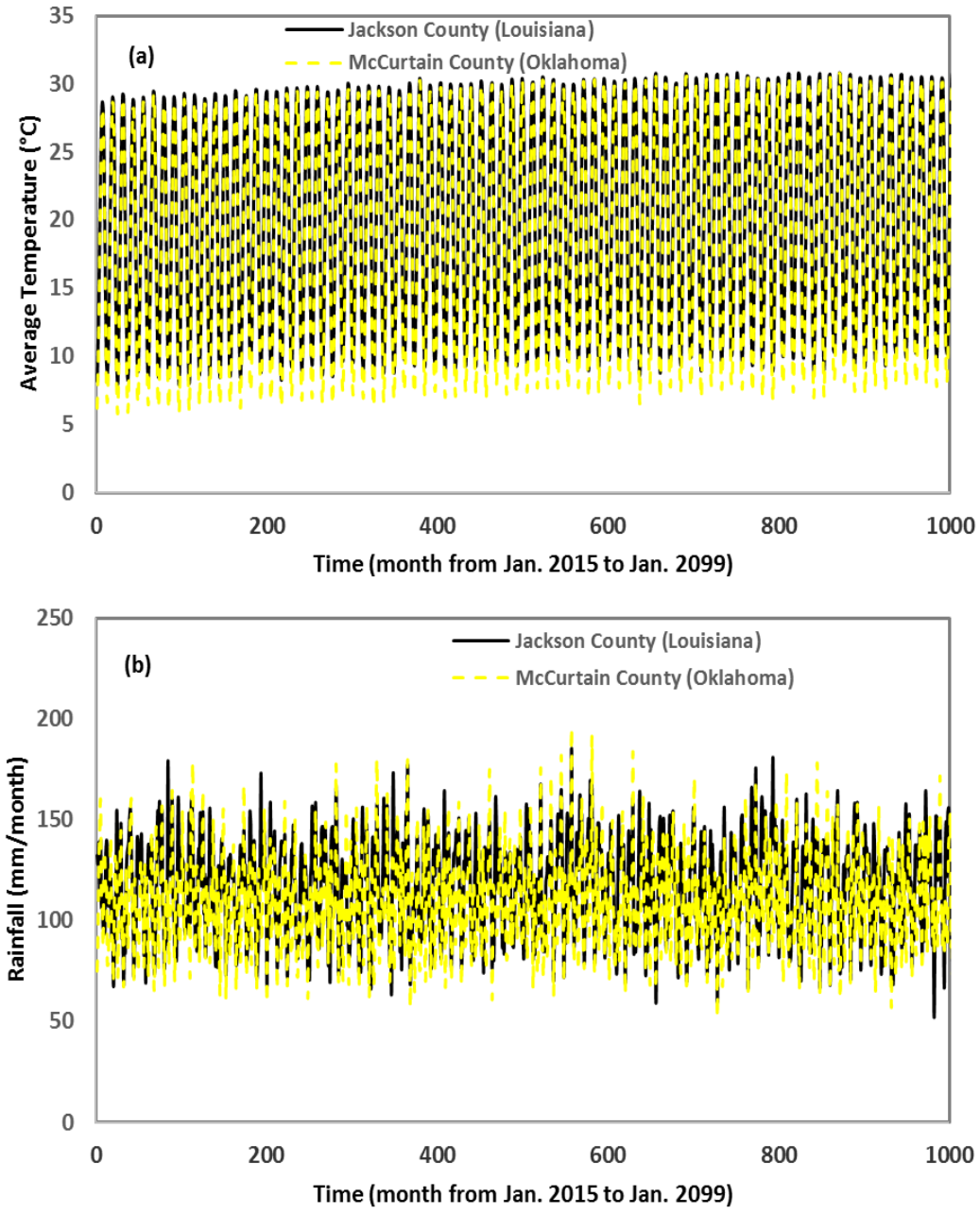

Figure A.2. Average air temperature (a) and precipitation (b) comparison between Louisiana and Oklahoma (Jackson and McCurtain counties)

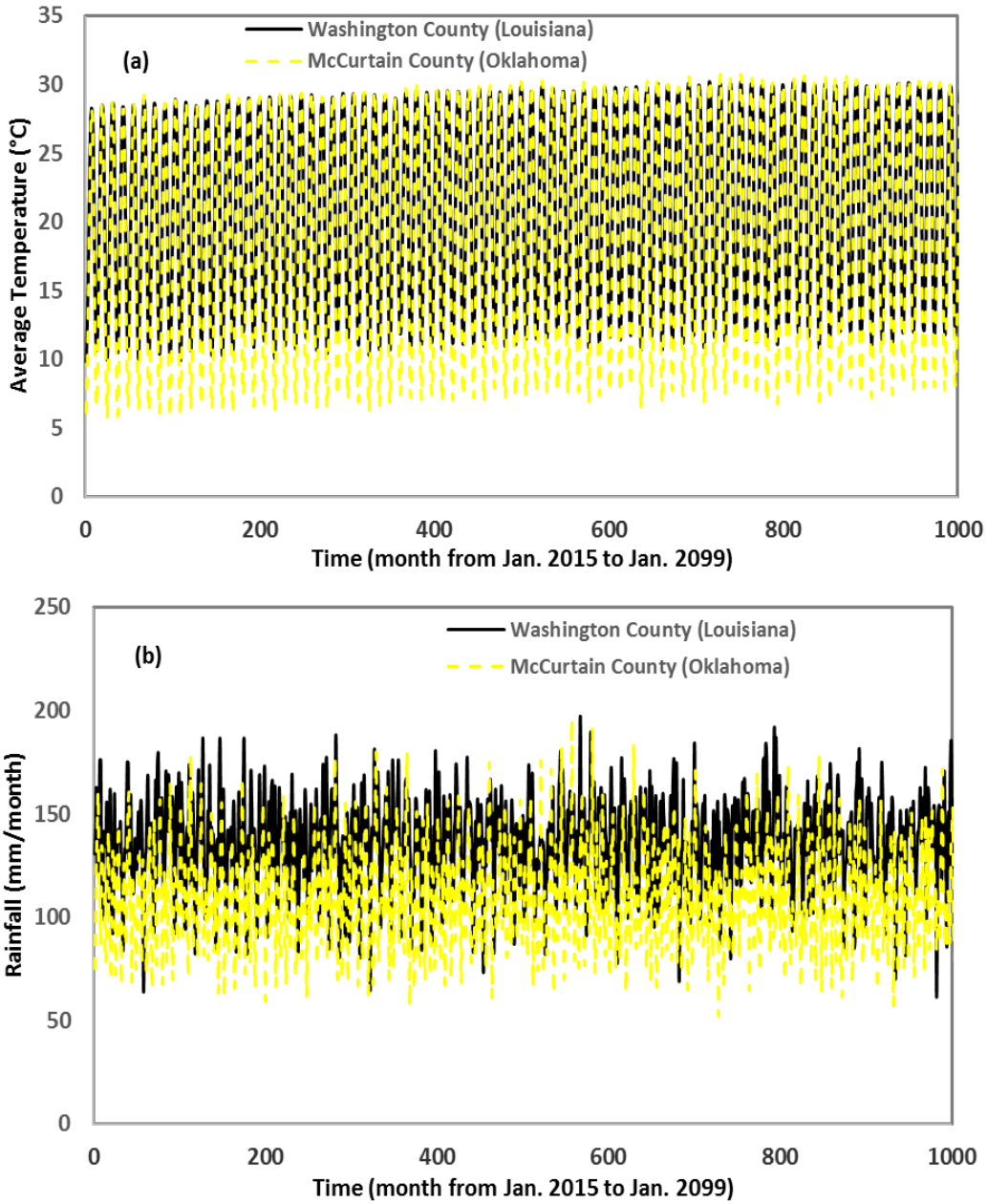

Figure A.3. Average air temperature (a) and precipitation (b) comparison between Louisiana and Oklahoma (Washington and McCurtain counties)

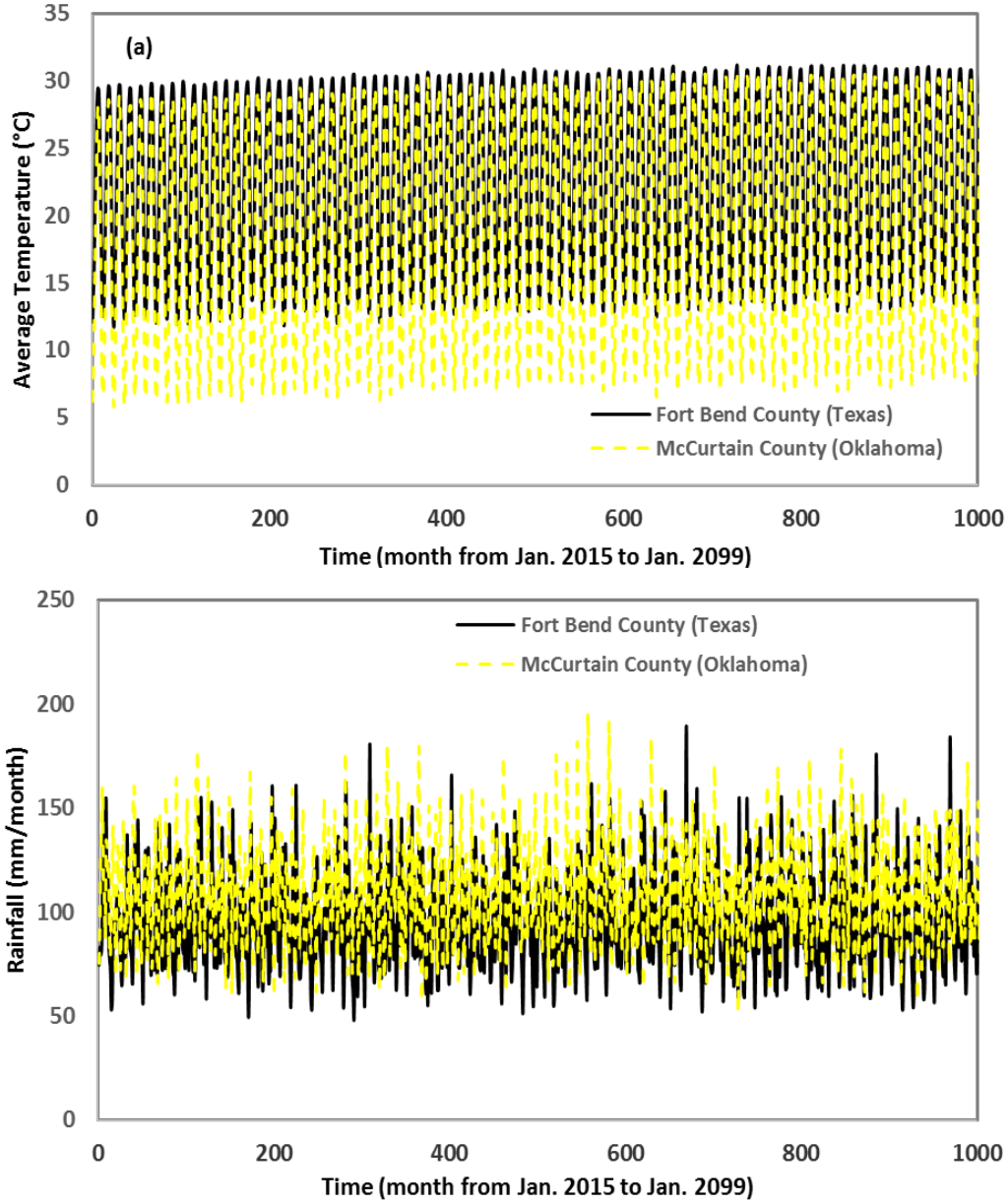

Figure A.4. Average air temperature (a) and precipitation (b) comparison between Texas and Oklahoma (Fort Bend and McCurtain counties)

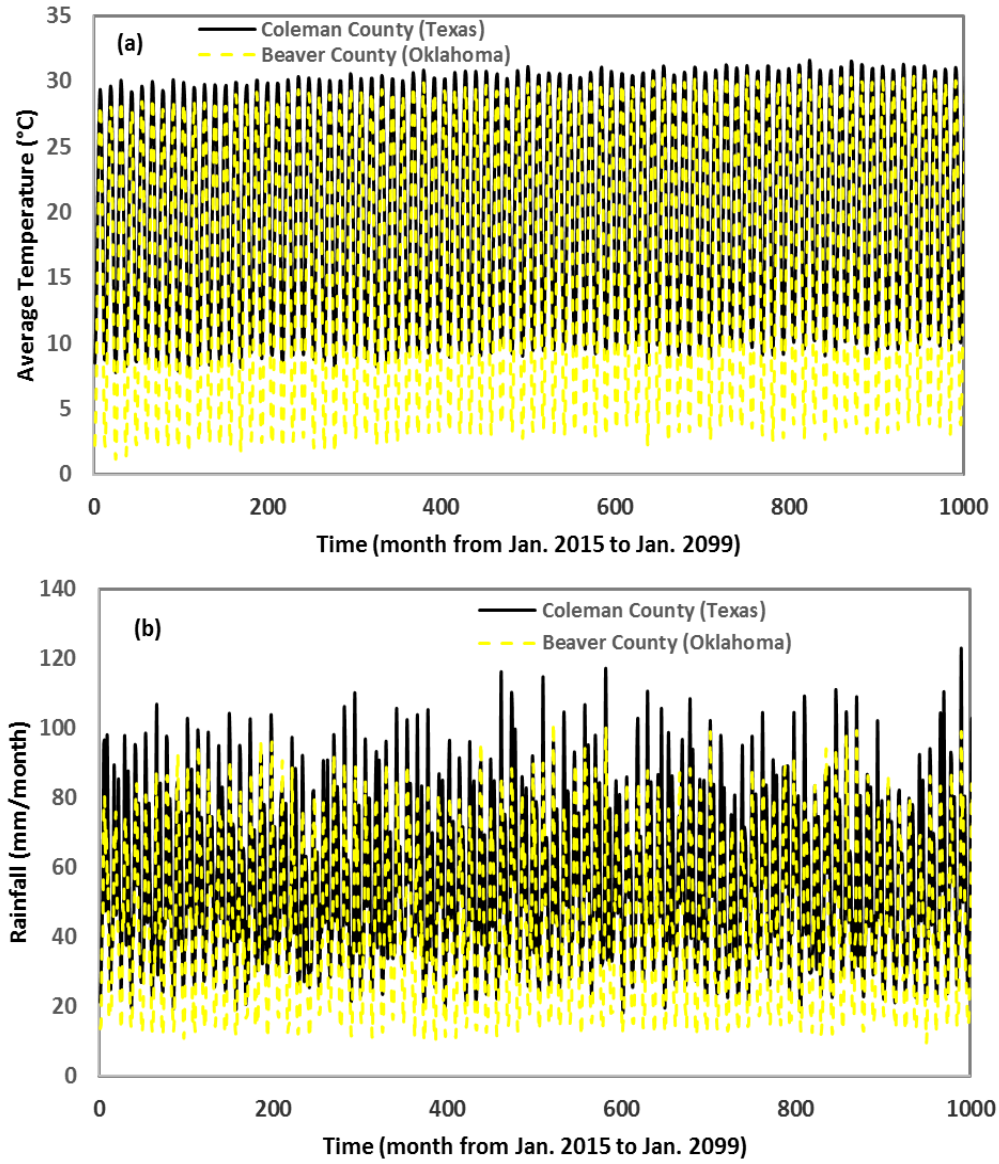

Figure A.5. Average air temperature (a) and precipitation (b) comparison between Texas and Oklahoma (Coleman and Beaver counties)